# NATIONAL ADVISORY COMMITTEE FOR AERONAUTICS

TECHNICAL MEMORANDUM 1393

## FLOW OF GAS THROUGH TURBINE LATTICES

By M. E. Deich

Translation

"Technical Gasdynamics." (Tekhnickeskaia gazodinamika) ch. 7, 1953.



NACA

Washington
May 1956

NATIONAL ADVISORY COMMITTEE FOR AERONAUTICS

TECHNICAL MEMORANDUM 1393

# FLOW OF GAS THROUGH TURBINE LATTICES*

By M. E. Deich

## 7-1. GEOMETRICAL AND GASDYNAMICAL PARAMETERS OF THE LATTICES; FUNDAMENTALS OF FLOW THROUGH LATTICES

The transformation of energy in a stage of a turbomachine is a result of the interaction of the gas flow with the stationary and rotating blades, which form the guide and impeller blade systems.

The lattices of a turbine in the general case represent systems of blades of the same shape uniformly arranged on a certain surface of revolution. A particular case of a three-dimensional lattice is an annular lattice with radial blades arranged between coaxial cylindrical surfaces of revolution.

In flowing through the lattice, the velocity and direction of the gas flow are changed, and a reaction force is thereby produced on the lattice. On the rotating lattices of a turbine this force performs work; the rotating lattices of compressors, on the contrary, increase the energy of the gas flowing through them. In stationary lattices an energy interchange with the surrounding medium does not occur; in this case the lattices bring about the required transformations of kinetic energy (velocity) and the deflection of the flow.

Depending on the flow conditions and the corresponding geometrical parameters of the blade profile, three fundamental types of lattices are distinguished:

(a) Converging flow type: the nozzle or guide (stationary) vanes and the reaction (rotating) lattices of turbines

*"Technical Gasdynamics." (Tekhnickeskaia gazodinamika) ch. 7, 1953, pp. 312-420.

(b) Action or impulse (rotating) lattices of turbines

(c) Diffuser: guide (stationary) and working (rotating) lattices of compressors.

Depending on the general direction of motion of the gas with respect to the axis of rotation, the lattices are divided into axial and radial types. In certain machine designs the gas flow moves at an angle to the axis of rotation (diagonal lattices).



The most important geometrical parameters of an annular (cylindrical) lattice are the mean diameter $d$, the length (height of the blade $l$, the width of the lattice $B$, the pitch of the blades on the mean diameter $t$, the chord $b$, and other blade profile parameters (fig. 7-1).

There exist several methods of specifying the shape of a blade profile. The universal method of coordinates (fig. 7-2(a)) has great advantages. The methods shown in figures 7-2(b) and (c) are based on the idea of the mean line of a profile; the mean line may represent the geometric loci of the centers of inscribed circles or the centers of the chords connecting the points of tangency. The mean line is defined by coordinates, and the thickness distribution about the mean line is then independently given. For specifying the profiles of turbine lattices, consisting most frequently of thick, sharply curved profiles with small pitch, the methods shown in figure 7-2(b) and (c) are inconvenient. The determination of the fundamental dimensions, the construction of the profile, or its checking require complicated graphical work. The most widespread method of constructing the profile from a small number of adjoining arcs of circles and segments of straight lines (fig. 7-2(d)) is arbitrary and tedious.

If the ratio of the mean diameter of the lattice $d$ to the height of the blade $l$ is large, the lattice may, for the purpose of simplifying the problem, be considered as a straight row lattice. The shape of the space between the blades along the height may then be considered as constant. In the simplest case, assuming that the diameter of the lattice and the number of the blades increase without limit, we obtain a plane infinite lattice (fig. 7-1(c)).

The passage from the cylindrical to the plane lattice is effected in the following manner: We pass two coaxial cylindrical sections of the annular lattice through the middle diameter $d$ and through the diameter $d + \Delta d$. Assuming $\Delta d$ to be small, we develop the resulting annular lattice of very small height on a plane. Increasing the number of blades to infinity, we obtain the plane infinite lattice shown in figure 7-1(c).

The assumption of plane cross sections, that is, used as the basis of the investigations and computations of modern turbomachines, was fruitfully applied by N. E. Joukowsky in 1890. The value of this assumption has been confirmed by numerous experiments.

The geometrical characteristics of lattices are usually given in nondimensional form. For example, the relative pitch of the profile is determined by the formulas

$$\bar{t} = \frac{t}{b} \quad \text{or} \quad \bar{t}_B = \frac{t}{B}$$

The relative height (or length) of the blade,

$$\bar{l}_b = \frac{l}{b}$$

In certain cases in investigating the three-dimensional flow in a lattice, it is more convenient to define the relative height as

$$\bar{l}_a = \frac{l}{a_2}$$

where $a_2$ is the width of the minimum cross section of the passage (fig. 7-1).

A rectilinear lattice is referred to as a system of coordinates x, y, z where the direction x is termed the axis of the lattice (fig. 7-1(b)). All profiles must coincide in the translational displacement along the axis of the lattice. The pitch t of the lattice is equal to the distance between any two corresponding points.

For a given profile shape, the shape of the interblade passage of the lattice depends, in addition to the pitch, on the angle $\beta_y$, which is defined as the angle between the axis of the lattice and the chord of the profile (fig. 7-1(c)). In the practical construction of turbine lattices, the position of a profile in the lattice is often specified by the geometrical angle of the exit edge $\beta_{2n}$ (the angle between the tangent to the mean line at the trailing edge and the axis of the lattice). In certain cases, for a straight-backed profile, the angle $\beta_{2n}$ is measured from the direction of the suction surface at the trailing edge.

In the design of the blade lattices it is necessary, besides satisfying a number of structural requirements, to ensure that the given transformation of energy obtains with minimum losses. A detailed study of the flow process over the blades of the lattice is thus required. One of the important problems is that of establishing the effect of the shape of the blades and of other geometric parameters of the lattice on

the mechanical efficiency over a wide range of Mach and Reynolds numbers and inlet flow angles.

The flow process of a gas through the lattices of a turbomachine is a very complicated hydromechanical process. The theoretical solution of the corresponding problem of the unsteady three-dimensional motion of a viscous compressible fluid presents great difficulties. A good approach to the solution of this problem, as in general to the solution of most technical problems, consists of the investigation of simplified models which retain most of the essential characteristics of the actual process. Succeeding analyses then develop the effect of secondary factors.

At the present time the most highly developed theory is that of the steady two-dimensional flow through the lattice of an ideal incompressible fluid. Such a flow may be considered as the limiting case of the actual flow in a lattice at small flow velocities (small Mach numbers, $M < 0.3 - 0.5$) and with small effect of the viscosity (large Reynolds numbers, $Re > 10^4 - 10^5$).

Within the frame of such a simplified scheme it is possible to establish the fundamental characteristics of a potential flow in a lattice. However, the solutions obtainable with these limitations require an essential correction. The effects of the viscosity and of the compressibility must be evaluated by theoretical and experimental methods. The results of other tests permit evaluating certain features of the three-dimensional flow in lattices and obtaining the characteristics of the lattices required for the thermodynamic computation of the stages of the turbomachine.

Let us consider several features of a plane potential flow of an ideal incompressible fluid for the case of the flow over the blades of a reaction turbine (fig. 7-3). On account of the repeated character of the flow, it is sufficient to study the flow in a single interblade passage or the flow about a single blade. In figure 7-3(a) the continuous curves represent the streamlines $\Psi$ = constant; the dotted curves represent the equipotential lines $\Phi$ = constant, normal to the streamlines. A sufficiently dense network of these lines gives a good characterization of the flow. The velocity $c$ at any point of the flow is equal to

$$c = \frac{d\Phi}{dS} = -\frac{d\Psi}{dn} \tag{7-1}$$

where $S$ and $n$ are the curvilinear distances along the streamlines and equipotential lines, respectively.

The differentials may be approximately replaced by finite increments, and we thus obtain

$$c \approx \frac{\Delta\Phi}{\Delta S} \approx -\frac{\Delta\Psi}{\Delta n}$$

If $\Delta\Phi = \Delta\Psi = \text{constant}$ at each point, then $\Delta S \approx \Delta n$. In this case, the individual elements of the orthogonal network of lines, $\Phi = \text{constant}$ and $\Psi = \text{constant}$, become squares in the limit (as $\Delta S \to 0$ and $\Delta n \to 0$). The flow network of an ideal incompressible fluid therefore is termed a square network.



At subsonic velocities, the losses in available energy are produced by the effect of viscosity, by periodic fluctuations of the flow, and by the high degree of turbulence of the flow. When the velocities are nearly sonic or when they are supersonic, the losses are caused by the irreversible process of the discontinuous energy transformation. The magnitude of the losses determines, to a large extent, the mechanical efficiency of the turbomachine.

The hodograph plane (fig. 7-3(b)) provides another important method of representing the flow. At each point along a streamline or equipotential lines (fig. 7-3(a)) the velocity has a definite magnitude and direction. When these velocity vectors associated with a given streamline or equipotential line are drawn from a common origin and their termini are connected (fig. 7-3(b)), the corresponding streamline or equipotential line is established in the hodograph plane. The streamlines and potential lines thus drawn also form a square network. This network may now be conceived to represent a flow in the usual sense. The streamlines that originally represented the blades are the boundaries for the new flow. The new flow itself is produced by a so-called vortex-source and a vortex-sink. The vortex source is located at the end of the velocity vector $c_1$ (the velocity at an infinite distance ahead of the lattice). The vortex-sink is at the end of the vector $c_2$ (the velocity at an infinite distance behind the lattice). The origin 0 and the termini of $c_1$ and $c_2$ form the velocity triangle of the lattice. From the equality of the flow rate ahead of and behind the lattice,

$$c_1 t \sin \beta_1 = c_2 t \sin \beta_2$$

it follows that the projections of the velocities $c_1$ and $c_2$ on the normal to the axis of the lattice are equal or that the straight line passing through the ends of the vectors $c_1$ and $c_2$ in the plane of the hodograph is parallel to the axis of the lattice. Considering the velocity hodograph of the lattice, we may arrive at the conclusion that, at points on the suction surface of the blade where the tangent to the blade surface is parallel to the upstream and downstream flow directions, the corresponding velocities should be greater than $c_1$ and $c_2$, respectively.

Of great interest is the distribution of the velocity or pressure on the surface of the blade. Figure 7-3(c) shows the approximate distribution of the relative velocities $\bar{c} = c/c_2$ and relative pressures $\bar{p} = (p - p_2)\Big/\frac{1}{2}\rho c_2^2 = 1 - \bar{c}^2$ as a function of the distance S along the profile. If the magnitude $c_1$ and the direction $\beta_1$ of the velocity at infinity ahead of the profile are known and also the position of the point of convergence of the flow $O_2$ (at the trailing edge), the flow through a given lattice is determined. In the case of an ideal incompressible fluid, a change in the magnitude of the velocity $c_1$ does not alter the shape of the streamlines or equipotential lines. Neither does it alter the relative velocity $\bar{c}$ or the relative pressure $\bar{p}$.

At finite distances from the lattice, the field of velocities and pressures is not uniform. The streamlines (for $\beta_1 \neq 90^\circ$) are wave shaped, and their shape is generally different from that at infinity; moreover, it periodically varies along the cascade axis. In correspondence with the conditions of continuity and in the absence of vorticity, the mean velocity along any line ab (fig. 7-3(a)) between two points separated by an integral number of periods t of the lattice is equal to the velocity at infinity. One of the streamlines approaching the leading edge of the profile actually branches at the leading edge. At the branching point $O_1$ (also called the entry point) the velocity becomes equal to zero and the pressure is at a maximum. Starting from the branch point, at which S = 0 (fig. 7-3(c)), the velocity along the profile sharply increases. Depending on the shape of the leading edge and also on the direction of the inlet velocity (inlet angle $\beta_1$), the velocity near the branch point may have one or two maxima. At the convex side of the profile the velocity is on the average greater, and the pressure less, than on its concave side. The general character of the velocity distribution over the profile may be evaluated by considering the width of the interblade passage and the curvature of the profile contour. In particular, a narrowing of the passage, characteristic of a turbine lattice of the reaction type, leads to an acceleration of the flow; in an impulse turbine having approximately constant passage width and curvature, the velocity and pressure change only slightly in the direction of flow (fig. 7-4); in a compressor lattice, the interblade passage widens and the velocity correspondingly decreases (fig. 7-4A).

An increase in the curvature of the convex parts of the blade leads to an increase in velocity, and vice versa. For a discontinuous change in curvature at the points of junction of arcs of circles, for example, the theoretical curves of the velocity and pressure distributions have an infinite slope. At projecting angles of the profile, the velocity theoretically increases to infinity, while at internal angles it drops to zero.

In view of the fact that these characteristics in the distribution of the velocity can not exist in an actual flow, the blade contours of modern lattices are designed with a smoothly changing curvature.

Near both the leading edge and a trailing edge of finite thickness,[1] the velocity may have one or two maxima; at the actual leading and trailing edges, the velocity must drop to zero. The actual trailing edge is the point of the tail where the curvature is greatest. At a large distance behind the lattice, the direction of flow is determined by the angle $\beta_2$.

Figure 7-5 shows the approximate effect of the inlet angle $\beta_1$, the pitch $t$, and the blade setting angle $\beta_y$ on the distribution of the relative velocity over a blade of the reaction-type turbine lattice. A change in the angle $\beta_1$ (fig. 7-5(a)) causes the branch point $O_1$ to be displaced along the profile. The design entry angle to the lattice may be considered as the angle for which the point $O_1$ coincides with the point of maximum curvature at the leading edge of the profile. In this case maximums of the velocity at the leading edge are either absent or are least sharply expressed. With a decrease in the entry angle, the branch point is shifted toward the concave part of the profile, and the velocity in the flow around the leading edge sharply increases. The vector to the exit velocity $c_2$ turns in the same direction as the vector of the inlet velocity; for example, on decreasing the angle $\beta_1$ from its design value, the exit angle $\beta_2$ increases. It should be remarked that the effect of inlet flow angle on outlet flow angle is very small in conventional turbine lattices. When the pitch $t$ is increased by a translational shift of the profile (fig. 7-5(b)) while keeping the inlet flow angle $\beta_1$ constant, the branch point $O_1$ is slightly displaced toward the concave part of the profile; correspondingly, the velocity distribution at the leading edge changes somewhat. On the convex side of the blade the velocity increases, while on the concave side it decreases. The exit angle $\beta_2$ increases. A change in the setting angle of the profiles (obtained by rotating them while maintaining the same pitch and inlet flow angle) changes the exit angle $\beta_2$. The change in $\beta_2$ is practically the same as the change in setting angle (fig. 7-5(c)). On rotating the profiles in the direction of decrease of the exit angle $\beta_2$, the corresponding velocities on the profile decrease; the branch point $O_1$ is displaced toward the concave part of the profile, in connection with which the velocity distribution at the leading edge changes in a way similar to that for a decrease of the inlet angle $\beta_1$.

---

[1]The case of an infinitely thin edge is not considered because it has no practical significance.

When the static pressure on a profile increases in the direction of flow (such as in diffuser elements) the flow of a real viscous fluid may separate from the blade. Experience shows that the static pressure is constant over parts of the profile behind the point of separation. The features of a flow with separation can be approximately taken into account in a so-called stream model of the flow of an ideal fluid. A zone of constant pressure is assumed to exist in this flow. At the boundary between this zone and the main flow, the velocity is constant, at the value which corresponds to the static pressure in the zones. In the plane of the hodograph, arcs of circles correspond to the boundaries of the separated zones. The radius of an arc is equal to the velocity at the boundary of the zone. Flow separation always occurs at the trailing edge of a blade. The separated flow region theoretically extends an infinite distance downstream of the lattice. For the same inlet and exit flow angles the velocity behind the lattice is greater with separation than it would be with no separation. At the boundaries of the separated flow region, discontinuous change in velocity would theoretically occur. In the actual flow of a viscous fluid, infinitely large forces would then be introduced which would prevent such a discontinuity from existing. In a real flow, therefore, the boundaries between the separated region and the main flow break up into individual vortices which are carried downstream by the flow. The presence of frictional forces also causes low pressure regions to exist in the separated region immediately behind the edges. Beyond this region the flow is rapidly equalized; this phenomenon leads to an increase in the pressure, decrease in the exit angle, and losses of kinetic energy similar to the losses in sudden expansion. The parameters of the equalizing flow are obtained by the simultaneous application of the equations of continuity, momentum, and energy (see sec. 7-7).



## 7-2. THEORETICAL METHODS OF INVESTIGATION OF PLANE POTENTIAL FLOW OF INCOMPRESSIBLE FLUID THROUGH A LATTICE

There are two problems in the theory of lattices that have the greatest significance. One of these, termed the direct problem, consists in determining the velocities of the potential flow field through a given lattice for a given velocity at infinity ahead of the lattice, and a given position of the rear stagnation point $O_2$ on the profile. Of greatest interest is the velocity at infinity behind the lattice. The determination of these quantities may be considered as the fundamental object of the solution of the direct problem. The inverse problem is that of theoretically constructing the lattice when the flow about it is either known or easily determined for a given velocity triangle. Of

practical importance is the problem of constructing such a lattice with a velocity distribution over the surface of a profile which is rational and which assumes small kinetic-energy losses in the actual flow.

It was remarked previously that for the flow of an incompressible fluid the shape of the streamlines, the shape of the equipotential lines, and the magnitude of the relative velocities do not depend on the absolute magnitude of the flow velocity. Moreover, for the same boundaries, the different potential flows of an incompressible fluid may be summed. For example, any flow of an ideal incompressible fluid through a lattice may be considered as the sum of two or several flows through the same lattice. In figure 7-6 the flow through the lattice is represented as the sum of two flows: a noncirculatory (irrotational) (fig. 7-6(b)) and a circulatory axial (fig. 7-6(c)). In the irrotational flow there is no circulation of velocity about the profile, or, in other words, the lattice does not change the direction of the flow; moreover, this direction is chosen such that the point of convergence of the flow is on the trailing edge. In a rotational-axial flow the direction of the velocity at infinity is parallel to the axis of the lattice; the magnitude of the circulation or the ratio $\Delta c_2/\Delta c_1 = m$ is chosen such that the velocity at the trailing edge is equal to zero. Any flow through a lattice (with the point of flow convergence on the trailing edge) may be obtained by summation of the irrotational and rotational-axial flows. In particular, the velocities at infinity ahead of and behind the lattice will be equal to the vector sum. The velocities on the surface of the profile itself will be equal to the algebraic sum of the corresponding velocities in the irrotational and rotational-axial flows. If it is taken into account that the magnitudes of the relative velocities do not depend on their absolute values in each of these flows, it is possible to find in a simple manner two important properties of the flow of an incompressible fluid through a lattice.

First, there exists a linear relation between the cotangents of the inlet and outlet flow angles of any given lattice. From the velocity triangle (fig. 7-6(a)), notice that

$$\frac{\cot \beta_0 - \cot \beta_2}{\cot \beta_0 - \cot \beta_1} = \frac{\Delta c_2}{\Delta c_1} = m = \text{constant} \qquad (7\text{-}2)$$

where $\cot \beta_1$ corresponds to the angle $\beta_1$ assumed in figure 7-6(a). For a given lattice, the magnitude of the coefficient $m$ can be computed theoretically. For a lattice of flat plates in particular, the coefficient $m$ is related to the relative pitch $t/b$ and the setting angle $\beta_0$ by the equation

$$\frac{\pi b}{t} = 2 \cos \beta_0 \arctan \frac{1 - m}{1 + m} \cot \beta_0 + \sin \beta_0 \ln \frac{1}{m} \qquad (7\text{-}3)$$

As may be seen from the graph of figure 7-7, the coefficient m decreases with a decrease in pitch, so that the exit angle $\beta_2$ approaches the setting angle $\beta_0$ of the flat plates.

To any lattice of airfoils there corresponds a unique equivalent flat plate lattice which has a coefficient m of the same magnitude, and the same direction of the irrotational flow. The equivalent flat-plate lattice for any inlet angle $\beta_1$ has the same exit angle $\beta_2$ as the given lattice of airfoils. In present-day turbine lattices the ratio $b/t$[2] of an equivalent plate lattice is not less than 1.3; the angle $\beta_0$ is between 15° and 40°, and the angle $\beta_1$ is between 90° and 20°. The magnitude of the coefficient m is not greater than 0.015; the angle of the velocity behind the lattice therefore differs from the angle $\beta_0$ for the equivalent flat plates by no more than 1°. For present-day compressor lattices this deviation may be as high as 3°.



Second, the magnitude of the relative velocity on the profile of any lattice depends linearly on the cotangent of the exit angle. In fact[3]

$$\bar{c} = \frac{c}{c_2} = \frac{c_{bu}}{c_2} + \frac{c_u}{c_2} = \frac{c_{bu}}{c_0} \cdot \frac{c_0}{c_2} + \frac{c_u}{\Delta c_1} \cdot \frac{\Delta c_1}{c_2}$$

Utilizing the obvious correlations (fig. 7-6(a)), $\bar{c}_{bu} = \frac{c_{bu}}{c_0}$ and $\bar{c}_u = \frac{c_u}{\Delta c_1}$ we obtain

$$\bar{c} = \bar{c}_{bu} \frac{\sin \beta_2}{\sin \beta_0} + \bar{c}_u(\cot \beta_0 - \cot \beta_1)\sin \beta_2 \qquad (7\text{-}4)$$

As was said, in present-day turbine lattices, $\beta_2 \approx \beta_0 = \text{constant}$, the direction of the velocity behind the lattice differs little from the direction of the irrotational flow for a wide range of inlet angles. Hence,

$$\bar{c} \approx \bar{c}_{bu} + \bar{c}_u(\cot \beta_2 - \cot \beta_1)\sin \beta_2 \qquad (7\text{-}4a)$$

---

[2]NACA note: This ratio is written as $t/b$ in original text.

[3]NACA note: $c_{bu}$ is the irrotational flow, fig. 7-6(b), and $c_u$ is the circulatory flow, fig. 7-6(c).

$$\left[\frac{c_0}{c_2} = \frac{\sin \beta_2}{\sin \beta_0}\right] \text{ and } \left[\frac{\Delta c_1}{c_2} = \frac{(\cot \beta_0 - \cot \beta_1)}{\csc \beta_2}\right]$$

At any point of the profile where $c_u = 0$ (fig. 7-6(c)) the relative velocity $\overline{c}$ does not depend on the inlet angle. If the distribution of the relative velocities $\overline{c}$ is known for two values of the inlet angle $\beta_1$, then the distribution $\overline{c}$ can be computed for angle $\beta_1$ with the aid of equation (7-4a).

Of practical significance in the theory of the two-dimensional motions of an incompressible fluid is the mathematical theory of the functions of a complex variable. Without entering the mathematical side of this problem, the discussion of which is given in any modern course of hydrodynamics, we shall nevertheless make use of the important concept of conformal transformation or mapping.

Conformal transformation may be defined as the continuous geometrical transformation (extension and compression or conversely) of a part of the plane (region) in which at each point of the region the extension or compression occurs uniformly in all directions about this point. In such a transformation the magnitudes of the angle between the tangents to any two curves passing through each point of the region are preserved as is also the shape of infinitely small figures, as is indicated by the term conformal transformation. Exceptions may be represented only by individual (singular) points of the region.

Every orthogonal square network in any conformal transformation may go over into a second orthogonal square network. This property explains the significance of conformal transformation in the investigation of the flow of an ideal incompressible fluid. Any conformal mapping of a region of flow translates an orthogonal square network of curves $\Phi$ = constant and $\Psi$ = constant of this flow into a new orthogonal square network, which may be taken as a network of a second flow in the conformally transformed region with equal values of the velocity potential and stream function at the corresponding points. The velocities of flow change inversely proportional to the extension at each point of the region.

In this way, the problem of determining the flow of an ideal fluid reduces to the mathematical problem of conformally transforming the given region into a simpler one in which the flow of an ideal fluid is initially known or else can be easily computed. After finding the conformal transformation of the points of the required region, the velocity is computed by differentiation ($c = d\Phi/dS$). Several examples of the conformal transformation of lattices are shown in figure 7-8.

The above defined equivalent lattice of plates is obtained by means of such a conformal transformation in which the flow region outside the airfoil lattice is transformed into the flow region outside the plate lattice. The infinity of the plane of the lattice of airfoils goes over without extension or rotation into the infinity of the plane of the plate

lattice. The pitch of the lattice is maintained, and the rear stagnation point of the flow at the outlet edge of the airfoil goes over into the given edge of the plates. It should be remarked that the conformal transformation is completely determined by the above condition. The noncirculatory flow through the airfoil lattice (fig. 7-8(a)) corresponds to the noncirculatory flow through the lattice of plates (fig. 7-8(b)). The singular points, at which the conformality of the transformation does not hold, are the edges of the equivalent plates. Considering the corresponding noncirculatory flows about the equivalent lattices of plates and airfoils, we note that the length of the equivalent plates, for equal pitch of the lattices, should be greater than the half perimeter of the profile. This property permits the parameters of the equivalent plate lattice to be approximately evaluated.



A clear picture of conformal transformation may be obtained in the following manner: The flow region of the lattice is assumed to be a plane in which an ideally elastic film is stretched without friction over the contours of the profiles and on which is drawn the network of lines $\Phi$ = constant and $\Psi$ = constant of any flow through the lattice. This film may then be stretched over the contours of any lattice which can be a conformal transformation of the given one. In the transition all the points of the film are displaced in a definite manner, both along the contours and in the flow region. The correspondence of points in a conformal transformation is thus achieved. The network of lines $\Phi$ = constant and $\Psi$ = constant of the flow through one lattice goes over into the network of the same lines of the equivalent flow of the other lattice.

Of great significance is the conformal transformation of a lattice of airfoil profiles into a lattice of circles (fig. 7-8(c)). In contrast to the equivalent network of plates, characterized by two parameters ($t/b$ and $\beta_0$), the equivalent network of circles is determined by only one parameter, the relative diameter (density of the lattice) $2r/t = 2\overline{r}$. As a result, lattices of profiles corresponding to different equivalent lattices of plates can have one and the same equivalent lattice of circles. The point $O_2$ in the circle lattice is not uniquely determined by the relative diameter, however.

An example of the conformal transformation of the region of flow in one period of a profile lattice into a bounded region is shown in figure 7-8(d). Infinity ahead of the lattice corresponds to the center of the circle ($\infty_1$); the infinity behind the lattice corresponds to a certain point on the horizontal radius ($\infty_2$); the flow lines in a period to a segment between the points $\infty_1$ and $\infty_2$. As in the case of the equivalent lattice of circles, the region of transformation is characterized by only a single parameter, the ratio of the distance between the points

$\infty_1$ and $\infty_2$ to the radius of the circle. For modern turbine lattices this ratio is generally greater than 0.99. The points corresponding to the uniformly arranged points of the profile contour are very irregularly arranged over the circumference of the circle; the greater part of the circle corresponds to practically only the leading edge of the profile, while the remaining part of the profile contour becomes a small arc near the point $\infty_2$. In a conformal transformation of the type considered (in which an infinite distance from the origin in one flow field is only a finite distance from the origin in the other) the displacement of a pitch ahead of or behind the lattice corresponds, respectively, to a passage around the point $\infty_1$ or $\infty_2$. The flow about the lattice is transformed into a flow of a special form produced by a vortex source at the point $\infty_1$ and a vortex sink at the point $\infty_2$. In the regions of the conformal transformation considered, the lattices are relatively simply determined by the potential flow of an incompressible fluid.

The problem of the flow about a lattice of plates was first solved by S. A. Chaplygin (in 1912) and then by the more simple method of N. E. Joukowsky. Their work laid the foundation for the theoretical investigations of the flow about hydrodynamic lattices. Approximate methods of determining the flows about lattices of circles were worked out by N. E. Kochin and E. L. Blokh. An exact solution was given by G. S. Samoilovich. B. L. Ginzburg constructed tables of values of the velocity potential and the velocities on a circle as functions of the central angle $\theta$ for transverse, longitudinal, and purely circulatory flows about lattices of circles with values of the spacing $2\overline{r} = 0.20 - 0.90$ (for circles in contact $2\overline{r} = 1.0$). By summing the flows considered, any flow through a circle lattice can be obtained (fig. 7-9). The values of the velocity potentials and the magnitudes of the velocities on a circle are obtained by summation from tabulated values multiplied by certain constants, the magnitudes of which are found from the given direction of the velocity at infinity ahead of the lattice and the condition of zero velocity at the branch points of the flow given on the circle. By making use of the solution for the lattices of circles, the solution of the direct problem, that is, the determination of the velocity on the surface of the blade in the given lattice for given inlet angle, reduces to the problem of obtaining an equivalent lattice of circles and then obtaining a conformal correspondence of the points of the blade contour in the lattice with the points of the circle in the equivalent circle lattice. The analogous problem of the mapping of the outside region of a single blade on a circle has been well studied and at the present time presents no essential difficulties. For a lattice of blades the problem is more complicated. An approximate solution of this problem has been given by N. E. Kochin starting from the known conformal correspondence of a single profile and a circle. The method of Kochin, however, is suitable in practice only for lattices of small spacing.

The exact solution obtained by G. S. Samoilovich may broadly be described as follows. First, by one of the known methods, a conformal transformation is obtained which maps the exterior of a single circle into the exterior of a single profile (fig. 7-10(a)). Then, from the condition of conformal correspondence of the exterior of the lattice of profiles and the exterior of the lattice of circles, the spacing of the equivalent lattice of circles $2\overline{r}$ (fig. 7-10(b)) is obtained. The spacing $2\overline{r}$ depends on the pitch of the profile lattice and the angle at which they are set. In the example considered, $2\overline{r} = 0.85$. When the blades are more closely spaced by decreasing the pitch or rotating them, the spacing density of the equivalent lattice of circles increases. The flow is then related to the flow about a unit circle. For determining the velocity distribution on a profile there is computed the displacement function $\Delta\theta$ equal to the difference in the central angles of points on a unit circle and on a circle in the equivalent circle lattice corresponding to the same point of the profile. The displacement function $\Delta\theta$ determines the correspondence of points of the profile in the profile and circle lattices. By making use of previously computed values of the velocity potential or the velocity on the circle, the velocity distribution on a profile of the lattice is determined for any given inlet angle $\beta_1$.

In figure 7-11 a comparison is shown of the experimental and theoretical distribution of the nondimensional pressure $\overline{p}$ over the profile of a lattice for the example considered with $\beta_1 = 90^\circ$. The experimental values $\overline{p}$ were obtained by measuring the pressure in the middle section of the experimental blades at small air velocities. The scatter of the test points for different $M_2$ numbers is found to be within the limits of accuracy of the measurements. There should be noted the characteristic divergence between the experimental and theoretical values of $\overline{p}$ on the back of the blade, produced by separation of the flow.

The velocity at each point of the blade in a lattice differs from the velocity at the same point of an isolated blade (for equal magnitude and direction of the velocity of the approaching flow and the same rear stagnation point $O_2$); first, because of the difference in the distribution of the velocity potential on a circle in a lattice of circles and an isolated circle; and second, because of the displacement of the corresponding point on a circle in the circle lattice.

The use of the method of conformal transformation permits determining the velocity distribution on a profile of a lattice for any inlet angle $\beta_1$ whenever one flow about it is known. Suppose, for example, there is known the distribution of the velocity potential $\Phi$ on a profile of the lattice with pitch $t = 1$ for irrotational flow with inlet angle $\beta_1 = 90^\circ$ and velocity at infinity $c_1 = c_2 = 1$ (fig. 7-12(a)).

This is sufficient for obtaining the equivalent lattice of circles and the correspondence of the points of the profile in the lattice with the circle in the circle lattice. Using the tables of distribution of the velocity potential on a circle for the corresponding flow about the lattice of circles makes it possible to construct the difference in potential $\Delta\Phi_{12}$ at the forward and rear stagnation points as a function of the lattice spacing with $t = 1$ and $c_1 = c_2 = 1$ (fig. 7-12(b)). The value of $\Delta\Phi_{12}$ in the circle lattice coincides with the same potential difference in the profile lattice for the single value of the spacing $2r/t$ characterizing the equivalent lattice of circles (fig. 7-12(c)). The conformal correspondence of the points of the profile and the circle is found by equating the known velocity potentials $\Phi$ on the profile in the lattice with those on a circle in the equivalent circle lattice (fig. 7-13). For determining the velocity distribution on the profile for any inlet angle $\beta_1$, it is necessary to determine, by employing tables of flow about circle lattices, the distribution of the velocity potential $\Phi$ or velocity $c_k$ on a circle in the circle lattice. The proper inlet flow angle $\beta_1$ must be used, and the rear stagnation point of the circle must correspond to the trailing edge of the profile (fig. 7-12). From the known correspondence of the points of the profile and circle in the lattices it is possible to construct the velocity potential as a function of the length of arc of the profile, the differentiation of which will give the required velocity distribution over the profile of the lattice ($c = d\Phi/dS$). With the described method of determining the velocity, the number of operations of differentiation is equal to the number of inlet angles for which the velocity distribution is determined. Repeated differentiation may be avoided if use is made of the formula

$$c = \frac{d\Phi}{dS} = \frac{d\Phi}{d\theta} \cdot \frac{d\theta}{dS} = c_k \frac{d\theta}{dS}$$

The velocity $c_k$ on a circle of the lattice of circles is determined for any inlet angle with the aid of tables, and the derivative $d\theta/dS$ is obtained only once from the graph shown in figure 7-13.

If the distribution of the velocity $c$ on a profile of the lattice is known, then to determine the conformal correspondence it is necessary first to find the velocity potential

$$\Phi = \int_0^S c\,dS$$

where it is assumed that $S = 0$ (or $\Phi = 0$) at the branch point.

Practically, for lattices with the spacings that are actually employed in turbines, the above problem is solved considerably simplified

by the method of conformal mapping of the lattice, not on a lattice of circles but on the interior of a circle (fig. 7-8(d)). In this case, it may be approximately assumed that the sink ($\infty_2$) is situated on the circle, and the velocity at each point of the profile computed for any inlet angle $\beta_1$ by the formula

$$c' = \frac{\sin\left(\frac{\theta}{2} - \beta_1'\right)}{\sin\left(\frac{\theta}{2} - \beta_1\right)} \frac{c_1'}{c_1} c$$

in which the angle in the circle $\theta$ is determined graphically from the equation

$$\Phi = \frac{1}{\pi} c_1 t \sin \beta_1 \left(\frac{\theta}{2} \cot \beta_1 - \ln \sin \frac{\theta}{2}\right)$$

The primes denote the magnitudes determined for a new inlet angle ($\beta_1$). At the branching point the velocity potential $\Phi' = 0$ and $\theta = 2\beta_1'$.

The converse problem of the theory of hydrodynamic lattices, as already stated, consists in the theoretical construction of lattices satisfying definite conditions. In the construction of theoretical lattices, there is generally given the velocity potential of the flow, and there is then obtained the shape of the profile that corresponds to it. The methods of theoretical lattices (like the methods of theoretical profiles in airfoil theory) permitted determining, in a sufficiently simple manner, the effect of the individual geometrical parameters of airfoil lattices of certain special shapes on their hydrodynamic characteristics. A classical example is the previously mentioned dependence between the inlet and outlet angles for a lattice of plates. Moreover, the methods of theoretical lattices up to the present time make use of certain approximate devices for solving the direct problem.

After sufficiently effective general methods of solution of the direct problem have been worked out, artificial devices for constructing theoretical lattices have to a considerable degree lost their practical significance. Of some practical interest, however, are those methods of constructing theoretical lattices that assure obtaining hydrodynamically a suitable velocity distribution on the profile and correspondingly small losses of the actual viscous flow of a compressible fluid about the constructed lattice.

The losses of kinetic energy in the flow of a real fluid (as compared with an ideal fluid) about a lattice may be determined with the aid of the boundary-layer theory, if the theoretical distribution of the velocity on the profile is known.

With account taken of what has been said, of all possible velocity distributions, the most suitable hydrodynamically may be considered that for which the losses in friction are a minimum and the condition of continuous flow is satisfied over the entire profile. (See section 7-6.)

Any continuous velocity distribution having a minimum number of diffuser parts and a minimum velocity on the concave side of the profile may be considered as practically suitable.

One of the simplest methods of constructing theoretical lattices that permits satisfying a number of conditions with regard to the velocity distribution is the method of the hodograph. This method was first applied to problems of the flow about lattices by N. E. Joukowsky, who in 1890 considered a case of the flow about a lattice of plates with the stream uniting at their edges. The possibility of applying the hodograph method for constructing lattices with hydrodynamically suitable velocity distribution was pointed out by Weinig. A practical application of the hodograph method was obtained by L. A. Simonov, who employed it for constructing theoretical profiles and lattices.

The construction of lattices by the method of the hodograph is based on the fact that the region of flow through a lattice of an ideal incompressible fluid is conformally transformed into another region in its velocity hodograph (see fig. 7-3). As has already been said, to the flow about a lattice in the region of the hodograph there corresponds a special flow of an ideal incompressible fluid produced by a vortex source at the end of the vector $c_1$ and a vortex sink at the end of the vector $c_2$ (see fig. 7-3). Taking into account that to a displacement by a pitch ahead of or behind the lattice there corresponds a passage around the vortex source or sink, we can determine the flow rate of the source or sink,

$$Q_1 = c_1 t \sin \beta_1 = - Q_2 = c_2 t \sin \beta_2$$

the circulation of the vortex source,

$$\Gamma_1 = c_1 t \cos \beta_1$$

and the circulation of the vortex sink

$$\Gamma_2 = - c_2 t \cos \beta_2$$

At the branching point $O_1$ and the rear stagnation point $O_2$, the velocity is equal to zero. Hence, the corresponding points of the flow in the region of the hodograph coincide with the point $c = 0$. For constructing the lattice, there are given the vectors $c_1 = c_2$ and the contour of the hodograph enveloping these vectors.

Let us consider in greater detail the procedure of constructing the stream flow through a lattice (fig. 7-14). It should be remarked that the direct problem of determining the flow through a given lattice (with no rear stagnation points in the stream) has no effective solution, and the method of the hodograph is practically the only one which permits constructing such flows.

The contour of the hodograph of the flow through a lattice with convergence point of the stream at the trailing edge (fig. 7-14(a)) passes through the point $c = 0$ and through the end of the vector $c_2$. The arc $S_1S_2$ corresponds to the boundaries of the flows between one infinity and the other in the plane of the lattice. In the case considered of a turbine lattice for a given hodograph, the absence of diffuser parts on the profile may be assured (fig. 7-14(d)).



To construct the lattice, it is necessary to find the flow of an ideal incompressible fluid in the plane of the hodograph, because of a vortex source at the end of the vector $c_1$ with circulation

$$\Gamma = c_1 t \cos \beta_1$$

and a sink at the end of the vector $c_2$. The flow rate from the source and sink is

$$Q = c_1 t \sin \beta_1$$

The magnitudes of the velocity and the nondimensional magnitude $\tau$ (see fig. 7-14(b)) are connected by the equation of continuity (see sec. 7-7)

$$c_1 t \sin \beta_1 = (1 - \tau) c_2 t \sin \beta_2, \text{ where } \tau = \frac{\Delta t}{t}$$

For constructing the profile, it is sufficient to find only the distribution of the velocity potential $\Phi$ over the contour of the hodograph by the method, for example, of conformal transformation of the hodograph into the interior of a circle (fig. 7-14(b)) for which the vortex source goes over into the center of the circle and the sink into the point of the circle $\theta = 0$. The conformal transformation of a given hodograph may be determined by some method of numerical mapping or with the aid of an electrical analog.

The velocity potential of the flow on a circle is, in the case considered, expressed by the simple formula

$$\Phi = \frac{1}{\pi}\left(\Gamma \frac{\theta}{2} - Q \ln \sin \frac{\theta}{2}\right)$$

At the branch point 0 of the flow, $d\Phi/d\theta = 0$ or $\cot \theta_0/2 = \Gamma/Q$, whence

$$\theta_0 = 2\beta_1$$

The coincidence of the branch point 0 in the hodograph plane with the point $c = 0$ is equivalent to the conformal correspondence of the point $c = 0$ and the point $\theta = \theta_0$. With the contour of the hodograph arbitrarily given, the branch point in the hodograph plane will not, in general, coincide with the point $c = 0$. The coincidence of these points is assured, however, by a suitable specification of the shape of the hodograph. In the example of figure 7-14, this coincidence was obtained by choosing the length of the segment P of the hodograph plane (fig. 7-14(a)).

After determining the velocity potential on the hodograph contour, the profile is constructed by graphical integration of the expression

$$dS = d\Phi/c$$

The accuracy of the computations and of the construction is checked by comparing the given and obtained boundary conditions $\sigma$. The neighboring profile of the lattice is at the pitch distance t (fig. 7-14(c)).

The velocity distribution over the profiles of the constructed lattice for given inlet angle corresponds to the given hodograph. The velocity distribution for any other inlet angle can be found simply. For this it is necessary to make use of the known conformal transformation of the region of the hodograph on the interior of a circle. Since the hodograph is, in turn, a conformal transformation of the flow region about the constructed lattice, the conformal correspondence of its exterior and interior on the circle is known. The change in the velocity potential $\Phi$, accompanying a change in the direction or magnitude of the velocity, is obtained in the circle as the change in the velocity potential of the flow due to a vortex source and sink with the changed strengths

$$\Gamma' = c_1' t \cos \beta_1', \quad Q' = c_1' t \sin \beta_1'$$

With the aid of evident substitutions and transformations we obtain

$$c' = \frac{d\Phi'}{dS} = \frac{d\Phi'}{d\Phi} c = \frac{d\Phi'}{d\theta} \cdot \frac{d\theta}{d\Phi} c = \frac{\Gamma' - Q' \cot \frac{\theta}{2}}{\Gamma - Q \cot \frac{\theta}{2}} c$$

$$= \frac{\cot \beta_1' - \cot \frac{\theta}{2}}{\cot \beta_1 - \cot \frac{\theta}{2}} \cdot \frac{c_1' \sin \beta_1'}{c_1 \sin \beta_1} c = \frac{\sin\left(\frac{\theta}{2} - \beta_1'\right) c_1'}{\sin\left(\frac{\theta}{2} - \beta_1\right) c_1} c \qquad (*)$$

where the primes denote the changed quantities.

We emphasize that formula (*), with change in inlet angle $\beta_1$, determines the magnitude of the velocity on the boundaries of the constructed flow with "solidified" streams passing off to infinity. Although the exit angle $\beta_2$ evidently does not change and the velocities at the boundaries of the stream zones are no longer relatively constant, the previously mentioned change in the exit angle in lattices of variable spacing and the change of velocity near the trailing edge are negligibly small. With account taken of these remarks, formula (*) permits computing with sufficient accuracy the velocity distribution on the profile of any lattice with change in the inlet angle if the velocity distribution for any one inlet angle is known. The exact solution of this problem (by obtaining the equivalent lattice of circles) has been described. The application of formula (*), in view of the evident advantage of simplicity of the computations, is justified in practically all cases where it is possible to neglect the effect of the inlet angle $\beta_1$ on the exit angle $\beta_2$. For computing the velocity distribution for several inlet angles $\beta_1'$, formula (*) can be applied only once, and then the linear dependence of the relative velocity $c/c_2$ on $\cot \beta_1$ must be employed.



## 7-3. ELECTRO-HYDRODYNAMIC ANALOGY

The distribution of the velocity potential in a lattice of airfoils for any irrotational flow about it may be experimentally obtained by the method of electro-hydrodynamic analogy (abbreviated EHDA). This method was first applied to problems of the theory of hydrodynamic lattices by L. A. Simonov. Until a general method of solution of the direct problem has been worked out, the method of EHDA is practically the only one which permits determining the flow about any arbitrary lattice with sufficient accuracy.

The EHDA method is based on the formal analogy between the differential equations which are satisfied by the velocity potential for the flow of an ideal incompressible fluid and by the electric potential for the flow of an electric current through a homogeneous conductor or semiconductor. By making use of this analogy, the theoretical computation of the velocity potential is replaced by the direct measurement of an electric potential.

The simplest and most widespread method of applying the EHDA is the following: A flow of an electrical current, analogous to the flow of an ideal incompressible fluid, is produced in a layer of water of constant thickness (10 to 25mm). The water is poured into a flat vessel (generally of rectangular shape) of nonconductive material. The electric current passes between the electrodes 1 arranged at opposite edges of the vessel (fig. 7-15). A small quantity of salt and carbonic acid which is

contained in the water assures sufficient conductivity. For avoiding the polarization of the electrodes in the electrolysis of the water, a low-frequency, variable current (generally using a circuit voltage of 110 or 220 volts alternating current) is connected to the electrodes. The blades of the lattice are made of an insulator material, such as paraffin or plastiline. Several blades of the lattice are studied; for all practical purposes, it is sufficient to study five blades. The measurement of the electric potentials in the bath is generally made by the compensation method. To the parallel current-conducting electrodes, a voltage divider (potentiometer) is connected, the movable contact of which is connected, through a zero current indicator (null indicator), to a feeler or probe situated at the point of measurement of the potential. The probe is a thin straight needle moving along the water perpendicular to its surface. The simplest and sufficiently accurate zero indicators of an alternating current are radio earphones or a speaker connected through a low-frequency amplifier. For the potentiometer, there is shown in figure 7-15 a water rheostat consisting of a long vessel filled with water. Under the conditions of exact design and horizontal position of the vessel, the electrical potentials are distributed proportionately to its length and can be measured in fractions of the applied voltage. To measure the potential, the moving contact is slid along the potentiometer and the reading of its scale taken at the instant the force of the sound in the earphones attains a minimum. The advantage of the described compensation method of measurement is the absence of the effect of the apparatus on the absolute value of the potential at the point of measurement.

Instead of an electrolytic bath, it is possible to use electroconductive paper. The blade shapes are then cut from the paper. In this case a direct-current source and highly sensitive galvanometers can be used.

The electro-hydrodynamic analogy may be conveniently applied to the direct problem in theory of hydrodynamic lattices. It may be used to establish the conformal transformation of a given lattice to the equivalent lattice of circles. According to the above described method (fig. 7-12), it is sufficient for this purpose to know the distribution of the velocity potential on a profile of the lattice for any convenient flow about it, as for example, an irrotational flow with $\beta_1 = \beta_2 = 90^\circ$, $c_1 = c_2 = 1$, and $t = 1$. The magnitude of the measured electric potentials (fig. 7-15) must then be divided by the potential drop (measured in the same units) over the distance of one pitch. This measurement must be made at a remote distance from the lattice and certainly not nearer to it than $2t$.

In obtaining the conformal transformation of a lattice of airfoil profiles into its equivalent lattice of circles with the aid of the EHDA,

the direct measurement of the potential distribution of the flow is conducted for the case of the flow with no circulation about the blades. With certain assumptions, the EHDA method can also be applied for directly measuring the velocity potential and even the velocity itself in any flow of an ideal fluid, including flow with stagnation point at trailing edge. The modeling scheme is indicated in figure 7-16. The exact form of the bounding walls (streamlines intersecting branch points) may in principle be obtained by the method of successive approximations; practically, however, with this method there may simultaneously be given with sufficient accuracy the magnitude of the inlet angle and the shape of the bounding streamlines. For measuring the magnitude of the velocity at any point of the flow, a probe 1 is used with two parallel needles placed in a holder at a small distance from each other. One then measures the difference in potential between the needles in the direction of the straight line passing through them. In measuring the velocity on the profile, both needles are set on the boundary of the model in the direction of flow. For measurements in the flow, the probe is rotated.

In concluding, we may remark that the EHDA method is employed also for investigating the flow of an ideal gas with subsonic velocities. For this purpose an electrolytic layer of variable thickness or a network model is applied. The electrical model in the plane of the velocity hodograph permits obtaining accurate solutions without successive approximations.

## 7-4. FORCES ACTING ON AN AIRFOIL IN A LATTICE; THEOREM OF JOUKOWSKY FOR LATTICES

For determining the forces acting on an airfoil, we isolate a portion of the flow, as shown in figures 7-17(a) and (b). The external boundaries of the isolated region are defined by the segments ab and dc, parallel to the axis of the lattice and of length equal to the pitch $t$. The lines ab and dc, strictly speaking, should be at an infinite distance from the lattice because the flow parameters along these lines are assumed to be constant. The inner boundary of the region is formed by the contour of the profile.

Since the streamlines ad and bc are equidistant throughout their length, the resultant of the forces acting on the surfaces defined by these lines are equal and opposite. The projections of the force with which the flow acts on the profile are denoted by $P_u$ and $P_a$. The magnitude of these forces may be determined from the momentum equation. In the direction normal to the axis of the lattice, the change in the momentum is equal to

$$m(c_{a1} - c_{a2}) = t(p_2 - p_1) - P_a$$

where $P_a$ is the component of the force P in the direction normal to the axis of the lattice; the mass rate of flow of the gas per second is determined from the formula

$$m = \rho_1 c_{a1} t = \rho_2 c_{a2} t$$

Then

$$P_a = t[(\rho_2 c_{a2}^2 - \rho_1 c_{a1}^2) + p_2 - p_1] \tag{7-5}$$

The projection of the force P on the axis of the lattice may be expressed by the equation

$$P_u = t\rho_1 c_{a1}(c_{u1} - c_{u2}) \tag{7-6}$$

The forces $P_u$ and $P_a$ refer to a profile having a unit span.

Equations (7-5) and (7-6) may be represented in another form by expressing the forces $P_u$ and $P_a$ in terms of the circulation $\Gamma$ and the flow parameters at the inlet and outlet of the flow.

According to the equation of continuity,

$$\rho_1 c_{a1} = \rho_2 c_{a2} = \rho c_a$$

where $\rho$ is the mean density of the gas.

The velocity $c_a$ is chosen such that

$$c_a = \frac{c_{a1} + c_{a2}}{2}$$

It is easily shown that we then have

$$\rho = \frac{2\rho_1 \rho_2}{\rho_1 + \rho_2} \tag{7-7}$$

The circulation about the profile is equal to

$$\Gamma = t(c_{u1} - c_{u2}) \tag{7-8}$$

since the line integral along the equidistant lines ad and bc are equal and opposite.

After simple transformations, we obtain from equations (7-5) and (7-6)

$$P_a = t[p_2 - p_1 - \rho c_a(c_{a1} - c_{a2})] \tag{7-9}$$

$$P_u = \rho\Gamma c_a \tag{7-10}$$

We make use of the equation of energy

$$\frac{c_1^2}{2} + \frac{k}{k-1}\frac{p_1}{\rho_1} = \frac{c_2^2}{2} + \frac{k}{k-1}\frac{p_2}{\rho_2}$$

Since

$$c_1^2 = c_{a1}^2 + c_{u1}^2$$

$$c_2^2 = c_{a2}^2 + c_{u2}^2$$

$$\frac{c_1^2 - c_2^2}{2} = c_a(c_{a1} - c_{a2}) + c_u(c_{u1} - c_{u2}) \tag{7-11}$$

where

$$c_u = \frac{c_{u1} + c_{u2}}{2}$$

and we obtain from the equation of energy

$$c_a(c_{a1} - c_{a2}) = \frac{k}{k-1}\left(\frac{p_2}{\rho_2} - \frac{p_1}{\rho_1}\right) - c_u(c_{u1} - c_{u2})$$

Substituting this expression in equation (7-9) and taking into account formula (7-8) we obtain

$$P_a = t\left[p_2 - p_1 - \frac{k}{k-1}\rho\left(\frac{p_2}{\rho_2} - \frac{p_1}{\rho_1}\right)\right] + \rho\Gamma c_u \tag{7-12}$$

$$Pu = \rho\Gamma c_a \tag{7-13}$$

The force $P_a$ given by expression (7-12) is conveniently represented in the form of a sum of two forces

$$P_a = P_{a1} + \Delta P_a$$

where

$$P_{al} = \rho \Gamma c_u$$

and

$$\Delta P_a = t\left[p_2 - p_1 - \frac{k}{k-1}\rho\left(\frac{p_2}{\rho_2} - \frac{p_1}{\rho_1}\right)\right] \tag{7-14}$$

The resultant of the forces $P_{al}$ and $P_u$ we will denote by $P_y$ and the over-all resultant force by $P$ (see fig. 7-17).

It is evident that

$$\vec{P}_y = \vec{P}_u + \vec{P}_{al}$$

$$\vec{P} = \vec{P}_u + \vec{P}_a$$

or

$$\vec{P} = \vec{P}_y + \Delta\vec{P}_a$$

The force $P_y$ is determined by the formula

$$P_y = \sqrt{P_u^2 + P_{al}^2}$$

Substituting the values $P_u$ and $P_{al}$ we obtain

$$P_y = \rho \Gamma \sqrt{c_u^2 + c_a^2}$$

But

$$c_u^2 + c_a^2 = c^2$$

where $c$ is the mean vector velocity

$$\vec{c} = \frac{\vec{c}_1 + \vec{c}_2}{2}$$

Hence, the expression for $P_y$ in the flow about a lattice has the same form as the lift force of an isolated airfoil:

$$P_y = \rho \Gamma c \tag{7-15}$$

The direction of the force $P_y$ is perpendicular to the direction of the mean vector velocity $c$. This follows from the obvious equation

$$\tan \beta = \frac{c_a}{c_u} = \frac{P_u}{P_{al}}$$

Thus, the Joukowsky force acting on an airfoil in a lattice is equal to the product of the mean density of the gas and the velocity circulation about the airfoil and the mean vector velocity. The direction of the force $P_y$ is determined by the rotation of the velocity vector $c$ by $90^\circ$ in the direction opposite to that of the circulation.



We recall that the mean density $\rho$ corresponds to the mean specific volume; that is,

$$\frac{1}{\rho} = \frac{1}{2}\left(\frac{1}{\rho_1} + \frac{1}{\rho_2}\right)$$

Thus we have established that, in contrast to the isolated profile, the resultant force acting on the profile in a lattice is equal to the sum of the Joukowsky force ($P_y$) and the additional force ($\Delta P_a$) perpendicular to the axis of the lattice:

$$\vec{P} = \vec{P}_y + \Delta\vec{P}_a$$

It is important to note that the characters of the forces $P_y$ and $\Delta P_a$ are different. Whereas the force $P_y$ depends on the circulation of the flow and becomes zero for $\Gamma = 0$, the force $\Delta P_a$ does not depend directly on the circulation.[4]

The force acting on the profile was determined for the general motion of a gas. With the aid of the obtained relations it is not difficult to investigate the magnitude of the aerodynamic force for certain special cases. Thus, for example, in passing from the lattice to the isolated profile it is necessary to increase the pitch of the lattice to an infinitely large value. At an infinite distance from the profile the equations $p_2 = p_1$ and $\rho_2 = \rho_1$ must be valid; hence, $\Delta P_a = 0$ and $P_u = 0$. In the case of isentropic flow about the isolated profile, the the resultant force acting on the profile is therefore equal to the Joukowsky force

$$P = P_y = \rho\Gamma c$$

---

[4]NACA note: This result is at least partially dependent on the selection of the mean velocity and mean density.

where $\rho$ and $c$ are the density and velocity of the flow, respectively. The direction of the force is perpendicular to the direction of the velocity of the approaching flow.

Passing to the case of the flow of an incompressible fluid about a lattice, it must be observed first of all that in equation (7-14) the second term on the right side is proportional to the change of the potential energy of the flow (with account taken of the hydraulic losses); that is,

$$\frac{k}{k-1}\left(\frac{p_2}{\rho_2} - \frac{p_1}{\rho_1}\right) = \frac{c_1^2 - c_2^2}{2}$$

In this case of an incompressible fluid, $\rho_1 = \rho_2 = \rho$, and the energy equation gives

$$\frac{c_1^2 - c_2^2}{2} = \frac{p_{2t} - p_1}{\rho}$$

where $p_{2t}$ is the theoretical pressure in the absence of losses. Hence,

$$\Delta P_a = -t(p_{2t} - p_2)$$

The pressure difference $p_{2t} = p_2$ is equal to the pressure loss in the lattice

$$p_{2t} - p_2 = \Delta p_n$$

and

$$\Delta P_a = -t\Delta P_n$$

Thus, in the case of the flow of an incompressible fluid about a lattice, the additional force is negative and is determined by the losses of pressure in the lattice (the pressure loss $\Delta p_n$ should not be confused with the pressure difference $p_2 - p_1$).

In the absence of losses, $\Delta p_n = 0$ and $\Delta P_a = 0$. In this case the resultant force is equal to the Joukowsky force

$$P = P_y = \rho\Gamma c$$

This result for the lattice was obtained by N. E. Joukowsky in 1912.[5]

## 7-5. FUNDAMENTAL CHARACTERISTICS OF LATTICES

For evaluating a lattice, energy characteristics are generally introduced. This procedure is different from that used for isolated airfoils. The need of energy considerations is determined by the procedure adopted for thermodynamic analyses. The energy characteristics permit evaluating the effectiveness of the process of energy transformation in the stages of the turbomachines. The component forces acting on an airfoil in the lattice are expressed in terms of the dynamic pressure of the flow at the inlet to the lattice or behind it. In the latter case the formulas for determining the peripheral and radial forces are assumed in the form

$$C_u' = \frac{2P_u}{kp_2M_2^2b} \tag{7-16}$$

[Note: $C_u'$ is a coefficient.]

and

$$C_a' = \frac{2P_a}{kp_2M_2^2b} \tag{7-17}$$

where $p_2$ and $M_2$ are the static pressure and nondimensional velocity behind the lattice.

Analogously, the other aerodynamic coefficients $C_x$ and $C_y$ may be determined. These are employed mainly in the computation of compressor lattices.

In choosing the fundamental geometrical parameter of the lattice, the pitch, it is convenient to employ the concept of peripheral force determined as the ratio

$$C_u = \frac{P_u}{P_u'}$$

[5]The possibility of generalizing the Joukowsky theorem to the case of the flow of a compressible fluid through a lattice was first pointed out by B. S. Stechnkin in 1944. The exact solution was obtained by L. I. Sedov in 1948. The basis of the approximate theorem of Joukowsky for lattices in the flow of a compressible fluid was proposed by L. G. Loitsyanskii in 1949. The generalized theorem of Joukowsky presented in this section for a lattice in an adiabatic flow was given by A. N. Sherstyuk.

where $P'_u$ is the peripheral force on unit length of the profile corresponding to the "ideal" rectangular distribution of the tangential pressure (fig. 7-18). Evidently, for an incompressible fluid (with low inlet velocity)

$$P'_u = (p_1 - p_2)B = \frac{\rho}{2} c_2^2 B$$

The magnitude $P_u$ is determined by formula (7-6); then

$$C_u = \frac{t}{B} \cdot \frac{2c_a(c_{u1} - c_{u2})}{c_2^2}$$

Noting that

$$c_2 = \frac{c_a}{\sin \beta_2} \quad \text{and} \quad (c_{u1} - c_{u2}) = c_a(\cot \beta_1 + \cot \beta_2)$$

we obtain finally

$$C_u = \frac{2 \sin \beta_2 \sin(\beta_1 + \beta_2)}{\sin \beta_1} \cdot \frac{t}{B} \tag{7-18}$$

The most important of the energy characteristics of the lattice is the efficiency defined as the ratio of the actual kinetic energy behind the lattice to the kinetic energy that should have been available if there were no losses,

$$\eta_p = H_{02}/H_{01}$$

or, after simple transformations

$$\eta_p = 1 - \frac{2}{k - 1} \frac{1}{M_{2t}^2} \left[ \left( \frac{p_{01}}{p_{02}} \right)^{\frac{k-1}{k}} - 1 \right] \tag{7-19}$$

where $p_{01}$, $p_{02}$ are the stagnation pressures ahead of and behind the lattice and $M_{2t}$ is the Mach number behind the lattice in the case of isentropic flow.

Formula (7-19) is suitable for determining the efficiency of a compressor lattice.

The coefficient of losses of kinetic energy is defined by the obvious expression

$$\zeta_p = 1 - \eta_p \tag{7-20}$$

The real flow at the inlet and outlet of the lattice is nonuniform; the velocities, angles of outflow, and static pressures vary along the pitch. The equations of continuity, momentum, and energy must then be written in integral form. Thus, the equation of continuity for the sections ahead of and behind the lattice can be written in the form

$$\int_0^t \rho_1 c_1 \sin \beta_1 dt = \int_0^t \rho_2 c_2 \sin \beta_2 dt$$

Introducing a reduced flow rate $q$, we obtain after elementary transformations[6]

$$\int_0^t \frac{p_{01} q_1}{\sqrt{T_{01}}} \sin \beta_1 dt = \int_0^t \frac{p_{02} q_2}{\sqrt{T_{02}}} \sin \beta_2 dt$$

For $T_{01} = T_{02} = T_0 = \text{constant}$, averaging of the equation of continuity gives

$$(p_0 q \sin \beta)_{cp} = \frac{1}{t} \int_0^t p_0 q \sin \beta \, dt$$

The peripheral force is in this case determined from the equation

$$P_u = \int_0^t \rho_1 c_1^2 \sin \beta_1 \cos \beta_1 dt - \int_0^t \rho_2 c_2^2 \sin \beta_2 \cos \beta_2 dt$$

or, again introducing the reduced flow rate $q$, we obtain[7]

$$P_u = k\varepsilon_* \left[ \int_0^t p_{01} q_1 \lambda_1 \sin 2\beta_1 dt - \int_0^t p_{02} q_2 \lambda_2 \sin 2\beta_2 dt \right]$$

---

[6] NACA note:

$$q = \sqrt{\frac{\gamma}{gR}} \frac{P}{P_0} \frac{T_0}{t} \frac{C}{\sqrt{\gamma g R T}}$$

[7] NACA note: $\lambda = \frac{c}{a_*}$ where $a_*$ is the speed of sound when $c$ is sonic. See eq. (7-25).

Averaging of the expressions under the integral sign gives

$$(p_0 q\lambda \sin 2\beta)'_{cp} = \frac{1}{t}\int_0^t p_0 q\lambda \sin 2\beta dt$$

From the equation of energy, the temperature of the flow behind the lattice is averaged, and the following expression is involved:

$$(p_0 q\lambda^2 \sin \beta)''_{cp} = \frac{1}{t}\int_0^t p_0 q\lambda^2 \sin \beta dt$$

For determining the nondimensional characteristics of the lattice, it is necessary to formulate the concept of an ideal (theoretical) process in the lattice for a nonuniform flow. An ideal process may be considered an isentropic process for which in the section investigated there remain unchanged, as in a real process, the field of static pressures and the directions of the velocities. According to another definition of an ideal process, the angles at the inlet and outlet of the lattice are equal to the mean of the angles $\beta_1$ and $\beta_2$ determined by the momentum equation.

The average values, by the equation of momentum, of the projections of the velocity behind the lattice are equal to

$$(c_2 \cos \beta_2)_{cp} = \frac{kg}{G}\varepsilon_* \int_0^t p_{02} q_2 \lambda_2 \cos \beta_2 \sin \beta_2 dt$$

$$(c_2 \sin \beta_2)_{cp} = \frac{kg}{G}\varepsilon_* \int_0^t p_{02} q_2 \lambda_2 \sin^2 \beta_2 dt$$

where $G$ is the flow rate of the gas through one channel of the lattice. The mean angle is then

$$\beta_{2_{cp}} = \arctan \frac{2\int_0^t p_{02} q_2 \lambda_2 \sin^2 \beta_2 dt}{\int_0^t p_{02} q_2 \lambda_2 \sin 2\beta_2 dt} \qquad (7\text{-}21)$$

Besides the efficiency in the computations of a stage, there is employed a coefficient of discharge equal to the ratio of the actual discharge to the discharge in the ideal process[8]

$$\mu_p = \frac{\int_0^t p_{02} q_2 \sin \beta_2 dt}{p_{01}(q_2 \sin \beta_2)'_{cp}} \tag{7-22}$$

and a coefficient of momentum (often termed coefficient of velocity)

$$\varphi_p = \frac{\int_0^t p_{02} q_2 \lambda_2 \sin 2\beta_2 dt}{p_{01}(q_2 \lambda_2 \sin \beta_2)'_{cp}} \tag{7-23}$$

which is the ratio of the momentums of the flow in the real and ideal processes.

The efficiency of the lattice in a nonuniform flow is computed by the formula

$$\eta_p = \frac{\int_0^t p_{02} q_2 \lambda_2^2 \sin \beta_2 dt}{p_{01}(q_2 \lambda_2^2 \sin \beta_2)''_{cp}} \tag{7-24}$$

For an approximate determination of $\eta_p$, equation (7-19) may be used, substituting in it the mean dynamic pressure behind the lattice. In the denominator of equations (7-21) to (7-24), the functions $q_{2t}$ and $\lambda_{2t}$ may be approximately determined from the pressure ratio $p_{2m}/p_{01}$, where the mean static pressure behind the lattice is

$$p_{2m} = \frac{1}{t} \int_0^t p \, dt$$

---

[8]The index t denotes that the parameters refer to an ideal process in the lattice. [NACA note: The prime in eqs. (7-22) and (7-23) and the double prime in eq. (7-24) are not defined in the text. They denote ideal conditions for which the author claims he uses the index t. Later in the text he does use t in $q_{2t}$ and $\lambda_{2t}$ to denote ideal conditions.]

In working up the results of tests of lattices, the local coefficients $\mu_i$, $\varphi_i$, and $\eta_i$ are used which are defined for each streamline by the formulas

$$\mu_i = \frac{q_2}{q_{2t}}; \quad \varphi_i = \frac{\lambda_2}{\lambda_{2t}} \quad \text{and} \quad \eta_i = \frac{\lambda_2^2}{\lambda_{2t}^2}$$

## 7-6. FRICTION LOSSES IN PLANE LATTICE AT SUBSONIC VELOCITIES

In the flow about a lattice the losses of kinetic energy produced by friction in the boundary layer and the formation of eddies in the wake behind the trailing edges are termed profile losses.

The part of the profile losses due to the friction may be evaluated if the velocity (or pressure) distribution over the contour of the profile is known. The determination of the structure of the boundary layer formed on the profile, the establishing of the points of transition and separation of the layer is an important part of the problem of profile losses in lattices. The theoretical and experimental investigations of the boundary layer in lattices permit determining to a first approximation the losses in friction for the continuous flow about a profile and finding the thickness distribution of the boundary layer on the profile.

The scheme of formation of the boundary layer on a profile in a plane lattice is shown in figure 7-19(a). Making use of the graph of the velocity distribution of the external flow, we follow the character of the change of the layer on the concave and convex surfaces of the blade. On the concave surface behind the branch point the thickness of the layer at first slightly increases. At the points of increasing curvatures where the velocity of the external flow either does not change or drops (the diffuser region on the concave surface) the thickness of the boundary layer increases. At these points of the profile there occurs the transition of the laminar into the turbulent layer or even a separation of the layer.

On the converging part of the concave surface where the pressure drops sharply, the thickness of the boundary layer decreases and attains minimum values at the point of departure from the profile. On the convex surface, in the direction toward the narrow section, the thickness of the layer likewise decreases, and at the points of maximum curvature of the profile it is a minimum.

Along the convex surface in the oblique section, there is noted a sharp increase in the thickness of the layer reaching a maximum value at the trailing edge. On this part of the profile (diffuser part of the convex surface) the flow as a rule has a positive pressure gradient which may lead to separation (fig. 7-19(b)).

The boundary layer on the profile may be computed if the velocity distribution of the external flow is given and the condition of the boundary layer (whether it is laminar or turbulent) is known. The existing methods of computing the boundary layer do not take into account the effect of the turbulence of the external flow and of strong curvature of the profile. In designing a lattice, the factor of practically most importance is the determining of the position of the point of transition from the laminar into the turbulent flow and the conditions of continuous flow about the profile. As computations and tests have shown, the transition point most often coincides with the point of minimum pressure on the profile or is somewhat shifted in the diffuser region. In those cases where the flow is strongly turbulent or when local regions are formed in which $dp/dx > 0$, in the converging part of the channel, the transition point may be displaced against the flow.



The computation of the turbulent parts of the boundary layer is conducted as a function of the character of the velocity potential distribution. In the converging parts or the parts of constant pressure, $(dp/dx \leq 0)$ in the case of small velocities (incompressible flow), the momentum thickness $\delta^{**}$ is computed on the assumption that the velocity distribution in the boundary layer is given by an exponential law.

In the work of N. M. Markov, there is shown the satisfactory agreement of the experimental data with the computed results. On figure 7-20 is given the velocity distribution in the boundary layer on the convex surface of the blade of a turbine lattice near the exit edge.

The character of the change of the momentum thickness $\delta^{**}$ along the blade of a turbine lattice may be seen in figure 7-21(a) and (b), where the experimental values of $\delta^{**}$ are also indicated. For computing the layer, the experimental curves of the velocity distribution $\lambda_0$ of the external flow were used. As may be seen from the curves in figure 7-21, the results of the computation satisfactorily agree with the test data.

On the basis of the computational results of the boundary layer on the concave and convex surfaces of the blade, the friction loss coefficient in the lattice is computed.

The fundamental characteristics of the lattice may be expressed in terms of the known parameters of the boundary layer, $\delta_2^*$ and $\delta_2^{**}$, which are determined at the exit edge of the blade. Denoting as before (see fig. 7-19(a)) by $u_2$ and $\rho_2$ the velocity and density at a point in the boundary layer at the exit edge, and by $u_{20}$ the velocity at the external boundary of the boundary layer in the same section (the velocity of the potential flow), we set up the equation for the coefficient $\zeta_T$ of the friction losses.

The kinetic-energy loss in the boundary layer may be expressed by the equation

$$\Delta h_T = \frac{1}{2}\int_0^{\delta_n} \rho_2 u_2 (u_{20}^2 - u_2^2)dy$$

We transform this equation into the form

$$\Delta h_T = \frac{1}{2}\int_0^{\delta_n} \left(1 - \frac{u_2^2}{u_{20}^2}\right)\frac{u_2}{u_{20}}\, u_{20}^3 \rho_2 \frac{\rho_0}{\rho_0}\, dy$$

It is not difficult to obtain

$$\frac{\rho_2}{\rho_0}\rho_0 = \frac{p_0}{gRT_0}\frac{\left(1 - \frac{k-1}{k+1}\lambda_{20}^2\right)^{\frac{k}{k-1}}}{1 - \frac{k-1}{k+1}\lambda_2^2} \tag{7-25}$$

since[9]

$$\frac{\rho_2}{\rho_0} = \frac{T_0}{T_2}\cdot\frac{p_2}{p_0} = \frac{\left(1 - \frac{k-1}{k+1}\lambda_{20}^2\right)^{\frac{k}{k-1}}}{1 - \frac{k-1}{k+1}\lambda_2^2}$$

where

$$\lambda_2 = \frac{u_2}{a_*} \quad \text{and} \quad \lambda_{20} = \frac{u_{20}}{a_*}$$

We set

$$\delta_2^{***} = \int_0^{\delta_n} \frac{1 - \frac{k-1}{k+1}\lambda_{20}^2}{1 - \frac{k-1}{k+1}\lambda_2^2}\left(1 - \frac{u_2^2}{u_{20}^2}\right)\frac{u_2}{u_{20}}\, dy \tag{7-26}$$

[9]NACA note: This presumes that the static pressure in the boundary layer is that of the mainstream and that the recovery factor within the boundary layer is unity.

Then referring to equation (7-25), the energy loss may be written in the form

$$\Delta h_T = \frac{1}{2} \delta_2^{***} \frac{p_0}{gRT_0} u_{20}^3$$

Summing the losses on the convex and concave surface of the blade, we obtain

$$\Delta h_{T,np} = \frac{1}{2} \frac{p_0}{gRT_0} \left[ (\delta_2^{***} u_{20}^3)_{cn} + (\delta_2^{***} u_{20}^3)_{bol} \right] \tag{7-27}$$



The magnitude $\delta^{***}$ has a concrete physical meaning; by analogy with the momentum-loss thickness $\delta^{**}$, $\delta^{***}$ is equal to the thickness of the fluid layer moving with the velocity $u_{20}$ outside the boundary layer, the kinetic energy of which is equal to the kinetic energy of the boundary layer.

The coefficient of losses in friction is

$$\zeta_T = \frac{\Delta h_{T,np}}{E_t} \tag{7-28}$$

where $E_t = Gc_{20}^2/2g$ is the kinetic energy of the flow behind the lattice for the isentropic process and $G$ is the actual flow rate of the gas through one channel of the lattice, which can be determined by the equation

$$G = G_t - g \left[ \int_0^{\delta_n} (\rho_{20} u_{20} - \rho_2 u_2)_{cn} dy + \int_0^{\delta_n} (\rho_{20} u_{20} - \rho_2 u_2)_{bol} dy \right]$$

where $\rho_{20}$ is the density at the outer boundary of the layer in the section at the exit edge and $G_t$ is the flow rate of the gas through one channel of the lattice in isentropic flow.

The above expression may be given in the form

$$G = G_t - \left[ (\delta^* u_{20})_{cn} + (\delta^* u_{20})_{bol} \right] \frac{p_0}{RT_0} \tag{7-29}$$

In equation (7-29)

$$\delta^* = \left(1 - \frac{k-1}{k+1}\lambda_{20}^2\right)^{\frac{1}{k-1}} \int_0^{\delta_n} \left(1 - \frac{1 - \frac{k-1}{k+1}\lambda_{20}^2}{1 - \frac{k-1}{k+1}\lambda_2^2} \cdot \frac{u_2}{u_{20}}\right) dy \quad (7\text{-}30)$$

The theoretical flow rate of the gas may be determined by the formula

$$G_t = g\rho_{2t}c_{2t}t \sin\beta_2 = \left(1 - \frac{k-1}{k+1}\lambda_{2t}^2\right)^{\frac{1}{k-1}} \frac{p_0}{RT_0} \lambda_{2t}a_*t \sin\beta_2 \quad (7\text{-}31)$$

Substituting expression (7-31) in equation (7-29), we obtain

$$G = \left[\left(1 - \frac{k-1}{k+1}\lambda_{2t}^2\right)^{\frac{1}{k-1}} \lambda_{2t}a_*t \sin\beta_2 - (\delta^* u_{20})_{cn} - (\delta^* u_{20})_{bol}\right] \frac{p_0}{RT_0} \quad (7\text{-}32)$$

By using equation (7-27), the equation for the loss coefficient (7-28) now assumes the form

$$\zeta_T = \frac{(\delta_2^{***}\lambda_{20}^3)_{cn} + (\delta_2^{***}\lambda_{20}^3)_{bol}}{\left[\left(1 - \frac{k-1}{k+1}\lambda_{2t}^2\right)^{\frac{1}{k-1}} \lambda_{2t}t \sin\beta_2 - (\delta^*\lambda_{20})_{cn} - (\delta^*\lambda_{20})_{bol}\lambda_{2t}^2\right]} \quad (7\text{-}33)$$

Bearing in mind that

$$G = \mu_p G_t = \mu_p \left(1 - \frac{k-1}{k+1}\lambda_t^2\right)^{\frac{1}{k-1}} \frac{p_0}{RT_0} \lambda_{2t}a_*t \sin\beta_2$$

formula (7-33) can be represented in the form

$$\zeta_T = \frac{(\delta_2^{***}\lambda_{20}^3)_{cn} + (\delta_2^{***}\lambda_{20}^3)_{bol}}{\mu_p\left(1 - \frac{k-1}{k+1}\lambda_{2t}^2\right)^{\frac{1}{k-1}} \lambda_{2t}^3 t \sin\beta_2}$$

or

$$\zeta_T = \frac{(H^{***}\delta_2^{**}\lambda_{20}^3)_{cn} + (H^{***}\delta_2^{**}\lambda_{20}^3)_{bol}}{\mu_p\left(1 - \frac{k-1}{k+1}\lambda_{2t}^2\right)^{\frac{1}{k-1}} \lambda_{2t}^3 t \sin\beta_2} \tag{7-34}$$

where

$$H^{***} = \frac{\delta^{***}}{\delta^{**}}$$

From a comparison of formulas (7-33) and (7-34), it follows that the flow-rate coefficient $\mu_p$ is equal to

$$\mu_p = 1 - \frac{(H^{*}\delta_2^{**}\lambda_{20})_{cn} + (H^{*}\delta_2^{**}\lambda_{20})_{bol}}{\left(1 - \frac{k-1}{k+1}\lambda_{2t}^2\right)^{\frac{1}{k-1}} \lambda_{2t} t \sin\beta_2} \tag{7-35}$$

where

$$H^{*} = \frac{\delta^{*}}{\delta^{**}}$$

For an incompressible fluid, there may be obtained from expressions (7-34) and (7-35)

$$\zeta_T = \frac{(H^{***}\delta_2^{**}u_{20}^3)_{cn} + (H^{***}\delta_2^{**}u_{20}^3)_{bol}}{\mu_p c_{2t}^3 t \sin\beta_2} \tag{7-36}$$

and

$$\mu_p = 1 - \frac{(H^* \delta_2^{**} u_{20})_{cn} + (H^* \delta_2^{**} u_{20})_{bol}}{c_{2t} t \sin \beta_2} \tag{7-37}$$

In this case (for the incompressible fluid), the values of $\delta_2^{**}$ and $\delta_2^{*}$ are determined by the formula given in table 4-1.

The magnitudes $H^{***}$ and $H^{*}$ entering equations (7-35) and (7-36) should be determined for the turbulent and laminar boundary layers individually.

It is evident that the values $H^{***}$ and $H^{*}$ and the magnitudes $\delta^{*}$ and $\delta^{**}$ depend on the velocity distribution in the boundary layer, that is, on the flow regime within the layer and on the character of the change in velocities of the external potential flow (the pressure gradient $dp/dx$).

N. M. Markov computed the values $H^{***}$ and $H^{*}$ for the turbulent layer using the assumption of an exponential velocity distribution law and for the laminar layer with $dp/dx = 0$. On figure 7-22(a) and (b) are given the values of $H^{***}$ and $H^{*}$ for the turbulent layer as a function of $Re^{**}$ and $\lambda_{20}$ and for the laminar layer as a function of $\lambda_{20}$.

As an example, we shall determine the theoretical magnitude of the profile losses in turbine lattices as a function of the inlet and exit angles $\beta_1$ and $\beta_2$. We assume that the velocity distribution on the profile is approximately that shown by the dotted curves in figure 7-23 for all inlet and exit angles. On the convex side of the profile $c_{cn}/c_2 = 1.1$ and on the concave side $c_{bol}/c_2 = 0.5$ approximately, [subscripts cn and bol denote convex and concave sides, respectively]. On this assumption, the density of the lattice $B/t$ for each pair of values of the angles should have a fully determined value (see sec. 7-5): From equation (7-18)

$$\frac{B}{t} = \frac{2 \sin \beta_2 \sin(\beta_1 + \beta_2)}{C_u \sin \beta_1}$$

where the coefficient of the peripheral force is

$$C_u = \frac{P_u}{B \frac{\rho c_2^2}{2}} = -\bar{p}_{cn} + \bar{p}_{bol}$$

$\overline{p}_{cn}$ and $\overline{p}_{bol}$ being the mean pressure coefficients on the convex and concave surfaces of the blade.

For the assumed values of $c_{cn}$ and $c_{bol}$

$$\overline{p}_{cn} = 1 - \left(\frac{c_{cn}}{c_2}\right)^2 = -0.21 \quad \text{and} \quad \overline{p}_{bol} = 1 - \left(\frac{c_{bol}}{c_2}\right)^2 = 0.75$$

that is, $C_u = 0.96$.

Assuming further that

$$u_{20} \approx c_{2t}$$

$$H^{***}_{cn} \approx H^{***}_{bol} \approx 2 \quad \text{and} \quad \mu_p = 1$$

we can represent the friction-loss coefficient of the lattice in the form

$$\zeta_T = 2 \frac{\delta^{**}_{cn} + \delta^{**}_{bol}}{t \sin \beta_2} \tag{7-38}$$

On the assumption of the exponential law of velocity distribution in the boundary layer (with exponent $n = 1/7$), the momentum thickness is equal to [Note: this expression is very similar to that of E. Truckenbrodt; cf. Schlicting, p. 470.]

$$\delta^{**} = 0.0973 \frac{0.37}{Re^{0.2}} \left[\int_0^S \left(\frac{c}{c_2}\right)^{3.86} dx\right]^{0.8} \tag{7-39}$$

In expression (7-39), we assume $Re = 10^5$, and to estimate the arc of the profile $S$ on the convex and the concave surfaces we evaluate approximately (fig. 7-23(a)):

$$S_{cn} = S_{bol} = \frac{1}{3} \frac{B}{\sin \beta_1} + \frac{2}{3} \frac{B}{\sin \beta_2} \tag{7-40}$$

The graphs in figure 7-23(b), where the friction loss coefficient[10] $\zeta_T$ is represented as a function of $\beta_1$ and $\beta_2$, are constructed with

[10]For the case of infinitely thin trailing edges the coefficient $\zeta_T$ is equal to the profile loss coefficient of the lattice.

the aid of formulas (7-38) to (7-40). The dotted curves correspond to constant values of B/t. Notwithstanding the considerable reservations with which the entire computation was made, the results are qualitatively well confirmed by experiment.

The friction losses depend on $\beta_1$ and $\beta_2$, increasing with decrease in these with the greatest influence exerted by $\beta_1$. For $\beta_1 \approx \beta_2$ (in lattices of the impulse type) the curves of equal $\zeta_T$ almost pass through the normal to the straight line $\beta_1 = \beta_2$; that is, in this case the losses depend essentially on the magnitude of the angle of rotation of the flow equal to

$$\Delta\beta = 180^\circ - (\beta_1 + \beta_2)$$

We may remark that the effect of Reynolds number on the friction loss coefficient in the lattice can easily be determined by computation.

## 7-7. EDGE LOSSES IN PLANE LATTICE AT SUBSONIC VELOCITIES

The eddy losses at the trailing edge constitute the second component of the profile losses in a plane lattice. The flow leaving the trailing edges always separates. As a result of the separation there is an interaction between the boundary layers flowing off from the concave and convex surfaces behind the trailing edge; vortices thus arise which appear at the initial part of the wake. The photographs of the flow behind the lattice presented in figure 7-24 show the formation of the initial part of the wake.

A large influence on the wake is exerted by the distribution of the velocity in the boundary layer at the point where the flows from the convex and the concave surfaces unite and also by the difference in pressure at these points. Along the initial part of the wake, (including the region behind the trailing edge where a Kármán vortex street is formed with the usual chess arrangement of the vortices) the interaction between the eddy wake and the nucleus of the flow unifies many properties of the flow field behind the lattice. The static pressure of the flow increases and the outlet angle decreases. As a result, kinetic-energy losses arise, analogous to the losses in sudden expansion.

The parameters of the equalizing flow can be obtained by the simultaneous solution of the equations of continuity, momentum, and energy. The control surfaces shown in figure 7-25 are selected. These surfaces are equally spaced, when measured along the lattice axis; and they enclose the fluid involved in the study. The above equations can be written for the following assumptions: (a) the density of the flow changes

little as it moves downstream (from secs. 2-2 to 2'-2'); (b) the field of velocities and pressures are homogeneous between the wakes and completely across the section 2'-2'.

The equation of continuity can then be represented in the form

$$\rho c_2(t - \Delta t)\sin \beta_{2n} = c_{2\infty}\rho t \sin \beta_{2\infty}$$

or

$$c_2(1 - \tau)\sin \beta_{2n} = c_{2\infty}\sin \beta_{2\infty} \tag{7-41}$$



where

$$\tau = \frac{\Delta t}{t}$$

The momentum equation in the direction of the axis of the lattice gives

$$c_2^2\cos \beta_{2n}\rho(t - \Delta t)\sin \beta_{2n} = c_{2\infty}^2\cos \beta_{2\infty}\rho t \sin \beta_{2\infty}$$

or, with account taken of (7-41), we obtain

$$c_2\cos \beta_{2n} = c_{2\infty}\cos \beta_{2\infty} \tag{7-42}$$

The momentum equation in the direction perpendicular to the lattice axis can be written in the form

$$c_2^2\rho \sin^2\beta_{2n}(t - \Delta t) + p_2(t - \Delta t) + p_{kp}\Delta t = c_{2\infty}^2\rho \sin^2\beta_{2\infty}t + p_{2\infty}t \tag{7-43}$$

From equations (7-41) and (7-42) there is easily obtained

$$\beta_{2\infty} = \arctan[(1 - \tau)\tan \beta_{2n}] \tag{7-44}$$

Equation (7-43) permits finding the increase in pressure behind the lattice

$$\Delta p_{2\infty} = \frac{2}{\rho c_2^2}\left[c_2^2\rho \sin^2\beta_{2n}(1 - \tau) - c_{2\infty}^2\rho \sin^2\beta_{2\infty} + (p_{kp} - p_2)\tau\right]$$

Taking into account expression (7-41), we obtain

$$\overline{\Delta p}_{2\infty} = \frac{p_{2\infty} - p_2}{\frac{1}{2}\rho c_2^2} = [2(1 - \tau)\sin^2\beta_{2n} + \bar{p}_{kp}]\tau \qquad (7\text{-}45)$$

For determining the theoretical velocity at infinity behind the lattice, we make use of the equation of energy which for the assumption made $\rho_2 = \rho_{2\infty} = \rho$ may be represented in the form

$$\frac{(c'_{2\infty})^2}{2} + \frac{p_{2\infty}}{\rho} = \frac{c_2^2}{2} + \frac{p_2}{\rho} \qquad (7\text{-}46)$$

where $c'_{2\infty}$ is the theoretical velocity in the section 2'-2'.

From expression (7-46), we obtain

$$\left(\frac{c'_{2\infty}}{c_2}\right)^2 = 1 - \Delta\bar{p}_{2\infty} \qquad (7\text{-}46a)$$

The velocity $c_2$ is expressed in terms of $c_{2\infty}$ with the aid of equations (7-41) and (7-44), thus

$$\frac{c_{2\infty}^2}{c_2^2} = (1 - \tau)^2\sin^2\beta_{2n} + \cos^2\beta_{2n} = 1 - \tau(2 - \tau)\sin^2\beta_{2n}$$

and we have

$$\left(\frac{c_{2\infty}}{c'_{2\infty}}\right) = \frac{1 - \tau(2 - \tau)\sin^2\beta_{2n}}{1 - \Delta\bar{p}_{2\infty}} = \varphi_{kp}^2 \qquad (7\text{-}47)$$

The coefficient of edge losses is[11]

$$\zeta_{kp} = 1 - \varphi_{kp}^2 = \frac{\tau\sin^2\beta_{2n} - \bar{p}_{kp}}{1 - \Delta\bar{p}_{2\infty}}\tau \qquad (7\text{-}48)$$

[11] Formulas (7-45) to (7-48) given here were obtained by G. Y. Stepanovich.

The nondimensional pressure behind the edges entering equations (7-45) and (7-48) is

$$\bar{p}_{kp} = \frac{p_{kp} - p_2}{\frac{1}{2}\rho c_2^2}$$

and it must be determined from experimental data.

With an accuracy up to magnitudes of the second order as compared with $\tau$ the coefficient of edge losses is expressed by the formula

$$\zeta_{kp} \approx - \bar{p}_{kp}\tau$$

For small velocities, according to test data (see below)

$$\bar{p}_{kp} \approx - 0.1$$

From the above arguments, it is seen that the edge losses are directly proportional to $\tau$.

According to test data, the equalization of the flow behind the lattice occurs very rapidly at first, and the rate of equalization is a function of the geometrical parameters of the profile and the lattice, and is quite dependent on the thickness of the edge. The region of intensive mixing ends at a distance $y = (1.3 \text{ to } 1.7\ t)$ behind the trailing edge. This is confirmed by the graphs in figure 7-26 in which are given the results of an investigation of the wake behind a reaction lattice according to the data of R. M. Yablonik. Figure 7-26(a) shows curves of local loss coefficients of the wake at different distances behind the reaction lattice. On figure 7-26(b) is shown the variation of the coefficient of nonuniformity in the flow field behind the lattice. This coefficient is defined by the formula

$$\nu = \frac{c_{a,max} - c_{a,min}}{2c_{a,m}}$$

where

$c_{a,max}$ and $c_{a,min}$ maximum and minimum values of component velocity $c_a$ in the given section

$c_{a,m}$ mean value of velocity $c_a$ in the same section

A detailed investigation of the flow behind the trailing edge of a reaction lattice was conducted by B. M. Yakub. The results of these tests reveal certain effects of the shape of the edges on the flow

structure in the eddy wake. Measurements of static pressure on both sides of the wake show that there is a considerable nonuniformity in the pressure field along the boundaries of the wake (fig. 7-27). Moreover, the static pressure along the wake boundaries changes periodically.

As the flow leaves the concave surface of a blade, its pressure must drop, while on the concave surface it must increase. Further, behind the principal edge vortex, the static pressure decreases on both sides of the wake, it then again increases somewhat, and so on. Finally, there is a complete equalization of the field of flow. From figure 7-27 it is seen also that the amplitude of the fluctuations of the static pressure depends on the shape of the edge. By making a two-sided taper (sharpening of the edges b and c in figure 7-27) it was possible to decrease somewhat the nonuniformity of the static-pressure field.

The tests showed that a sharpened edge of the type b raises the efficiency of the lattice, as compared with the normal edges, by 1 percent and that an edge of type c increased the efficiency by 2.5 percent (for a medium velocity of flow). It should be remarked that, notwithstanding their high effectiveness, the forming of very sharp edges of the type c introduces serious difficulties because such an edge rapidly deteriorates under actual operating conditions.

## 7-8. SEVERAL RESULTS OF EXPERIMENTAL INVESTIGATIONS OF PLANE LATTICES AT SMALL SUBSONIC VELOCITIES

Systematic investigations of the effect of the geometric parameters of the lattices on the magnitude of the profile losses at small velocities were conducted in the M. I. Kalinin Laboratory, the I. I. Polzunov Institute, the F. E. Dzerzhinskii Institute, and in other scientific research organizations and institutes.

We shall consider as an example several results of an experimental investigation of the effect of the pitch, the blade angle, and the angle of incidence of the flow on the velocity distribution over the profile of an impulse and reaction type lattice.

Figure 7-28 shows the velocity distribution over the profile[12] of a reaction turbine according to the data of N. A. Sknar. With increase in pitch, the flow about the back of the profile becomes impaired. Along a considerable part of the convex surface, the pressure gradient is positive (see curve for $\overline{t} = 0.904$ on fig. 7-28). In this diffusing region a boundary layer is formed, and its thickness increases and in certain

[12]The local velocities are made dimensionless by dividing them by the vector mean velocity.

cases separates. With increasing pitch the nonuniformity of the flow in the passages between the blades increases; the velocities on the convex side increase, while on the concave side they decrease. At high values of the pitch, the flow about a profile in the lattice approximates the flow about a single profile (fig. 7-28).

The effect of the blade setting on the velocity distribution over the profile is shown in figure 7-29(a). The maximum favorable velocity distribution for a given profile is obtained at a setting angle $\beta_y \approx 50^\circ$. In this case both along the upper and lower surface the velocities increase more uniformly.



A change in the inlet angle of the flow (fig. 7-29(b)) greatly affects the velocity distribution along the profile. Large inlet angles tend to impair the flow along the concave surface, while small angles similarly affect the flow along the convex surface.

The investigation of an impulse lattice conducted by E. A. Gukasova shows that, similar to the reaction lattice, a change in pitch causes a considerable change in the velocity distribution along the profile (fig. 7-30). For all values of the pitch an adverse pressure gradient is found immediately behind the leading edge. The diffusing region extends over the greater part of the concave surface, and only near the outlet part does the flow reaccelerate. On the convex surface of the blade behind the leading edge, the flow accelerates and reaches a maximum velocity downstream of the part of greatest curvature. We note that, as for the impulse lattice, diffuser regions are formed near the trailing edge of the upper surface for all regimes.

With decreasing pitch, the nonuniformity of the velocity field in the channel between the blades decreases. A similar trend accompanies an increase in the inlet angle of the flow; as $\beta_1$ increases, the flow on the concave surface accelerates while the flow on the convex surface slows down. A decrease in the inlet angle is accompanied by the appearance of adverse pressure gradients near the inlet of both the convex and concave surfaces. For inlet angles somewhat higher than the profile angle $\beta_{1n}$, the most favorable general velocity distribution is found.

The change of the coefficient of profile losses in impulse and reaction lattices as a function of the pitch and inlet angle may be seen in figure 7-31. The curves show that for each lattice there exists a definite optimum pitch for the minimum profile losses. Thus, for example, for the reaction lattice having the profile shown in figure 7-28, the optimum pitch is $\bar{t}_{opt} = 0.673$. For the impulse lattice, $\bar{t}_{opt} \approx 0.50\text{-}0.60$.

In spite of the favorable velocity distribution, in a closely spaced lattice ($\overline{t} < \overline{t}_{opt}$) the loss coefficient is relatively high because of the greater losses produced by friction. Decreasing the pitch also causes an increase in the coefficient of edge losses.

The curves in figure 7-31 show that for all pitches a decrease in the inlet angle (below the optimum) has a sharper effect on the efficiency than an increase in the angle. An increase in $\zeta_p$ also noted for $\beta_1 > \beta_{1n}$ for the impulse lattice of large pitch. It should be emphasized that as a rule the values of the optimum inlet angles exceed the geometric angle of the profile.

From the results of the investigations, it can be concluded that the experimental determination of the optimum pitch must be carried out over a wide range of inlet angles.

The tests show that the direction of the equalized flow behind the lattice may with sufficient accuracy be determined by formula (7-44). The familiar formula given in the literature for determining the effective (actual) angle of the flow

$$\beta_{2e} = \text{arc sin} \frac{a_2}{t} \tag{7-49}$$

gives somewhat lowered values of $\beta_2$. More closely agreeing values of $\beta_{2e}$ with test results are obtained by formula

$$\beta_{2e} = \text{arc sin} \frac{a_2}{t - \Delta t} \tag{7-50}$$

At small velocities tests confirm that for all practical purposes, the outlet flow angles of a reaction lattice depend only slightly on the direction of the flow at inlet, that is, on the angle $\beta_1$ (fig. 7-32). The angle $\beta_2$ is, however, influenced to a large extent by the pitch and the setting angle of the profile. With an increase in $\beta_y$ and $\overline{t}$, the angle $\beta_2$ increases.[13]

Similar results are obtained also for the impulse lattice. In this case, however, the deviation between experimental and computed values of the outlet angles increases. According to the data of a number of tests the outlet flow angle increases somewhat, as the inlet flow angle increases.

---

[13]Analysis of formula (7-44) leads to the same results.

Immediately behind the lattice, the field of the flow angles is nonuniform; the angles $\beta_2$ vary along the pitch (fig. 7-33). The greatest changes in $\beta_2$ are found near the boundaries of the trailing eddy wake. With increasing distance from the lattice, the flow equalizes and the values of the local angles approach the mean value $\beta_{2\infty}$.

The nonuniformity of the field behind the lattice depends on the inlet flow angle. With either a decrease or a considerable increase in the inlet angle, the nonuniformity of the flow at the outlet increases. Particularly unfavorable is a decrease in the inlet angle.

The results of numerous tests of lattices at small velocities in a uniform weakly turbulent flow permit drawing several general conclusions as to the character of the change in profile losses in lattices as a function of the parameters defining the flow regime (inlet angle $\beta_1$ and Reynolds number Re) and of the fundamental geometrical parameters of the profile and lattice.

A study of the effect of the angle of inlet flow, angle of the profile setting, and the pitch for fixed values of Re shows that, in the cases where a change in these magnitudes results in the formation of adverse pressure gradients on the profile, the boundary layer thickens, and the transition from a laminar to a turbulent boundary layer moves upstream. As a result, the friction losses increase. In certain cases the boundary layer may separate in the regions where diffusion occurs, a circumstance which leads to a sharp increase in the profile losses. A decrease in the inlet flow angle and an increase in the pitch increases the likelihood of adverse pressure gradients. In this connection, it should be remarked that in impulse lattices the losses as a rule are greater than in the reaction type which are characterized by a more favorable (converging) pressure distribution over the profile. The above considered tests showed that the minimum loss coefficient in an impulse lattice constitutes about 7 percent, while in the reaction lattice it is about 4 percent.

Changes in $\beta_1$, $\bar{t}$, and $\beta_y$ have an effect on the magnitude of the edge losses.

The effect of the Reynolds number on the efficiency of the lattice has not yet been sufficiently studied. The available data show that a change in Re has different effects on the profile losses in the lattice, depending on the inlet angle and the geometrical parameters of the lattice. If separation occurs on the profile, the profile losses tend to decrease markedly with an increase in $Re_2$. For nonseparating flow about the profile, the effect of $Re_2$ for the reaction lattice is small (fig. 7-34).

## 7-9. FLOW OF GAS THROUGH LATTICE AT LARGE SUBSONIC VELOCITIES; CRITICAL $M_*$ NUMBER FOR LATTICE

The fundamental characteristics of the potential flow of a compressible fluid in a lattice at subsonic velocities is qualitatively the same as that of incompressible flow. The network of streamlines $\psi$ = constant and equipotential lines $\Phi$ = constant remains orthogonal, but it is no longer square. The velocity at any point of the flow is

$$c = \frac{d\Phi}{dS} = \frac{\rho_0}{\rho}\frac{d\psi}{dn}$$

and, as a result, when $\Delta\Phi = \Delta\psi$ = constant, then $\Delta S/\Delta n \approx \rho/\rho_0 \leqslant 1$. In the plane of the hodograph, the network of lines $\Phi$ = constant and $\psi$ = constant is no longer orthogonal. According to the condition of equality of the flow rate ahead of and behind the lattice, we have

$$c_1\rho_1 t \sin\beta_1 = c_2\rho_2 t \sin\beta_2$$

For $c_1 < c_2$, the projection of the velocity $c_2$ on the normal to the axis of the lattice ($c_2\sin\beta_2$) becomes larger than the same projection of the velocity $c_1$. The distribution of the relative velocities $\bar{c} = c/c_2$, in contrast to the case of the incompressible fluid, depends on the absolute value of the velocity, or more accurately, on the Mach number $M$ at any definite point of the flow, for example, on $M_2 = c_2/a_2$.

An approximate method of estimating the velocity distribution over the profile may be used to establish the characteristic regimes of the flow about the lattice at subsonic velocities. The approximate method is based on the circumstance that in modern turbine lattices of high solidity the flow between the profiles may be considered as a flow in a channel.[14]

The flow velocity in an interblade passage of constant width and curvature (fig. 7-35) can be determined in a particularly simple manner. A comparison with more accurate theory shows that for a perfect gas the velocity distribution across the channel approximately satisfies the equation

$$c = \frac{R_{cn}}{R} c_{cn} \qquad (7\text{-}51)$$

---

[14]The method considered, proposed by A. Stodola, was developed subsequently by G. Y. Stepanov.

and in particular

$$c_{bol} = \frac{R_{cn}}{R_{bol}} c_{cn}$$

The velocity on the convex side of the profile $c_{cn}$ can be determined from the equation of continuity

$$c_1 \rho_1 t \sin \beta_1 = \int_{R_{cn}}^{R_{bol}} c\rho \, dR \tag{7-52}$$



In equation (7-52) it is convenient to transform to the nondimensional functions $q$ and $\lambda$

$$q_1 t \sin \beta_1 = \int_{R_{cn}}^{R_{bol}} q \, dR$$

Using expression (7-51), we obtain finally

$$q_1 t \sin \beta_1 = \lambda_{cn} R_{cn} \int_{\lambda_{cn}}^{\lambda_{bol}} q \, d\left(\frac{1}{\lambda}\right) = \lambda_{cn} R_{cn} I \Big|_{\lambda_{cn}}^{\lambda_{bol}} \tag{7-53}$$

Computation of the integral $I$ for small subsonic velocities gives (the constant of integration is omitted)

$$I_1 = m_1 \ln \frac{1}{\lambda} \tag{7-54}$$

where

$$m_1 = \left(\frac{k+1}{2}\right)^{\frac{1}{k-1}}$$

For a gas with $k = 1.4$ we obtain

$$I_2 = m_1 \left[\cosh^{-1} \frac{1}{m_2 \lambda} - \left(\frac{23}{15} - \frac{11}{15} m_2^2 \lambda^2 + \frac{1}{5} m_2^2 \lambda^4\right) \sqrt{1 - m_2^2 \lambda^2}\right] \tag{7-55}$$

where

$$m_2 = \sqrt{\frac{k-1}{k+1}}$$

For $k = 4/3$ we have

$$I_3 = m_1\left(\ln\frac{1}{\lambda} + \frac{3}{2}m_2^2\lambda^2 - \frac{3}{4}m_2^4\lambda^4 + \frac{1}{6}m_2^6\lambda^6\right) \tag{7-56}$$

If the computed function $I$ is used, the equation of continuity can be written in the form[15]

$$\frac{q_1 t \sin\beta_1}{R_{cn}} = \lambda_{cn}(I_{bol} - I_{cn}) \tag{7-57}$$

where $I_{cn}$ by equation (7-54) or (7-55) corresponds to $\lambda_{cn}$ and $I_{bol}$ corresponds to $\lambda_{bol} = R_{cn}/R_{bol}\lambda_{cn}$.

It is possible to apply the process of successive approximations for computing $\lambda_{cn}$ by equation (7-57), since the expression in parentheses depends little on $\lambda_{cn}$. In the first approximation

$$\lambda_{cn}^{(1)} = \frac{\lambda_1 t \sin\beta_1}{R_{cn}\ln\frac{R_{bol}}{R_{cn}}} \tag{7-58}$$

Then, in the following approximation, $I_{cn}$ and $I_{bol}$ are determined from $\lambda_{cn}^{(1)}$

$$\lambda_{cn}^{(2)} = \frac{q_1 t \sin\beta_1}{R_{cn}\left[I_{bol}^{(1)} - I_{cn}^{(1)}\right]} \tag{7-59}$$

and so forth. For $\lambda_{cn} < 0.5$ the first approximation (7-58) is sufficient. The solution of equation (7-57) is conveniently represented in the form of the graph shown in figure 7-36, which gives the magnitude $q_{cp} = q_1 t \sin\beta_1/(R_{bol} - R_{cn})$ as a function of $R_{cn}/R_{bol}$ for various values of $\lambda_{cn}$.

A critical value $q_{1*}$ and a corresponding $\lambda_{1*}$ or $M_{1*}$ denote critical flow in the lattice; that is, a condition where $\lambda_{cn} = 1$. In the curved channel for which $R_{cn}/R_{bol} < 1$, the graph in figure 7-36 indicates that the maximum flow is attained for some $\lambda_1 > \lambda_{1*}$.

---

[15]NACA note: Subscript cn refers to convex side, bol to concave side.

The above described method can also be applied for finding the velocity within an interblade passage of variable width and curvature. For this purpose it is necessary in the section of interest to inscribe circles as shown in figure 7-37 and to determine their diameter and also the radii of curvature $R'_{cn}$ and $R'_{bol}$ at the points of tangency of the circles. For computing the velocities $\lambda_{cn}$ and $\lambda_{bol}$, formulas (7-58) and (7-59) may be used substituting, for example,

$$R_{cn} = R'_{cn};\ R_{bol} = R'_{cn} + a$$

or

$$R_{bol} - R_{cn} = a;\ \frac{R_{cn}}{R_{bol}} = \frac{R'_{cn}}{R'_{bol}}$$

or $R_{bol} = R'_{bol}$, $R_{cn} = R'_{bol} - a$. The differences in the values of $\lambda_{cn}$ and $\lambda_{bol}$ obtained in each case characterize the error of the applied method. As an example, in figure 7-37 are compared the results of the exact solution (in the flow of an incompressible fluid) with the results of computations by the described method. The satisfactory agreement of the values of the velocities that is observed also in the other examples attests to the feasibility of applying this method for preliminary computations.[16]

Let us now consider flow of a gas through a reaction lattice when the velocities are nearly sonic. For a critical value of $M_2 = M_{2*}$ at a certain (critical) point of the profile, the critical velocity is reached. With further increases in $M_2$, the pressure distribution ahead of this critical point changes little. The pressure distribution behind the point of sonic velocity changes considerably. In the so-called diffusing (i.e., for subsonic flow) region behind this critical point, there is an increase in the supersonic velocity.

The experimental determination of the critical values $M_{2*}$ shows that its magnitude largely depends on the geometric parameters of the profile, the lattice, and the direction of the flow at the inlet. In a

---

[16]This method of computing the flow in a channel was based on the approximate determination of the length of the potential line and on the assumption that the distribution along it of the curvature of the streamlines differs little from the case of vortex flow. With a certain complication of the computations, this method can be rendered more accurate by the successive refinements in estimating the distribution of curvature.

reaction lattice for an entry angle $\beta_1 \approx \beta_{1n}$, the values of $M_{2*}$ decrease with increase of pitch because the local velocities on the convex surface at the points of maximum curvature increase. In figure 7-38 are shown the curves of maximum velocities on the back of the profile as a function of $M_2$. From these curves the values of $M_{2*}$ can be determined. For $1 > M_2 > M_{2*}$ on the convex side of the profile, local regions of supersonic velocities are formed, the boundaries of which are the lines of transition ($M = 1$) and a system of weak shocks.

Experiment shows that the supersonic zones may arise simultaneously in the flow region adjoining the trailing edge and the boundaries of the wake. Because of the lowered pressure behind the trailing edge, the velocities of the particles leaving the upper and lower surfaces (outside the boundary layer) increase. This acceleration may lead to the formation of zones of supersonic velocity adjoining the boundaries of the wake. In correspondence with experimental data obtained at a small pitch, the supersonic zones are formed first at the trailing edges themselves and then progress to the more curved part of the convex side of the profile in the interblade channel. For a large pitch, on the contrary, supersonic velocities arise first in the channel adjoining the convex surface of the blade. This is confirmed by the results of measurements of the pressure behind the trailing edges and of the minimum pressure on the convex surface of the profile in lattices of various pitches.

The critical values of the number $M_{2*}$ are shown in figure 7-39 for $\beta_1 \approx \beta_{1n}$ as a function of the pitch for a reaction lattice. It is seen from the graph that for each lattice there exists a pitch $\bar{t}_*$ for which the critical velocity is reached simultaneously on the back and behind the trailing edge of the profile.

In an impulse lattice,[17] the critical M number is lower than that of a reaction lattice, this fact is a result of the greater curvature of the impulse profile. Local supersonic regions in the impulse lattice may arise, depending on the inlet angle near the leading edge, on the convex surface and at the trailing edge.

The graphs shown in figures 7-40 and 7-41 characterize the effect of the number $M_2$ (and also $M_1$) on the pressure distribution over the profile for the two fundamental types of lattice. With an increase in $M_2$, the absolute values of the pressure coefficients increase. The characteristic points of the pressure diagram (points of minimum pressure) are displaced in the direction of the flow. For small angles $\beta_1$

[17]For the impulse lattice the critical M number is sometimes referred to the inlet velocity.

and large numbers $M_1$, experiment shows the displacement of the branch point $O_1$ along the concave surface of the profile.

The effect of compressibility shows up more markedly on the convex surface, where the pressures change more rapidly; the pressure gradient along the convex surface increases. Correspondingly, the flow in the diffusing region on the convex surface also changes. Since the minimum pressure on the profile decreases, the pressure gradient in the diffusing region of this surface increases. The pressure changes particularly sharply on the convex surface near the narrow section of the channel. Similarly, but more sharply, the effect of the compressibility reveals itself in the pressure distribution in an impulse lattice.

A change in the inlet flow angle at large supersonic velocities in an impulse lattice sharply affects the pressure distribution, particularly at the inlet part of the profile (fig. 7-42).

## 7-10. PROFILE LOSSES IN LATTICES AT LARGE SUBSONIC VELOCITIES

The results of experimental investigation permit estimating the change in the profile losses in various lattices at subsonic and near sonic velocities.

For $M_2 < M_{2*}$, with increasing flow velocity, the effect of the compressibility on the losses due to friction depends on the one hand on the change in the pressure distribution over the profile. Increasing the velocity increases the diffusion on the convex surface and, hence, increases the losses. On the other hand, increasing the velocity changes the velocity distribution within the boundary layer itself; and this tends to decrease the losses.

The investigation of the wake at large subsonic velocities shows that the pressure behind the trailing edge drops with increasing value of $M_2$; this behavior is particulary acute when the velocity is approximately sonic. In figure 7-43 is shown the dependence of $\overline{p}_{kp}$ on $M_2$ for a rounded trailing edge. It is seen that with an increase in $M_2$, the value of $\overline{p}_{kp}$ decreases and reaches a minimum value at $M_2 \approx 0.9 - 1.0$. With a further increase in $M_2$, the pressure behind the trailing edge increases. The intensity of the vortice behind the trailing edge and the width and depth of the wake are increased (fig. 7-44). At the same time, for $M_2 < 1$, the extent of the smoothed out part of the flow behind the lattice increases.

For an approximate estimate of $\zeta_{kp}$ at large subsonic velocities, formula (7-48) may be employed, substituting the test values of $\overline{p}_{kp}$ (fig. 7-43). Thus, taking into account the fact that the trailing-edge losses increase, with an increase in $M_2$, the character of the change of the coefficient of profile losses as a function of $M_2$ is determined by whichever of the above-mentioned factors is the deciding one. In the final analysis, this answer depends on the geometric parameters of the profile and lattice.

In reaction lattices the approach to near sonic velocities while $M_2 < M_{2*}$ does not lead to any considerable increase in the losses if the flow in the interblade channel is without separation.

We recall that the resistance coefficient of a single profile sharply increases in the zone of near sonic velocities. In the flow about a single profile, the local shock waves have a considerably greater intensity, and in many cases the flow separates to the impairment of the flow. The energy losses in the local shock waves of a lattice are not large, and they evidently do not appreciably increase the loss coefficient.

In a reaction lattice, thanks to the converging flow, the local shock waves within the channel do not, as a rule lead to separation. In those cases where the flow separates at supersonic velocities, however, the loss coefficient increases more rapidly with increase in $M_2$.

Figure 7-45 gives $\zeta_p$ curves for several reaction lattices consisting of different profiles and for two impulse lattices. We note that since the test lattices had different profiles, the dotted curves in figure 7-45 do not characterize the effect of pitch alone.

The effect of the incompressibility on the profile losses is more marked for impulse lattices. The curves in figure 7-45 clearly confirm this conclusion.[18] It should be emphasized that, for large velocities, a change in the inlet angle has a particularly marked effect on the loss coefficient in the impulse lattice $\zeta_p$. In passing to large inlet angles ($\beta_1' > \beta_{1n}$), the losses in the impulse lattice decrease.

---

[18]The results of the test were obtained on an apparatus with constant back pressure. With increase in the number $M_2$ there is a simultaneous increase in $Re_2$. As was pointed out in the preceding section, the increase in $Re_2$ leads to a lowering of the losses. It may be assumed that for $Re_2$ = constant the change of $\zeta_p$ as a function of $M_2$ would be somewhat sharper.

Detailed investigations of the flow structure show that an increase in $M_2$ leads to an increasing nonuniformity of the field behind the lattice (figs. 7-46 and 7-47).

Analysis of the effect of compressibility on the flow structure in lattices permits drawing the conclusion that the optimum pitch of the profiles decreases as the velocity increases. With decreasing pitch, the nonuniformity of the distribution of the flow between the blades is reduced.



Of practical interest, is the change of the flow direction behind the lattice as a function of $M_2$. Tests show that for $M_2 \leqslant M_{2*}$ the compressibility has only a slight effect on the magnitude of the mean angle behind the lattice. For the majority of reaction lattices, there is first noted a certain decrease and then an increase in $\beta_2$ with increase in $M_2$. For $M_2 > M_{2*}$, the mean angle as a rule increases with increase in $M_2$ (fig. 7-48).

## 7-11. FLOW OF A GAS THROUGH REACTION LATTICES AT SUPERSONIC PRESSURE DROPS

In conventional guide and reaction lattices, the flow velocities at the inlet are subsonic; the transition to supersonic velocities occurs in the interblade passages. We will first consider the fundamental properties and structure of the flow in plane reaction lattices for supersonic pressure drops when

$$p_2/p_{02} > \varepsilon_*$$

The successive change of the supersonic regimes of the flow in a lattice is shown schematically in figure 7-49. In the narrow zone of an interblade passage the critical velocity is established.[19] Behind the trailing edge the pressure is below critical. In the flow about the point A (fig. 7-49(a)) the pressure drops and the fan of expansion ABC fall on the convex side of the neighboring profile and are then reflected from it. The initial and reflected expansion of waves overexpand the flow; that is, the static pressure behind the wave ABC is less than

[19]The transition surface coincides approximately with the narrowest section of the passage. Actually, as a consequence of the nonuniformity of the flow in the converging part and the effect of viscosity, the transition surface has a certain curvature and is displaced upstream.

the pressure at infinity behind the lattice. The further development of the flow depends to a considerable extent on what pressure is established behind the trailing edge or AE. The bounding streamlines of the gas leaving the concave and convex surfaces of the profile approach each other and are then sharply deflected at a certain distance behind the edge. At the boundaries of the initial part of the wake, a system of weak shocks arises which merge with the oblique shock FC, which is formed at the points of discontinuity of the wake.

The oblique shock interacting with the boundary layer on the convex surface of the profile is reflected[20] and again impinges on the trailing wake. Depending on the mean $M_{kp}$ number in this section of the wake, the reflected shock either intersects the wake ($M_{kp} > 1$) or is reflected from its boundary (if $M_{kp} < 1$). Thus, the flow moving along the convex surface of a profile successively passes through the primary and reflected expansion waves and the primary and reflected shocks.

The behavior of the bounding streamlines in passing off the edge depends essentially on the ratio of the pressures at the point D to the pressure behind the trailing edge. If the pressure of the flow at D is greater than that behind the edge section, then there is formed at the point D an expansion wave; and the flow about the edge is improved. The streamline leaves the profile not at point D, but at point E (fig. 7-49(a)). On account of the curvature of the wake EF and the rotating of the flow near the point E, there arises behind the expansion fan DLK a system of weak shocks merging with the curved shock FH, which arises at the point of turning of the boundary of the wake F. The system of the two shocks FC and FH forms the trailing shock of the profile.

If on passing through the system of waves, the pressure of the flow near the point D is below the pressure behind the edge, a shock arises at the point D. In this case the wake increases.

On passing through the system of expansion waves and oblique shocks, the individual streamlines are multiple and variously deformed. On intersecting the primary rarefaction wave, the streamline a-a deflects, turning by a certain angle with respect to the point A (the angle between the tangent to the streamline and the axis of the lattice increases). The reflected wave somewhat decreases the angle of deflection

---

[20] The reflection remains normal even at large angles of incidence of the primary shock ($\varepsilon_2 \rightarrow \varepsilon_*$), since the interaction of the shock with the boundary layer on the convex surface occurs in the zone of negative pressure gradients (the effect of the reflected rarefaction wave). Within a wide range of velocities, the separation of the layer in lattices with relatively small pitch is not observed.

of the streamline. On intersecting the primary shock, the streamline is sharply deflected in the opposite direction (the angle of the streamline with the axis of the lattice decreases). In passing through the reflected shock CP, the angle of the streamline with axis of the lattice again increases.

With an increase in the pressure drop through the lattice, the flow spectrum behind the minimum area section changes; the intensity and character of arrangement of the rarefaction waves and shocks change. The extent (and therefore the intensity) of the rarefaction wave increases. The angles of the primary, reflected, and edge shocks decrease. The point where the oblique shock FC falls (point C) is displaced downstream (fig. 7-49(b)). In correspondence with this, the character of the deformation of the individual streamlines likewise changes. With increase in $\varepsilon_2$ the mean outflow angle increases.



The expansion of the flow within the confines of the lattice ends for a certain relation of the pressures $\varepsilon_2 = \varepsilon_s$. For flow conditions near this limiting regime, the primary shock is curved and forms a certain small angle with the plane of the outlet section. The exact determination of the value $\varepsilon_s$ is therefore difficult. The limiting regime may be considered that for which the primary shock falls at the point D of the edge section (fig. 7-49(c)).

If $\varepsilon_2 < \varepsilon_s$, the expansion of the flow continues beyond the lattice (fig. 7-49(d)). The system of shocks at the trailing edge remains essentially as before, but the wake behind the edge is considerably diminished. The left branch of the tail shock (the shock FC in fig. 7-49) falls in the subsonic part of the wake of the neighboring profile and deforms its boundary; the pressure behind the edge increases. The intensity of the shock increases at the point D', and in certain cases separation of the flow occurs on convex surface of the blade (point D').

The wake behind the edge is greatly weakened. In such regimes separation is observed mainly in lattices with relatively large pitch. It should be remarked that for $\varepsilon_2 \ll \varepsilon_s$ the separations vanish as a rule. The primary shock falls in the supersonic part of the wake (fig. 7-49(e)). The pressure behind the edge drops, and the separation on the back is eliminated. Thus, a very characteristic property of the regimes $\varepsilon_2 < \varepsilon_s$ is the interaction of the primary shock with the wake at the edge.

The shock FC passing through the flow field behind the outlet section sharply decreases the angle of deflection of the flow. This is particularly well marked by the deflection of the wake near the edge.

The above considered schemes of flow are illustrated by photographs of the flow spectra behind the throat and at the exit from the reaction lattice (fig. 7-50). There is here seen the fundamental system of waves and shocks, the deformation of the wake behind the edge for different regimes, and also the interaction between the waves and shocks with the neighboring profiles and wakes.

The flow spectra are given for two lattices: $\bar{t} = 0.543$ (fig. 7-50) and $\bar{t} = 0.86$ (fig. 7-51). The photographs show that in the lattice of small pitch the flow is void of separation for all regimes. In the lattice of large pitch ($\bar{t} = 0.86$), separation of the flow on the back of the profile occurs for the regimes $\varepsilon_2 = 0.288 - 0.258$. In figure 7-51 (photographs (a) and (b)) there is clearly seen the vortex structure of the trailing wake and the considerable nonuniformity of the flow behind the lattice.

Figure 7-52 gives the pressure distribution behind the throat on the convex surface of a profile in a reaction lattice for various ratios $\varepsilon_2 = p_2/p_{01}$. The curves show the considerable nonuniformity of the pressure on the back of the blade. Behind the throat section (i.e., at the points 2 to 6) the expansion of the flow may be observed; the pressure at these points is lower than the pressure behind the lattice. The expansion ends with a sharp increase in the pressure at those points on the convex surface of the blade where the incident and reflected shocks interact with the boundary layer. With an increase in $\varepsilon_2$, the zones of maximum expansion on the convex surface as well as the sharp increase of pressure in the shocks are both displaced along the back toward the trailing edge.

In the regimes of limiting expansion ($\varepsilon_2 = \varepsilon_s$), the pressure along the back of the profile continuously drops. The pressure behind the expansion waves at all regimes $\varepsilon_2 \geqslant \varepsilon_s$ decreases as the pitch increases.

The effect of the pitch on the intensity of the shocks behind the throat is seen in figure 7-53. The character of the curves $\Delta p_2/p_{i,min}$ ($\Delta p_2$ is the increase in pressure through the shock wave impinging on the convex surface of incidence of the shock wave) depends on the pitch. With an increase in $\bar{t}$ the maximum intensity of the shocks at first decreases and then increases. At the same time, the maximum $\Delta p_2/p_{i,min}$ shifts in the direction of higher values of $\varepsilon_2$.

The detailed investigation of the flow in the sections behind the lattice shows that the distribution of the angles and the static pressures is very nonuniform. In figure 7-54(a) is shown the distribution of the local angles of deflection $\beta_{2i} - \beta_{2n}$ over the pitch of the lattice for two regimes. The upper curve corresponds to the flow conditions

shown in figure 7-49(c)($\varepsilon_2 \approx \varepsilon_s$). Ahead of the primary shock, the flow deflections are influenced by the expansion waves; the angles of the streamlines slightly decrease. At $\bar{x} = 0.4$ there is a sharp decrease in $\beta_{2i}$ due to the primary shock. At $\bar{x} > 0.4$ the local angles vary less sharply up to $\bar{x} \approx 0.9$.

From figure 7-54(b) it is seen that the distribution of the static pressures over the pitch is likewise very nonuniform. The static pressure varies with the system of waves and shocks traversing the section investigated.



A large effect on the spectrum of the flow behind the lattice is exerted by the setting angle of the profile (i.e., the angle at the exit). With a change in the angle $\beta_{2n}$ the geometrical parameters of the section behind the throat vary. For the same pressure drop in the lattice ($\varepsilon_2$), the arrangement of the fundamental system of waves and shocks in this section of the lattice varies.

With increase in $\beta_{2n}$ the length of the wall of the section BD (fig. 7-49) is shortened (the pitch is unchanged); the relative effect of the primary expansion wave increases; the angle of deflection increases with increase in $\beta_{2n}$.

The equalization of the flow behind the trailing edge for $M_2 > 1$ occurs at greater distances from the lattice than for $M_2 < 1$. The variation of the distribution curves of $p_{02}/p_{01}$ along the pitch as a function of $\bar{y}$ for $M_2 = 1.58$ is shown in figure 7-54(c).

We note that the equalization of the flow at supersonic velocities is accompanied by a decrease in the static pressure behind the trailing edges.

Supersonic reaction lattices are often used as nozzle lattices (for $\varepsilon_2 < \varepsilon_*$)(fig. 7-55). The interblade passages of such a lattice form supersonic nozzles. At design conditions supersonic velocities may be obtained in such lattices without any essential deviation angle of the flow. On the other hand, expansion may arise in the overhang section of the lattice at design conditions. The expansion wave is formed as a result of the lowering of the pressure behind the trailing edge. In the flow about the trailing edge, as in the subsonic lattice, a second shock at the trailing edge arises. Thus, the same general system of shocks and expansion waves, although they are weaker, is maintained also for the nominal operating regime of the supersonic lattice.

For the off-design regimes ($\varepsilon_2 < \varepsilon_{2comp}$), the fundamental system of waves and shocks is organized in a manner similar to that shown for lattices with converging channels. If, however, the ratio of the pressures $\varepsilon_2$ becomes larger than the computed one, the shocks are moved upstream into the interblade channel, the same way as they are in the one-dimensional supersonic nozzle. It should be borne in mind that, for the same value of $\varepsilon_2$, the shocks in the channels of the supersonic lattice are somewhat weaker than in the Laval nozzle and are situated near the outlet section.

The flow structure in a supersonic reaction lattice is shown in figure 7-56. At increased pressures behind the lattice, a system of two oblique shocks is situated within the channel (fig. 7-56(a)). With an increase in pressure behind the lattice the shocks move toward the outlet section (figs. 7-56(b), (c), and (d)). Near design operation (figs. 7-56(e) and (f)) primary and reflected shocks intersect on the convex surface; behind the lattice a trailing-edge shock may be seen.

The pressure distribution over the profile (fig. 7-57) agrees with the flow picture. At regimes where the relative pressure $\varepsilon_2$ is greater than computed, the pressure rises through the system of shocks. It is characteristic that there is no transverse pressure gradient in the channel between the blades of a supersonic lattice.[21] The velocity field behind a supersonic lattice possesses very great nonuniformity for $\varepsilon_2 < \varepsilon_*$ (fig. 7-57(b)).

## 7-12. IMPULSE LATTICES IN SUPERSONIC FLOW

When the velocities are practically sonic a $\lambda$-shaped shock is formed on the convex side of each profile of an impulse lattice. This system of shocks of small curvature merges to form the bow wave for the neighboring profile (fig. 7-58(a)). Immediately behind each bow wave the flow is subsonic. This scheme of flow evidently can take place only in the case in which the flow accelerates behind each bow wave and then reaccelerates to the velocity $M_1$ ahead of the following shock.

There acceleration of the flow occurs in the expansion waves forming in the flow about the leading edges. As the velocity of the oncoming flow increases, the bow becomes curved and moves toward the inlet edges of the profiles (fig. 7-58(b)). It may be assumed that for velocities corresponding to the flow scheme in figure 7-58(b) the flow behind

---

[21] It may be assumed that the tip losses in such lattices are small even with small blade heights.

the shocks will be turbulent. Because the effect of profiles is communicated upstream in the subsonic region, a nonuniform velocity distribution is established behind the leading shock. The velocities vary periodically in magnitude and direction along the lattice.

For a certain sufficiently large value of $M_1$ the right branches of the shocks merge forming a continuous wavy-shaped shock (fig. 7-58(c)). The left branches of the bow wave are turned into the concave surface of the profile. With further increase in the velocity $M_1$ the angles of the branches of the bow waves decrease; the shocks approach the inlet edges of the lattice. In certain cases at the inlet to the interblade channels there is formed the system of shocks shown in figure 7-58(d). In the system of intersecting and reflected shocks the pressure increases.



The envelope of this system of curved shocks lowers the velocity of the flow to a subsonic value. Supersonic velocities arise again as a result of the expansion on the convex surface. The flow about the trailing edge here occurs with the formation of the known system of expansion waves and shocks. Only for very large supersonic velocities at the inlet does the flow remain supersonic over the entire extent of the interblade channel.

The above considered schemes of formation of shocks at the inlet to an impulse lattice are confirmed by photographs of the flow. In figure 7-59 there are clearly seen the changes in the shape of the bow waves that accompany increases in $M_1$.

The pressure distribution over the profile at supersonic velocities (fig. 7-60(a)) shows that for $M_1 \leq 1.5$ the velocity over a large part of the concave surface is subsonic. For $M_1 > 1.12$, the velocities are supersonic at all points on the convex surface. The point of minimum pressure on the back in the overhang section is displaced with increasing $M_1$ toward the outlet section of the lattice.

The investigation of the flow behind an impulse lattice at supersonic velocities shows that the distribution of static pressures, velocities, and losses over the pitch is very nonuniform.

A change in the inlet angle of the flow greatly affects the structure and intensity of the bow waves, the pressure distribution over the profile, and the flow distribution between the wakes behind the lattice.

The form of the inlet edge of the profile and angle $\beta_{1n}$ have an effect on the structure and, in particular, the intensity of the bow waves. Ahead of an impulse lattice consisting of profiles of small curvature (large angles of the inlet edge $\beta_{1n}$) an over-all wave-shaped

shock is formed instead of the system of shocks shown in figure 7-58(b). The shape of this wave ahead of a lattice of plates for various inlet angles is seen in figure 7-61. Since the formation of such a shock ahead of the lattice is possible in the case where $M_1 \sin \beta_1 > 1$, the number $M_1$ corresponding to the type of shock considered increases as $\beta_1$ decreases.

## 7-13. LOSSES IN LATTICES AT NEAR SONIC AND SUPERSONIC VELOCITIES

The above considered properties of the flow of a gas in plane lattices of different types at large velocities permit an analysis of the behavior of the over-all characteristics of lattices accompanying a change of velocity of the flow ($M_1$ or $M_2$).[22] Figure 7-62(a) shows curves of the loss coefficients for reaction lattices as a function of $M_2$ and the inlet flow angle $\beta_1$. Figure 7-62(b) gives similar curves for impulse lattices.

The curves show that, depending on the entry angle, the pitch, and profile shape, the loss coefficient of reaction lattices may increase or decrease in the region of transonic velocities ($0.8 \leqslant M_2 \leqslant 1.2$). A marked increase of the losses in a lattice occurs at supersonic velocities ($M_2 > 1.2$). The value of $M_2$ for which this increase is observed decreases as the pitch is increased.

The loss coefficients of supersonic lattices increase very sharply with an increase in $M_2$ and reach a maximum value when the relative pressure in the lattice is nearly critical ($M_2 \approx 1$). With a further increase in $M_2$, the coefficient $\zeta_p$ decreases. The losses in a supersonic lattice are a minimum near the computational (design) value of $M_2$. For $M_2 > M_{2comp}$ the loss coefficient increases with the velocity.

From a comparison of the loss curves in a reaction supersonic lattice (fig. 7-62(a)) with those in a one-dimensional supersonic nozzle, it can be concluded that the variation of $\zeta_p$ with $M_2$ is qualitatively the same in both cases. It follows that the shocks in the interblade passages and the separations and vortex formations associated with them have the main influence on the effectiveness of such lattices at off-design regimes. The lowering of the losses in the lattice for $M_2 \leqslant 1$ is explained by the fact that at such regimes the wave and vortex losses

---

[22]The data presented in the present section refer only to lattices of definite geometric parameters.

decrease and then (for small $M_2$) entirely vanish (the interblade passage works as a Venturi tube). As in the case of the single nozzle, the losses in a supersonic lattice at the design and off-design regimes vary as a function of the passage parameter $F_1/F_*$.[23] With an increase in this parameter, the losses for design operation decrease somewhat and increase for $M_2 < M_{2comp}$.

Comparison of the losses in different reaction lattices leads to the conclusion that in a wide range of velocities, lattices with converging interblade channels possess a higher effectiveness than supersonic lattices. Evidently supersonic lattices are suitable for application in the range of large supersonic velocities, but they are only effective for the case where such turbine lattices will always operate near design conditions. The points of intersection of the curves (the points A and A' in fig. 7-62(a)) permit establishing ranges of rational application of the two types of lattices compared.

The losses in an impulse lattice at subsonic velocities increase with increase in the velocity more sharply than those in reaction lattices, and they reach maximum values for $M_1 \approx 0.8$ to 0.9 (fig. 7-62(b)). A further increase in the velocity leads to a certain lowering of the loss coefficient. Thus, in the zone of near sonic velocities $M_2 = 0.9$ to 1.3 the coefficient $\zeta_p$ of an impulse lattice decreases and becomes a minimum at $M_1 \approx 1.2$ to 1.4. For $M_1 > 1.4$ with increasing velocity, $\zeta_p$ again increases.[24]

The lowering of the loss coefficient in an impulse lattice at small supersonic velocities is explained by the improvement of the flow about the inlet edges and on the convex surface of the profile. For $M_2 = 0.7$ to 0.9 flow separations are formed near the inlet part and on the convex surface of the profile; the points of minimum pressure and separation are displaced downstream when supersonic velocities are achieved since the flow in the channel is converging behind the bow waves (fig. 7-60). Also change in the inlet angle has a particular effect on the magnitude of the loss coefficient at supersonic velocities for impulse lattices. For inlet angles less than $\beta_{1n}$ (a "blow" on the concave

---

[23] NACA note: Area ratio, see fig. 7-62(a).

[24] The data presented refer only to the given lattice. With a change in the shape of the profile and the pitch, the character of the dependence of $\zeta_p$ on $M$ may vary.

surface of the profile) the loss coefficient increases. The mean angle of the flow behind the lattice increases with an increase of velocity at supersonic velocities (deflection behind the throat).

## 7-14. COMPUTATION OF ANGLE OF DEFLECTION OF FLOW IN OVERHANG SECTION OF A REACTION LATTICE AT SUPERSONIC PRESSURE DROPS

There exist several methods of determining the angles of deflection of the flow behind the throat of the lattice. The most widespread methods of computation are based on the one-dimensional equations of flow. Assuming that the field of flow in the sections AB (fig. 7-63) and EF (chosen at a large distance behind the lattice) is uniform and neglecting the losses in the lattice up to section AB, the equation of continuity may be written in the form

$$\overline{AB}\rho_2 c_2 = \overline{EF}\rho_{2\infty} c_{2\infty} \sin \beta_{2\infty}$$

or, bearing in mind that for very thin trailing edges

$$\overline{AB} = \overline{EF} \sin \beta_{2n} = t \sin \beta_{2n}$$

we obtain

$$\rho_2 c_2 \sin \beta_{2n} = \rho_{2\infty} c_{2\infty} \sin \beta_{2\infty}$$

We divide both sides of this expression by $\rho_{*1} a_{*1}$; then

$$q_2 \sin \beta_{2n} = q_{2\infty} \frac{p_{02}}{p_{01}} \sin \beta_{2\infty}$$

Taking into account that $\beta_{2\infty} = \beta_{2n} + \delta$, where $\delta$ is the angle of inclination of the flow in the overhang section, we arrive at the equation

$$\delta = \arcsin\left(\frac{q_2}{q_{2\infty}} \cdot \frac{p_{01}}{p_{02}} \sin \beta_{2n}\right) - \beta_{2n} \qquad (7\text{-}60)$$

In the above equation $q_2$ and $q_{2\infty}$ are easily expressed in terms of the pressure ratios $p_2/p_{01}$ and $p_{2\infty}/p_{02}$.

For a reaction lattice, with $p_{2\infty}/p_{02} < \varepsilon_*$, the flow parameters in the section AB will have their critical values when $q_2 = 1$. For a supersonic lattice $q_2 = F_*/F_1 < 1$. By ignoring the losses, Bais related the flow at section AB to that at DH in a form similar to that of formula (7-60)

$$\delta = \arcsin\left(\frac{\sin \beta_{2n}}{q_{2\infty}}\right) - \beta_{2n} \tag{7-60a}$$

With account taken of the losses, formula (7-60a) can be written as

$$\delta = \arcsin\left(\frac{1}{q_{2\infty}} \frac{p_{01}}{p_{02}} \sin \beta_{2n}\right) - \beta_{2n}$$

Replacing $q_{2\infty}$ by $\lambda_{2t}$ and $\zeta_p$ and taking into account the fact that

$$\frac{p_{01}}{p_{02}} = \left(\frac{k-1}{2} M_{2t}^2 \zeta_p + 1\right)^{\frac{k}{k-1}} = \frac{1 - \frac{k-1}{k+1}\lambda_{2t}^2(1-\zeta_p)}{1 - \frac{k-1}{k+1}\lambda_{2t}^2}$$

we obtain after transformations

$$\delta = \arcsin\left[\left(\frac{2}{k+1}\right)^{\frac{1}{k-1}} \frac{1 - \frac{k-1}{k+1}\lambda_{2t}^2(1-\zeta_p)}{\lambda_{2t}\left(1 - \frac{k-1}{k+1}\lambda_{2t}^2\right)^{\frac{k}{k-1}}\sqrt{1-\zeta_p}} \sin \beta_{2n}\right] - \beta_{2n} \tag{7-60b}$$

Whence, it follows that with constant value of the theoretical outflow velocity $\lambda_{2t}$, the angle of deflection increases with an increase in the losses. According to equation (7-60a), the angle of deflection $\delta$ depends not only on the outflow velocity and the losses but also on the angle $\beta_{2n}$.

Formula (7-60) holds only for $\varepsilon_2 \geq \varepsilon_S$, that is, up to the point for which the primary expansion wave impinges on the convex surface of the blade. The angle of deflection corresponding to the limiting expansion over the convex surface of the blade is approximately determined by the relation

$$\delta_S = \alpha_{mS} - \beta_{2n}$$

where $\alpha_{mS}$ is the angle of the characteristic coinciding with the plane AD.

The pressure in the outlet section of the lattice for the regime considered may be determined by the formula

$$\varepsilon_S = \varepsilon_*(\sin \beta_{2n})^{\frac{2k}{k+1}} \tag{7-61}$$

In fact, since

$$\sin(\beta_{2n} + \delta_S) = \sin \alpha_{mS} = \frac{1}{M_{2S}} = \frac{\sin \beta_{2n}}{q_{2S}}$$

we have

$$\left(\frac{\varepsilon_*}{\varepsilon_S}\right)^{\frac{1}{k}} \sin \beta_{2n} = \left(\frac{k+1}{2} \varepsilon_S^{\frac{k-1}{k}}\right)^{\frac{1}{2}}$$

Solving this equation for $\varepsilon_S$, we arrive at formula (7-61).

Making use of the known relation between $\alpha_m$ and $\varepsilon$ and substituting in the particular case $\varepsilon_2 = \varepsilon_S$, we obtain

$$\delta_S = \arcsin \left[ \frac{\left(\frac{k-1}{k+1}\right)^{\frac{1}{2}}}{\sqrt{(\sin \beta_{2n})^{\frac{2(1-k)}{k+1}} - \frac{2}{k+1}}} \right] - \beta_{2n} \tag{7-62}$$

For the one-dimensional case of infinitely thin trailing edges and straight convex and concave surfaces, the exact solution may be obtained by simultaneously solving the equations of continuity, momentum, and energy.

By the equation of energy,

$$\frac{p_2}{\rho_2} + \frac{k-1}{k} \frac{c_2^2}{2} = \frac{p_{2\infty}}{\rho_{2\infty}} + \frac{k-1}{k} \frac{c^2}{2}$$

From the condition of continuity,

$$\frac{\rho_2}{\rho_{2\infty}} = \frac{\lambda_{2\infty}}{\lambda_2} \frac{\sin(\beta_{2n} + \delta)}{\sin \beta_{2n}}$$

Substituting this expression in the equation of energy, we obtain

$$\frac{k+1}{2k} = \frac{1}{k}\frac{p_{2\infty}}{p_2}\frac{\lambda_{2\infty}}{\lambda_2}\frac{\sin(\beta_{2n}+\delta)}{\sin\beta_{2n}} + \frac{k-1}{2k}\left(\frac{\lambda_{2\infty}}{\lambda_2}\right)^2 \tag{7-63}$$

We write the equation of momentum using the component in the direction of the trailing edges in the form

$$\rho_2 c_2^2 t \sin\beta_{2n} + p_2 t \sin\beta_{2n} = \rho_{2\infty} c_{2\infty}^2 t \sin\beta_{2\infty}\cos\delta + p_{2\infty} t \sin\beta_{2n}$$

or

$$\rho_2 c_2 a_* (\lambda_{2\infty}\cos\delta - \lambda_2) = p_2 - p_{2\infty}$$

Since

$$\rho_2 c_2 a_* = q_2 \rho_{*1} a_*^2 = k\varepsilon_* q_2 p_{01}$$

we obtain

$$\frac{\lambda_{2\infty}}{\lambda_2} = \left(\frac{p_2 - p_{2\infty}}{k\varepsilon_* q_2 p_{01}} + 1\right)\frac{1}{\cos\delta} \tag{7-64}$$

If in the section AB the parameters are critical, then

$$\frac{\lambda_{2\infty}}{\lambda_2} = \left[\frac{1}{k}\left(1 - \frac{\varepsilon_{2\infty}}{\varepsilon_*}\right) + 1\right]\frac{1}{\cos\delta}$$

The last expression together with equation (7-63) gives

$$\tan^2\delta + \frac{2k}{k-1}\frac{\varepsilon_{2\infty}}{\varepsilon_*}\frac{\cot\beta_{2n}\tan\delta}{k+1-\frac{\varepsilon_{2\infty}}{\varepsilon_*}} - \frac{k+1}{k-1}\left(\frac{1-\frac{\varepsilon_{2\infty}}{\varepsilon_*}}{k+1-\frac{\varepsilon_{2\infty}}{\varepsilon_*}}\right)^2 = 0$$

whence

$$\tan\delta = \frac{\sqrt{\left(\frac{k}{k-1}\frac{\varepsilon_{2\infty}}{\varepsilon_*}\cot\beta_{2n}\right)^2 + \frac{k+1}{k-1}\left(1-\frac{\varepsilon_{2\infty}}{\varepsilon_*}\right)^2} - \frac{k}{k-1}\frac{\varepsilon_{2\infty}}{\varepsilon_*}\cot\beta_{2n}}{k+1-\frac{\varepsilon_{2\infty}}{\varepsilon_*}} \tag{7-65}$$

Approximately, for $\delta \leq 10^{\circ}$, we obtain

$$\delta \approx \frac{k+1}{2k} \frac{\left(1 - \frac{\varepsilon_{2\infty}}{\varepsilon_*}\right)^2 \tan \beta_{2n}}{\frac{\varepsilon_{2\infty}}{\varepsilon_*}\left(1 + k - \frac{\varepsilon_{2\infty}}{\varepsilon_*}\right)} \qquad (7\text{-}65a)$$

The above accurate solution obtained by G. Y. Stepanov permits determining the wave losses in the lattice. The coefficient of wave losses is expressed by the formula

$$\zeta_b = 1 - \frac{\lambda_2^2}{\lambda_{2t}^2}$$

or after substituting for $\lambda_2$

$$\zeta_b = 1 - \frac{\left[\frac{1}{k}\left(1 - \frac{\varepsilon_2}{\varepsilon_*}\right) + 1\right]^2}{\frac{k+1}{k-1}\left[1 - \varepsilon_2^{\frac{k-1}{k}}\right]\cos^2\delta}$$

For computing the flow behind the throat of the lattice, the method of characteristics may be applied. We consider a lattice of plates of small curvature with straight, infinitely thin trailing edges (fig. 7-64(a)) and set up the boundary conditions at the point where the streamlines coming off the two sides of each plate merge. The streamline 1-1 moving along the convex surface of the plate intersects both the primary and reflected expansion waves, while the streamline 2-2 coming off the concave surface intersects only the primary waves. In the plane of the hodograph the region of the flow in the section AB is expressed by the point corresponding to the end of the vector $\lambda_1 = 1$ (fig. 7-64(b)). The velocity of the streamline 2-2 after passing through the primary expansion wave is determined by the vector $\lambda_2$, while the velocity of the streamline 1-1 after passing through both the primary and reflected waves is determined by the vector $\lambda_3$. The boundary conditions near the point A for two merging streamlines of gas are the conditions that the static pressures are equal and the velocity vectors are parallel. These conditions are satisfied if the oblique shocks $K_1$ and $K_2$ are formed at the point A, the direction of these shocks shown in figure 7-64(a). If the angle $\delta_1$ is small, the primary shock $K_1$ may be considered as a characteristic, while for computing the edge shock $K_2$ the method of characteristics may be used. We here neglect the wave losses in the shocks. It is evident that the direction of the shock $K_2$ coincides with the

normal to the epicycloid of the second family at the point d located at the center of the segment bc. With this simplification of the problem, the wake (which for an infinitely thin edge is considered to be between the streamlines 1-1 and 2-2) in the immediate neighborhood of the point A has the direction of the vector $\lambda_2$ (the dot-dash line in fig. 7-64(a)). The velocities and other parameters of the flow for the remaining streamlines are determined after computing the interaction of the primary and reflected expansion waves.



The entire region of flow behind the throat can be divided into three zones (fig. 7-64(a)): I - the zone of influence of the primary expansion wave (for the lattice considered, this region transforms into a point), II - the zone of interaction of the primary and reflected waves, and III - the zone of influence of the reflected wave (in the plane of the hodograph, this zone corresponds to the characteristic of the second family bc).

The region of interaction of the primary and reflected waves of rarefaction (zone II) may be computed once for all, using the minimum value of the angle $\beta_{2,min} = 7^\circ$ to $10^\circ$. For any other angle $\beta_{2n} > \beta_{2,min}$ the computation of the flow downstream of the throat is carried out in the following manner. We draw the x-axis at the given angle to CB (fig. 7-64(c)) and find the mean pressure in the section AB = t

$$p_S = \frac{1}{t}\int_0^t p_{Si}dx$$

characterizing the regime of the limiting expansion. For all regimes $\varepsilon_* > p_2/p_{01} > p_S/p_{01}$ the zone of interaction II will be bounded by the broken characteristics, for example, AB', AB", AB"' . . . (fig. 7-64(c)). To each value of the pressure drop in the lattice corresponds a fully determined position of the points B', B", B"' . . . . Carrying out successively the computation of the flow for different positions of the characteristics AB', AB", etc., we establish the distribution of the pressures (velocities and local angles) over the pitch AB in the zones II and III and obtain the mean pressure behind the lattice

$$p_{2,cp} = \frac{1}{t}\int_0^t p_{2i}dx$$

In this way the computation of the local parameters of the flow behind the lattice is conducted for the entire group of possible flow regimes in the lattice, and the relation is established between the position of the points B', B", etc., and the pressure drop in the lattice.

The mean angle of deflection of the flow for a given regime may be obtained from equation (7-21):

$$\tan(\beta_{2n} + \delta_{cp}) = \frac{2\int_0^t q_i \lambda_i \sin^2(\beta_{2n} + \delta_i)dx}{\int_0^t q_i \lambda_i \sin 2(\beta_{2n} + \delta_i)dx}$$

where $q_i$, $\lambda_i$, and $\delta_i$ are, respectively, the local reduced flow rate, nondimensional velocity, and angle of deflection.

For a lattice of profiles with finite thickness of the trailing edges, the computation of the flow in the overhang section by the method of characteristics is considerably more complicated. In this case it is necessary to know how the pressure varies behind the trailing edges as a function of the geometrical parameters of the profile and the lattice and of the flow regime. Such a relation

$$\frac{p_{kp}}{p_0} = f(M_2, \bar{t}, \bar{\tau})$$

can be established only experimentally. Then, replacing the actual lattice by a lattice of planes, the trailing edges of which serve as the sources of disturbances uniformly distributed in the field of sonic (or supersonic) flow, the intensity of the expansion waves may be found. From the boundary conditions at the edge the system of additional expansion waves and shocks is determined.

An important advantage of the method of characteristics is the possibility of constructing the spectrum of the flow on the convex section behind the throat and at different distances from the lattice and of determining the nonuniformity of the field of velocities and pressures in different sections.

A comparison of the most widespread and accurate methods of computing the deviation angles with test data (for two reaction lattices) is shown in figure 7-65. It is seen from the latter that, for lattices of small pitch and consisting of profiles with thin trailing edges, formula (7-65) and the method of characteristics give results that satisfactorily agree with experiment. For small values of $\delta(\varepsilon_2 \geq 0.35)$ the equation of continuity (7-60(b)) may likewise be used for approximate computations. For lattices of large pitch, only the method of characteristics gives results which are in good agreement with experiment.

## 7-15. CHARACTERISTIC FEATURES OF THREE-DIMENSIONAL FLOW IN LATTICES

As was already pointed out, the ring lattices of turbomachines consist of radially arranged blades of finite height (length). The shape of the interblade passages of the lattice varies in the radial direction. In condensation turbines, lattices with variable height blades are used. The guide lattices are always shrouded. Rotating lattices are sometimes designed without shrouds.

These construction features of real lattices have an important influence on the flow. The phenomena observed in three-dimensional lattices are not taken into account in the analyses of two-dimensional flow. On the basis of test data we shall analyze the special features of three-dimensional flow in a straight row of lattices.

In these lattices secondary flows are formed near the tips of the profile on the convex surface of the blade. The cause of formation of secondary flows in the interblade channels of a lattice is the viscosity of the gas and the transverse pressure gradient arising from the curvature of the channels.

Because of the increased pressure on the concave surface of the blade, the gas particles flow toward the convex surface of the blade (fig. 7-66(a)). For sufficiently high ratios $l/a_2$ (see fig. 7-66(b)), the secondary motion of the gas over the concave surface is only achieved with difficulty, because the particles must move over a long path over which there is friction. Such a flow from the concave surface to the convex surface of the neighboring profile is possible only in the boundary layer along the end walls bounding the channel. The peripheral flow of the gas in the boundary layer therefore starts on the concave surface at the tips of the profile (near the end walls) and continues over the end walls toward the convex surface of the blade. As experiment shows, there occurs a nonuniform distribution of the pressures over the height of the blade; the pressure is lower on the concave surface near the end walls, while at the tips of the convex surface of the blade the pressure is higher than it is in the middle section. Along the end walls of the channel, the pressure drops in the direction from the concave to the convex side of the blade. At the tips and along the convex surface of the blade, the boundary layer flowing from the end walls encounters the boundary layer moving along paths parallel to the end walls. As a result, near the tips of the blade and on the convex surface rapid growth of the boundary layer occurs; the thickness of the layer increases sharply. In the majority of cases this leads to a local separation of

the layer and therefore to the formation of vortices.[25] At the same time, because of the motion of the boundary layer from the concave surface to the convex surface of the blade, compensating flows are formed at the blade tips which are directed from the convex surface toward the concave surface. These flows, together with the boundary layer separation on the convex surface, form vortex regions (trailing vortex) near the ends (butt faces) of the channel walls.

In this way, at the convex surface of the blade near the tips, a vortex pair arises consisting of two vortices whose direction of rotation does not coincide with the direction of the circulation about the profile.[26] The vortices rotate toward one another in correspondence with the direction of motion of the gas in the boundary layers at the plane walls (figs. 7-66(b) and (c)) and induce a field of velocities normal to the streamlines of the primary flow (fig. 7-66(d)), which leads to a certain increase in the outlet angle of the flow from the lattice.

In the photographs of the wakes of the flow (fig. 7-67) there is clearly seen the secondary flow of the boundary layer on the end walls. Behind the points where the vortices arise, the secondary flow of the gas continues to be associated with the boundary layers on the plane walls and the convex surface of the blade; the vortices are enlarged toward the outlet section. On account of the growth of the vortices, their axes arrange themselves with a certain inclination to the plane walls.

At small ratios $l/a_2$, the vortex regions are propagated over the entire section of the channel forming a vortex pair characteristic of curved channels of square section. The over-all vorticity of the flow sharply increases.

---

[25]Depending on the shape of the profile and of the interblade channel and also on the flow regime in the lattice (inlet angle, $M_2$ and $Re_2$ numbers) the separation of the boundary layer on the convex surface may not occur. Tests show that separation does not occur for large inlet angles and small flow velocities.

[26]In connection with the question as to the mechanism of formation of secondary flows in the lattice, it should be remarked that attempts to make use of the theory and computation procedure of the induced drag of a wing of finite span for determining the tip losses in lattices did not give any essential results. The tip losses in a lattice and the induced drag of a wing have a different origin. It is sufficient to state that the tip phenomena in a lattice arise from the viscosity of the fluid, whereas the formation of trailing vortices from the tips of a wing of finite span are not directly connected with the viscosity; the tip vortices of a wing should exist for the flow of an ideal fluid also.

The experimental investigations confirm the occurrence of separation and vortices in a row of straight blades. The distribution of the dynamic pressure and the static pressure over the height of the blade near the convex side in the nucleus of the flow and at the concave side in the narrow section of the channel in figure 7-68(a) shows the characteristic variation of these parameters in vortex regions. In the vortex zone $\overline{p}_{0i}$ and $\overline{p}_i$ decrease; this decrease does not appear in the nucleus of the flow or at the concave surface. In the outlet section of the lattice the picture of the distribution of $\overline{p}_{0i}$ and $\overline{p}_i$ remains qualitatively the same (fig. 7-68(b)). The zones of reduced values of $p_{0i}$ are displaced from the plane walls. The dips in the curves are more marked.

The separation of the boundary layer on the back of the blade and the formation of vortices are a source of considerable loss of energy, particulary for relatively small blade heights. The change in the geometric parameters of the straight lattice and, in particular, of the relative height and pitch affects the magnitude of the tip losses.

With decrease in the height $\overline{l}_a$ the vortex regions approach each other (fig. 7-69(a)) and are slightly shifted toward the side walls. The strength of the vortices, within definite limits of the change of $\overline{l}_a$, practically does not change. Only for $\overline{l}_a \leq 2$ is there a noticeable increase in the effect of the vortices in the nuclear flow (the values of $\overline{p}_{0i}$ decrease). For lattices of height $\overline{l}_a < 1.7$, the entire flow in the channels is vortical and the pressure of complete stagnation in the nucleus is lowered.

From this it follows that the absolute magnitude of the losses in vortical regions does not change with decrease in the height of the blades up to certain limits. The relative losses change in inverse proportion to the height $\overline{l}_a$. With increase in the pitch of the profiles (fig. 7-69(b)) the strength of the tip vortices increases, and there occurs a certain displacement of the zone of maximum losses away from the end walls.

A large effect on the tip losses is exerted by the curvature of the interblade channels. As the curvature increases the losses increase. This trend is particularly intense for lattices of small height.

The flow regime, that is, the inlet flow angle and the $Re_2$ and $M_2$ numbers, has an effect on the magnitude of the tip losses. With an increase in the entry angle of the flow (fig. 7-70) the strength of the secondary flows decreases. We may note that at large entry angles the transverse pressure gradient in the interblade channels decreases. At the same

time there is a lowering of the intensity of the secondary flow of the boundary layer toward the convex surface of the blade, the thickness of the layer on the back decreases and the vorticity losses decrease. An increase in the velocity of the subsonic flow in the lattices leads to a decrease in the tip losses, a fact which is evidently explained by the decrease in thickness of the boundary layer.

The investigation of the three-dimensional flow in lattices of straight blades qualitatively shows the same change of the mean (averaged over the pitch) loss coefficients near the end walls for all lattices. With an increasing distance from the end walls, the loss coefficient sharply decreases at first and at a small distance reaches the minimum value beyond which it again increases. In the zone of lowering of $\zeta_p$ there is found a decrease in the thickness of the boundary layer on the convex surfaces and of the depth of the end dips. The character of the variation of $\zeta_p$ over the height for short blades for different velocities is seen in figure 7-71. The curves in figure 7-71 show clearly the decrease in $\zeta_p$ with an increase in $M_2$ for $M_2 < 1$.

CA-10 back

In correspondence with the above-mentioned effect of the curvature of the channels and the inlet angle, a certain relation must exist between the profile and tip losses. In lattices with large profile losses there are found also increased tip losses.[27] From a consideration of the scheme of formation of the tip losses in a straight lattice it follows that the measures taken to decrease the transverse pressure gradient in the interblade channel and therefore in lowering the strength of the peripheral flows in the boundary layers greatly decrease the tip losses. Of great importance is also the character of the velocity distribution over the height at the entry to the lattice. With a nonuniform velocity distribution over the height at the entry the tip losses increase. In this connection it should be remarked that the use of overlap[28] in the real lattices of turbomachines leads to a sharp increase in the tip losses.

In cylindrical lattices, the character of the tip phenomena changes somewhat. Because of the change of the pitch of the profile over the radius and the occurrence of a radial pressure gradient, the symmetry of the vortices arrangement is disturbed. Both vortices are displaced along the radius from the casing toward the hub of the annular lattice.

---

[27]It is assumed that all fundamental geometrical parameters of the lattices compared remain the same (pitch, setting angle, and height of blades).

[28]By overlap is meant the difference in heights of two neighboring lattices. As a rule the height of the rotating lattice is chosen to be greater than the height of the guide lattice.

The intensity of the upper vortex thereby increases, while that of the lower decreases (fig. 7-72). The radial pressure gradient in an annular lattice is the cause of the additional losses of energy since the peripheral flows in the boundary layer are increased by such gradient.

In conclusion it should be emphasized that, for lattices with small relative height, the value of the optimum pitch must be determined after account has been taken of the tip phenomena. The optimum pitch may decrease in comparison with that of a plane lattice.



## Classification of the Losses in Lattices

The results of theoretical and experimental investigations considered in this chapter of the flow of a gas through turbine lattices permit classifying the energy losses in lattices according to the following scheme:

A. Profile losses (in the plane lattice)

(1) Losses by friction in the boundary layer on the profile

(2) Vorticity losses by the separation of the flow on the profile

(3) Vorticity losses behind the trailing edge (edge losses)

B. Losses in three-dimensional lattices (in addition to those of group A)

(1) Losses produced by friction at the bounding walls of the lattice over the height and due to peripheral (secondary) flows in the boundary layers

(2) Losses in the thickened layers on the back of the blade and vorticity losses due to separation of the layer at the tips and the formation of vortices

C. Wave losses (in addition to those of groups A and B at near sonic and supersonic velocities)

In the general case, for the investigation of lattices of turbine stages under actual conditions, there are added the losses arising from the unsteadiness of the flow and the heat losses (when cooling is employed).

As was stated above, only the friction losses in the lattice can be determined by computation at the present time. The theoretical methods of computing a potential flow through a lattice and the semiempirical methods of computing the boundary layer permit solving this part of the problem with satisfactory accuracy. The total losses in a lattice can be determined only experimentally. The physically evident connection between the geometrical parameters of the profile and lattice and the magnitude of the losses does not at the present time have an exact mathematical expression.

Translated by S. Reiss
National Advisory Committee
for Aeronautics

## BIBLIOGRAPHY

1. Kochin, N. E.: Hydrodynamic Theory of Lattices. GITTL, 1949.

2. Simonov, L. A.: Computation of the Flow About Wing Profiles and the Construction of a Profile from the Distribution of the Velocities on Its Surface. PMM, vol. 11, no. 1, 1947.

3. Simonov, L. A.: Application of the Electrohydrodynamic Analogy to the Computation of Hydroturbines. Nauchnye zapiski ESMMI, vol. 6, 1940.

4. Samoilovich, G. S.: Computation of Hydrodynamic Lattices. Prikladnaya matematika i mekhanika, vol. 14, no. 2, 1950.

5. Ginzburg, B. L.: Computation of the Potential and Velocity of a Plane Parallel Flow About a Lattice of Circular Cylinders. Trudy TsKTI, no. 18, 1950.

6. Zhukovskii, M. I.: Computation of the Nonvortical Flow About a Lattice of Profiles with Variation of Pitch and Angle of Setting. Teploperedacha i aerogidrodinamika, no. 8, 1950.

7. Blokh, E. L.: Investigation of a Plane Lattice Consisting of Theoretical Profiles of Finite Thickness. Trudy TsAGI, no. 611, 1947.

8. Loitsianskii, L. G.: Resistance of a Lattice of Profiles in a Gas Flow with Subsonic Velocities. Prikladnaya matematika i mekhanika, vol. XIII, no. 2, 1949.

9. Deich, M. E.: The Problem of the Tip Losses in the Guide Vanes of Steam Turbines. Sovetskoe kotloturbostroenie, no. 6, 1945.

10. Markov, N. M.: Computation of the Aerodynamic Characteristics of a Plane Lattice of Profiles of Axial Turbomachines. Mashgiz, 1952.

11. Markov, N. M.: Experimental Investigation of the Boundary Layer in the Channel of a Reaction Turbine. Sovetskoe kotloturbostroenie, no. 6, 1946; Kotloturbostroenie, no. 2, 1947.

12. Stepanov, G. Y.: Hydrodynamic Investigations of Turbine Lattices. Obzornyi byulleten aviamotorostroeniya, no. 4 and 4, 1949.

13. Povkh, I. L.: The Effect of the Pitch on the Aerodynamic Characteristics of Turbine Profiles in a Lattice. Kotloturbostroenie, no. 6, 1948.

14. Povkh, I. L.: Computation of Efficiency and Resistance of Lattice Profiles. LPI, 1952.

15. Sknar, N. A.: Experimental Investigation of Reaction Lattices of Profiles. Teploperedacha i aerogidrodinamika, no. 18, 1950.

16. Gukasova, E. A.: Experimental Investigation of Impulse Lattices of Profiles. Teploperedacha i aerogidrodinamika, no. 18, 1950.

17. Dromov, A. G.: Effect of Periodic Variation of Flow in a Turbine Stage on the Losses of Impulse Blades. Izvestiya VTI, no. 1, 1948.

18. Yakub, B. M.: Investigation of the Flow Behind the Outlet Edges of Nozzles. Izvestiya VTI, no. 11, 1948.

19. Gurevich, Kh. A.: Effect of Pitch and Angle of Attack on the Aerodynamic Characteristics of Impulse Turbine Profiles. Trudy LPI im. M. I. Kalinina, no. 1, 1951.

20. Rodin, K. G.: On the Tip Losses of Energy in Turbine Blade Lattices, Trudy LPI im. M. I. Kalinina, no. 1, 1951.

21. Yablonik, R. M.: Some Results of Simultaneous Tests of Two Turbine Lattices. Trudy LPI im. M. I. Kalinina, no. 1, 1951.

22. Kirsanov, V. A.: Investigation of the Flow in Lattices of Turbine Profiles for Large Subsonic Velocities. TsKTI, 1952.

23. Stechkin, B. S.: Axial Compressors. izd. VVIA im. N. E. Zhukovskogo, 1947.

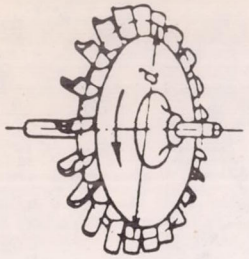

(a) Ring (cylindrical) lattice.

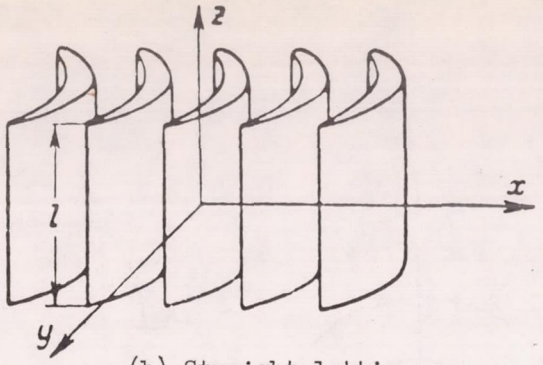


(b) Straight lattice.

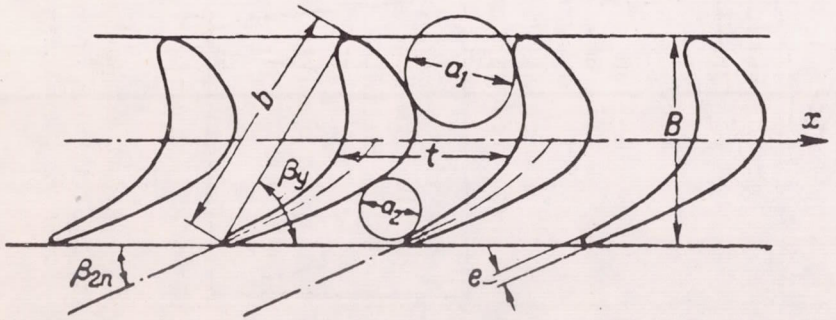


(c) Plane lattice.

Figure 7-1. - Geometrical parameters of lattice.

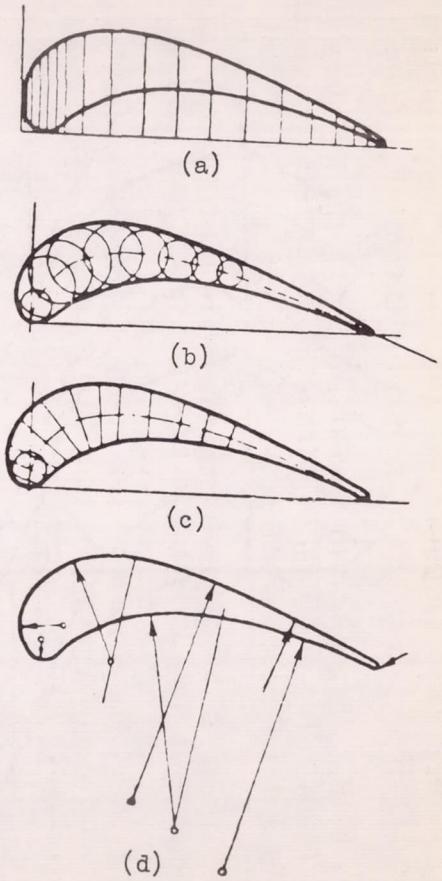


Figure 7-2. - Various methods of specifying profile of blade.

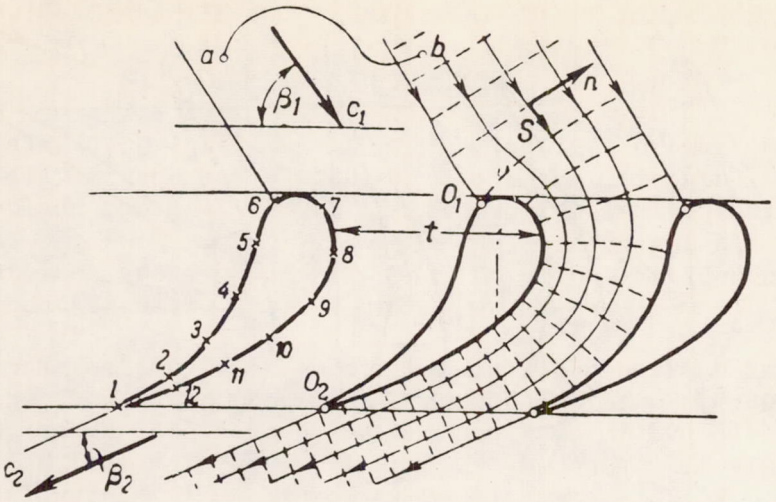


(a) Equipotential lines and streamlines.

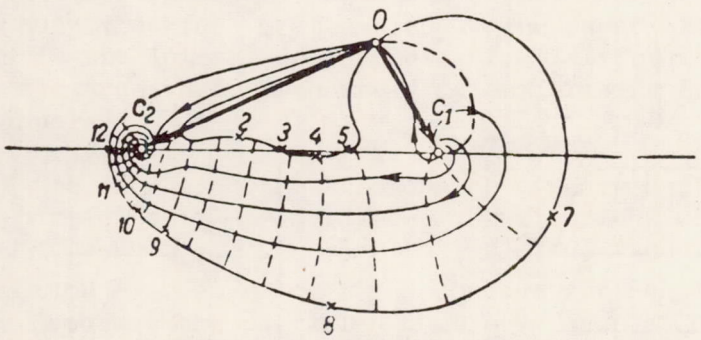


(b) Hodograph of velocity.

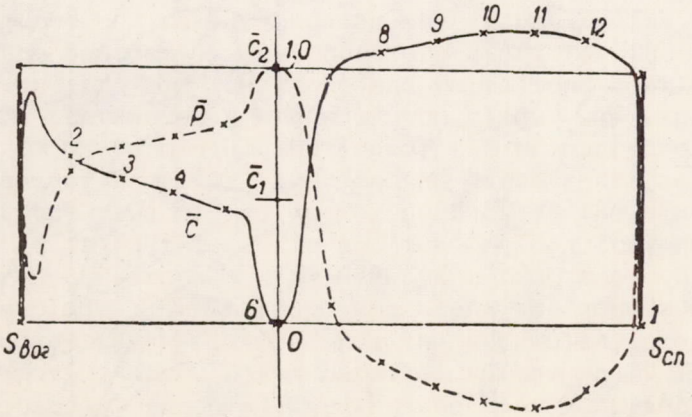


(c) Distribution of relative velocities and of pressure coefficients over the profile.

Figure 7-3. - Flow of ideal incompressible fluid through reaction lattice.

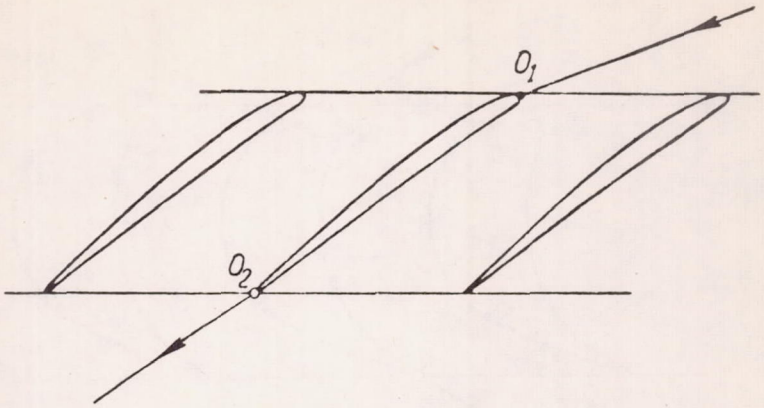


(a) Profile of lattice.

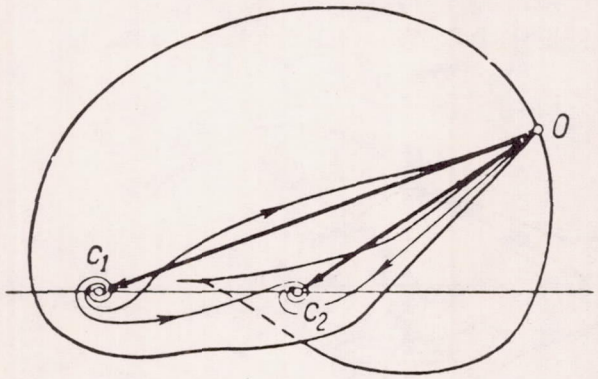


(b) Hodograph.

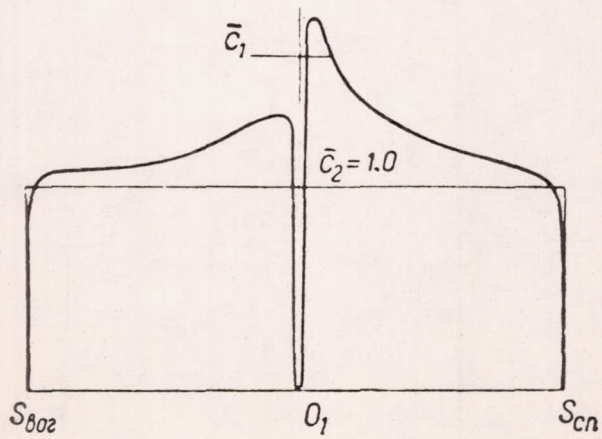


(c) Distribution of relative velocities over profile.

Figure 7-4 (A). - Flow of an ideal incompressible fluid through compressor lattice.

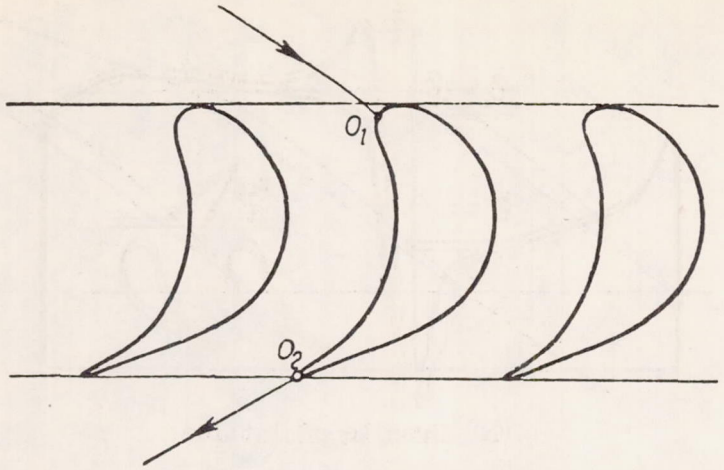


(a) Profile of impulse blade.

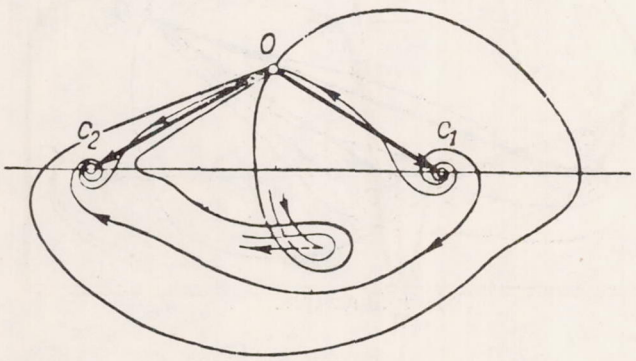


(b) Hodograph.

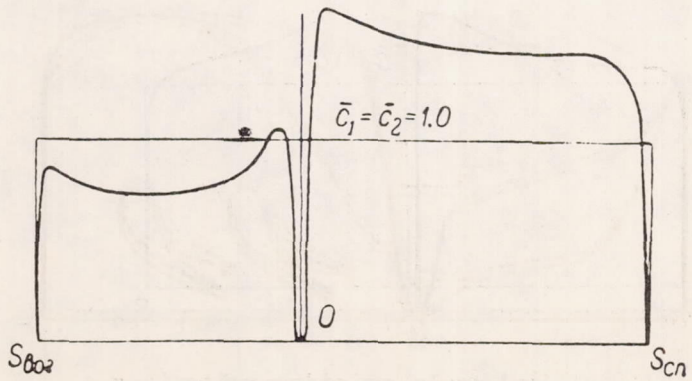


(c) Distribution of relative velocities over profile.

Figure 7-4. - Flow of ideal incompressible fluid through impulse lattice.

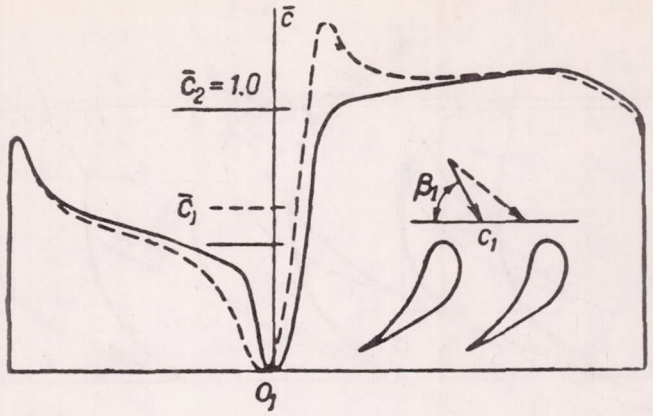


(a) Inlet angle $\beta_1$.

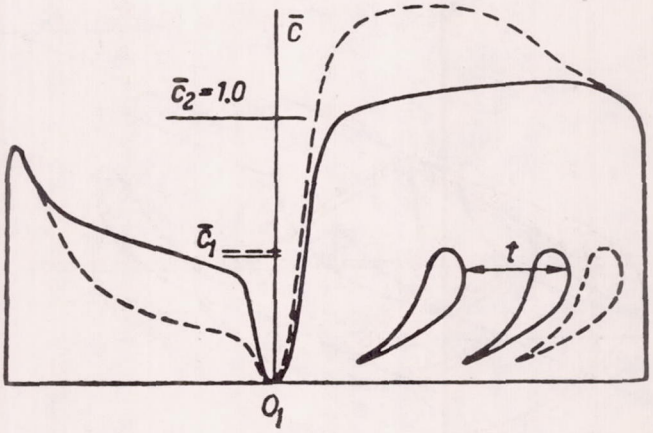


(b) Pitch t.

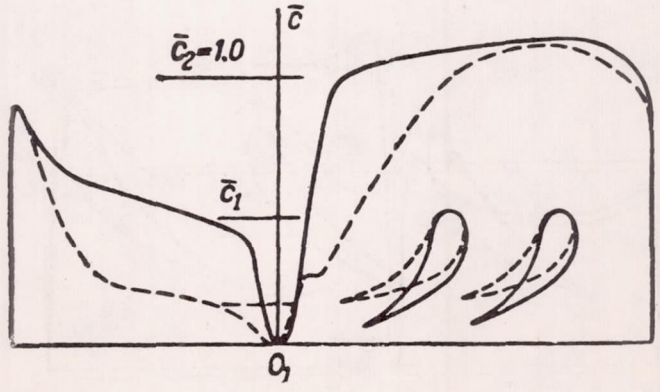


(c) Angle of setting $\beta_y$.

Figure 7-5. - Effect of inlet angle, pitch, and setting angle on relative velocity distribution over profile of lattice.

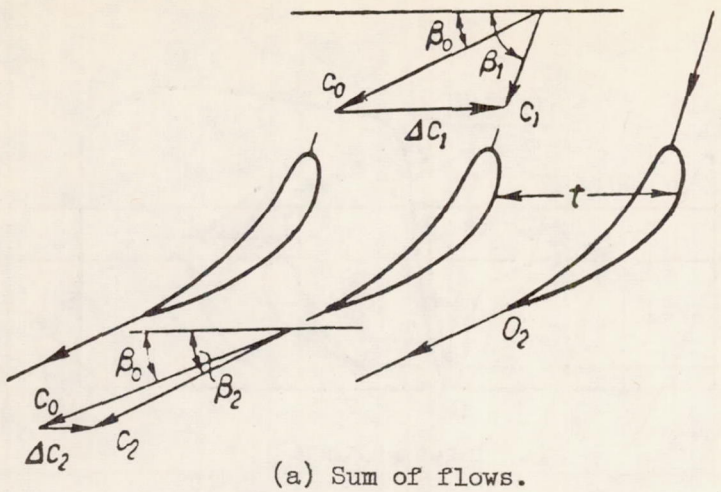


(a) Sum of flows.

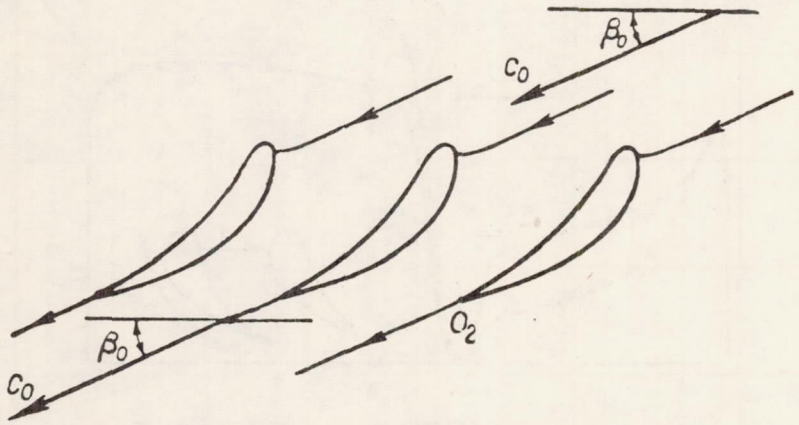


(b) Noncirculatory flows.

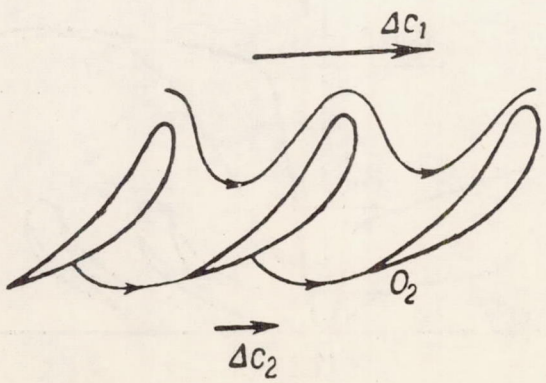


(c) Circulatory-axial flows.

Figure 7-6. - Flow of ideal incompressible fluid through lattice of blades.

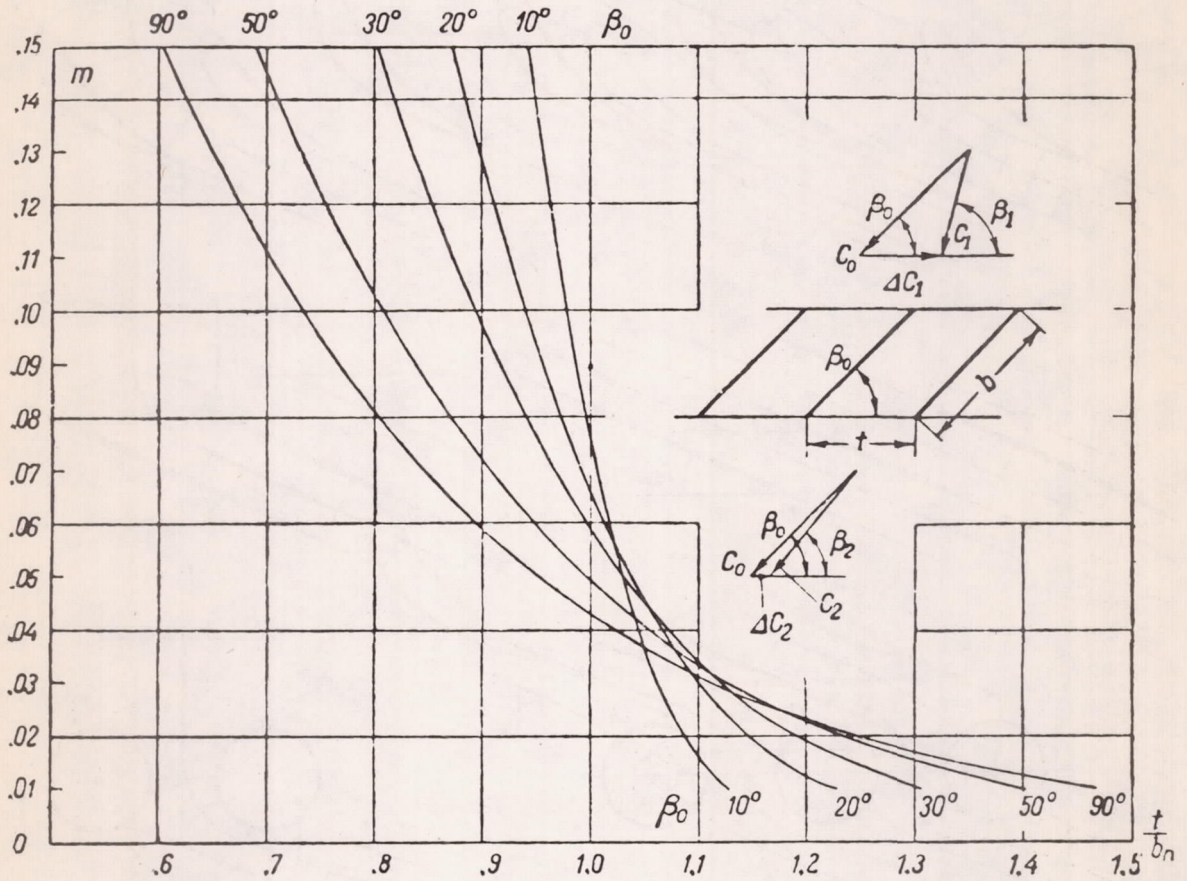


Figure 7-7. - Dependence of the coefficient $m = \Delta c_2/\Delta c_1$ on pitch and setting angle of lattice of plates. [NACA note: The abscissa should obviously be $\frac{bn}{t}$ instead of $\frac{t}{bn}$.]

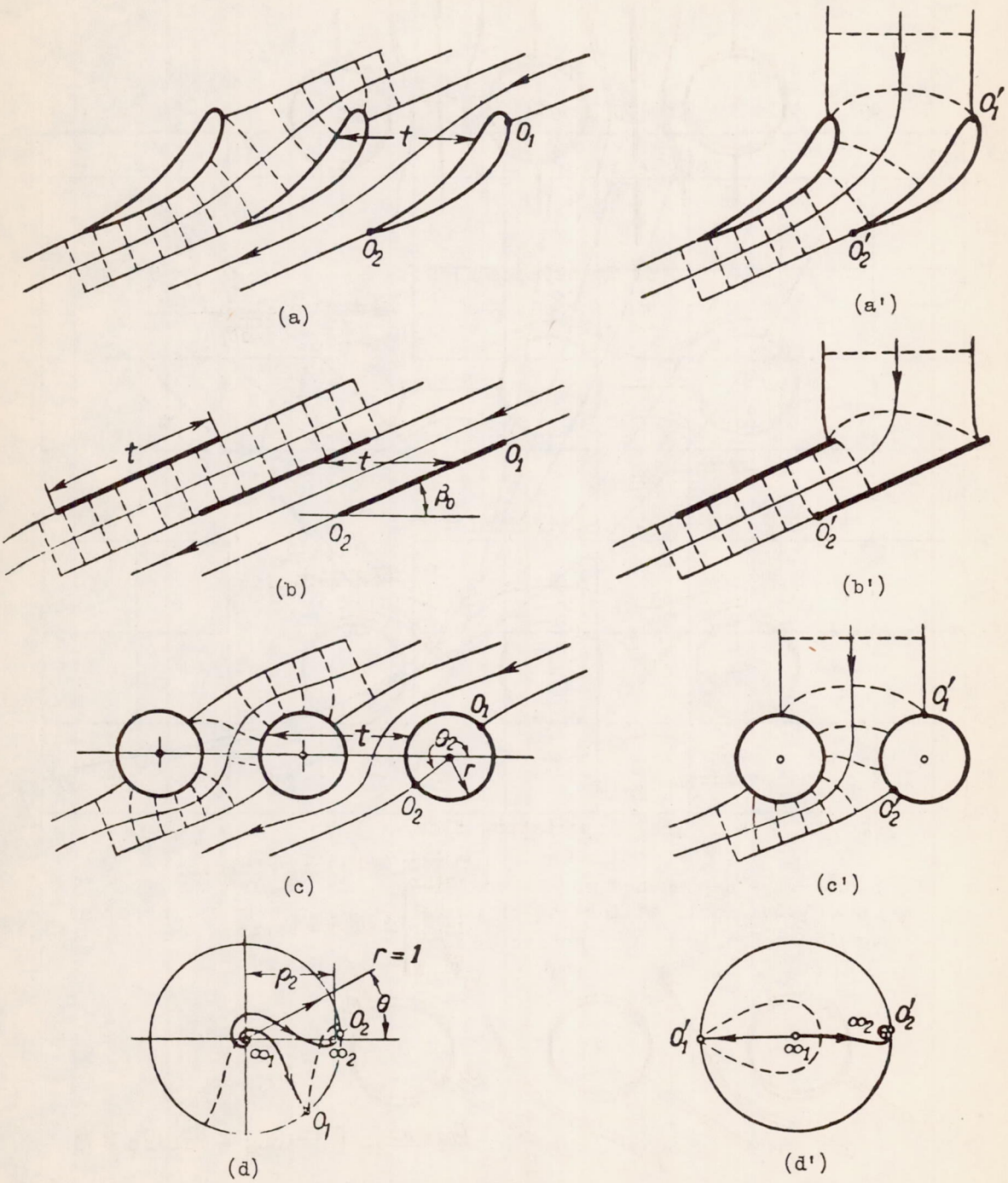


Figure 7-8. - Examples of conformal transformation of lattice.

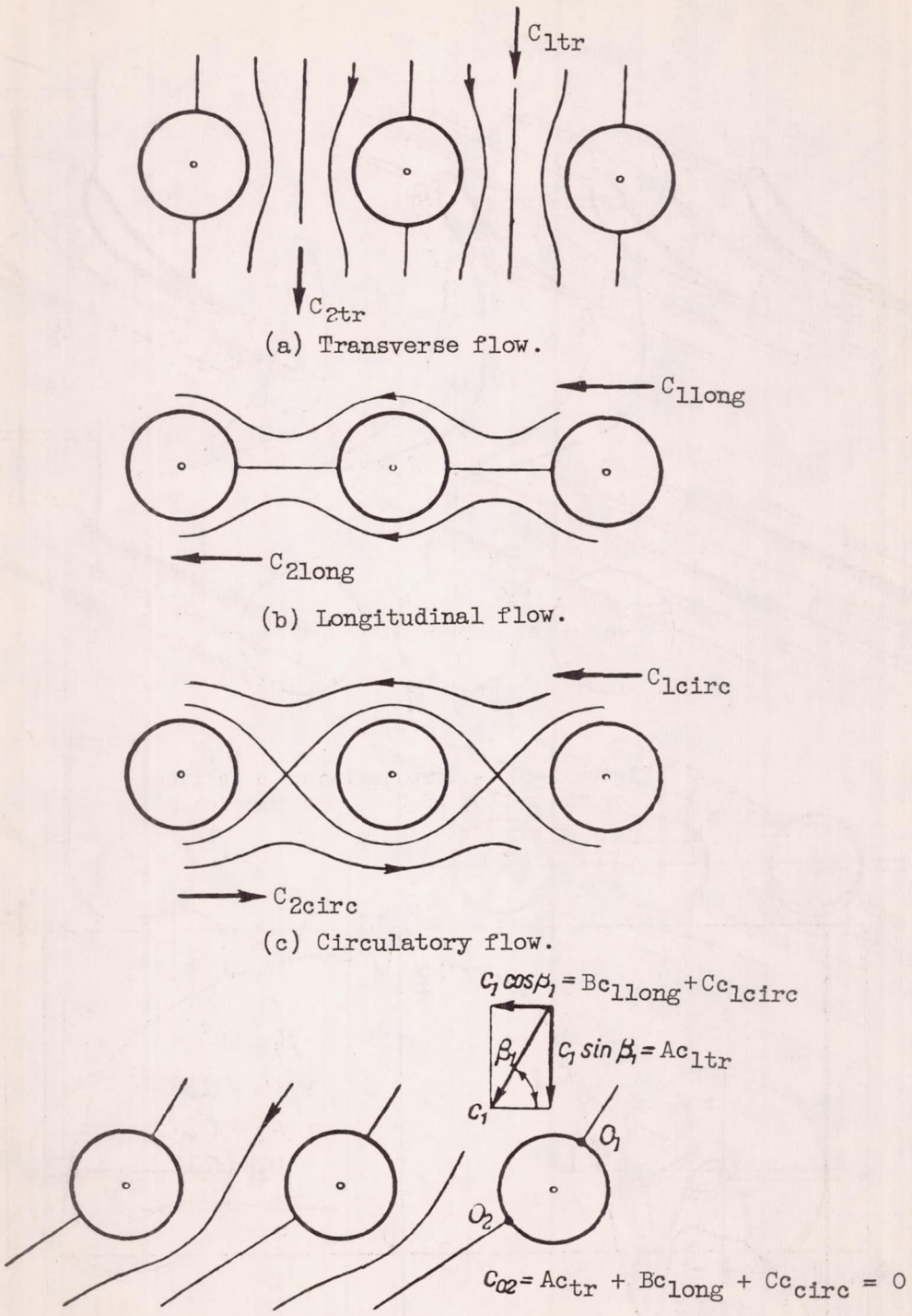


(a) Transverse flow.

(b) Longitudinal flow.

(c) Circulatory flow.

(d) Sum of flows.

Figure 7-9. - Flow of conformal transformation of lattice of circles.

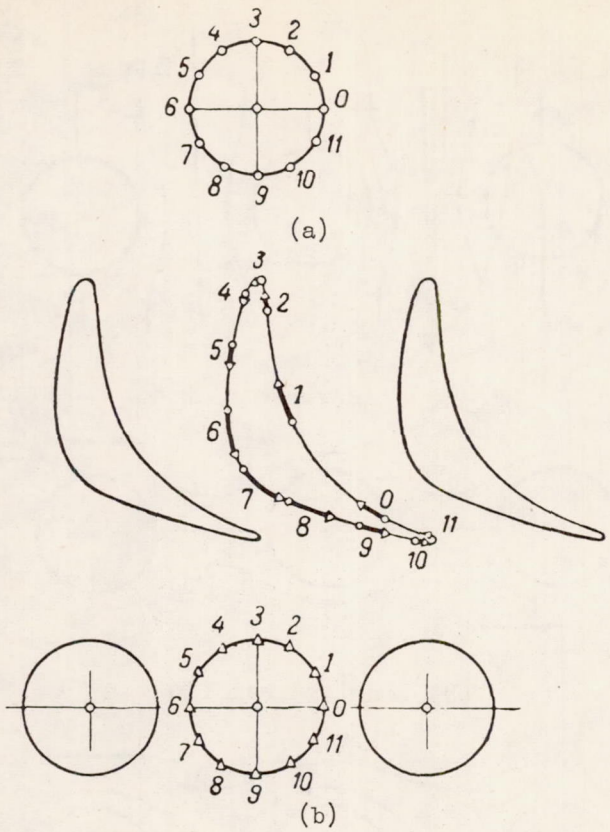


Figure 7-10. - Computation of a lattice by the method of G. S. Samoilovich.

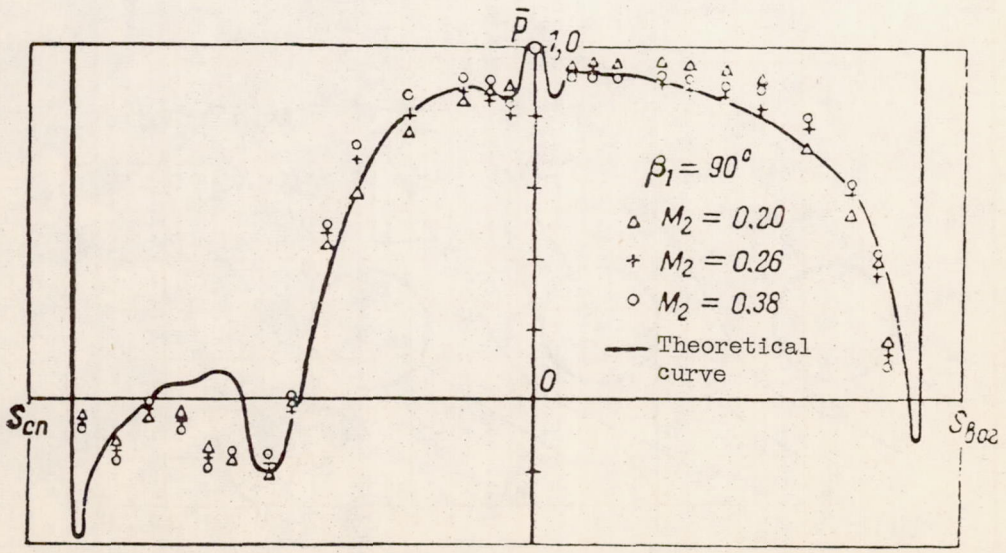


Figure 7-11. - Comparison of the theoretical and experimental pressure distribution over a lattice profile.

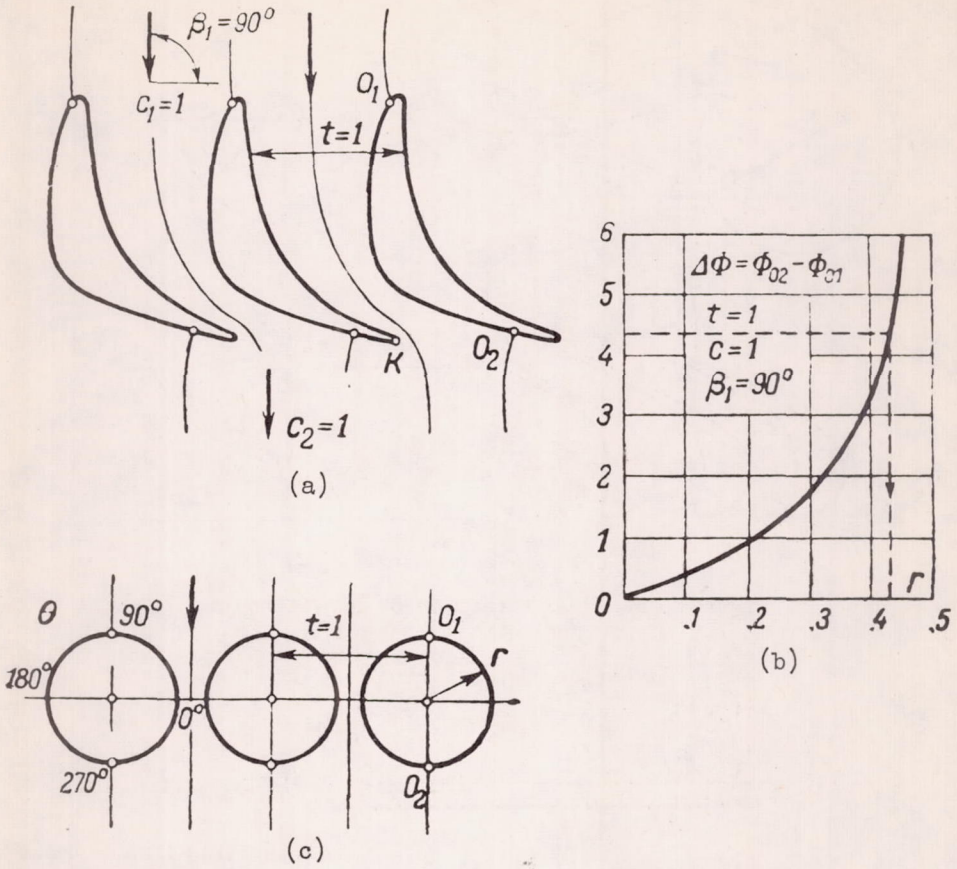


Figure 7-12. - Determination of an equivalent lattice of circles.

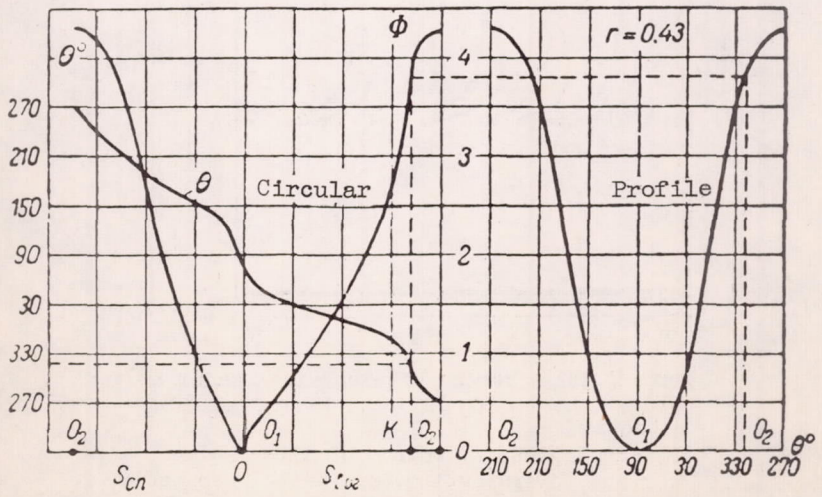


Figure 7-13. - Determination of the correspondence of the points of the profile with the circle ($t = 1$, $c_1 = 1$, $\beta_1 = 90^\circ$).

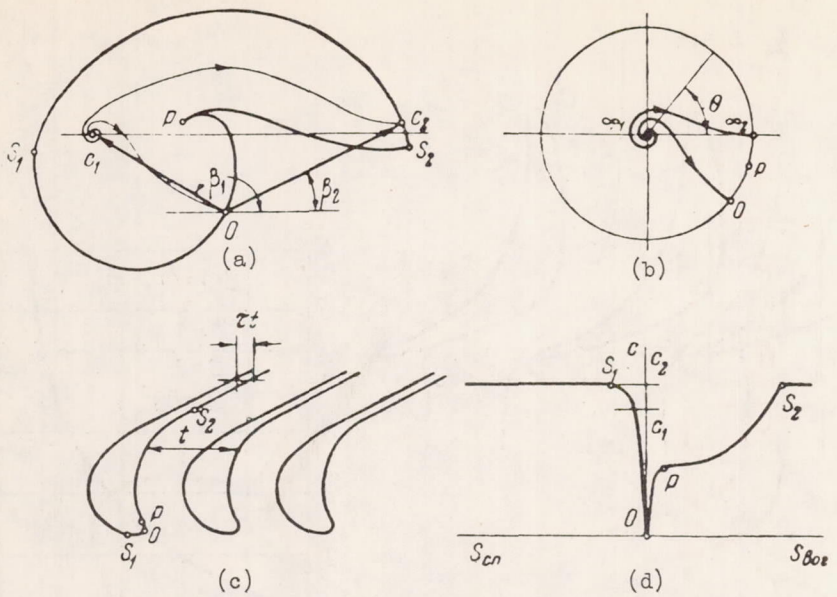


Figure 7-14. - Construction of flow stream.

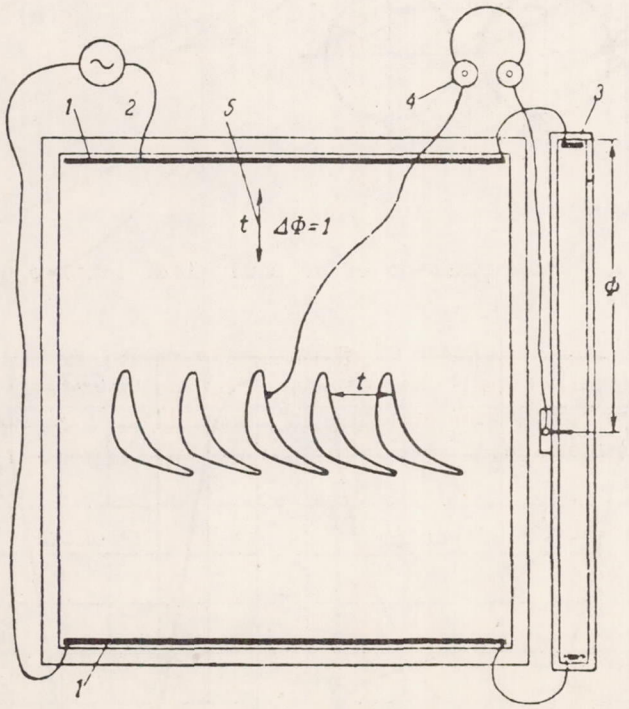


Figure 7-15. - Scheme of electrical model of flow without circulation. Measurement of potential.
1, electrodes; 2, source of alternating current; 3, potentiometer (water rheostat); 4, zero indicator (radio phones); 5, unit of potential.

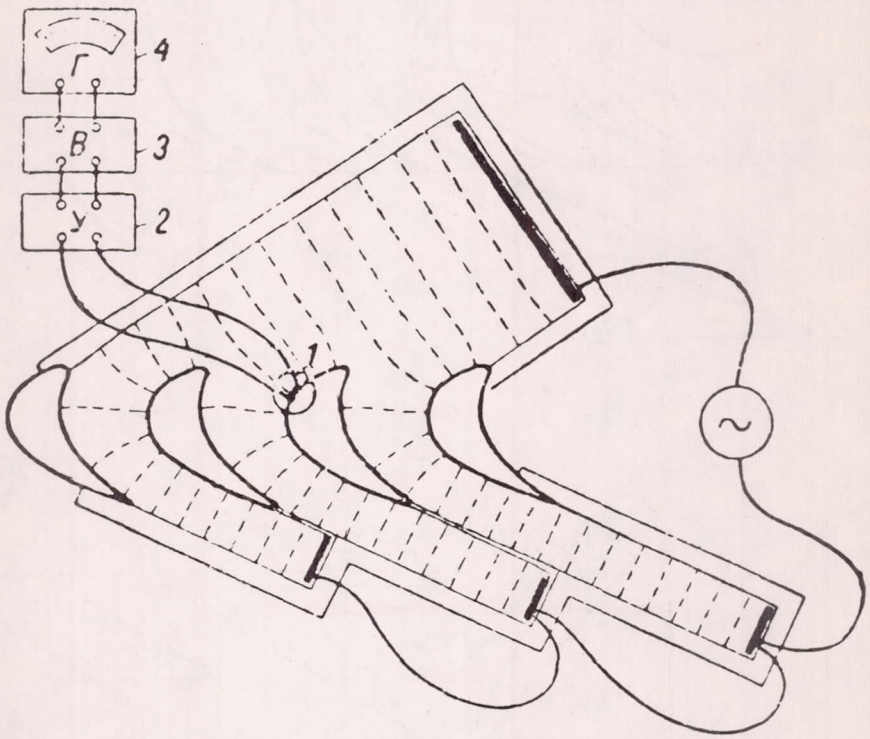


Figure 7-16. - Scheme of electrical model of flow with circulation. Measurement of velocities. 1, probe with two needles; 2, amplifier; 3, rectifier; 4, galvanometer; ----, equipotential lines.

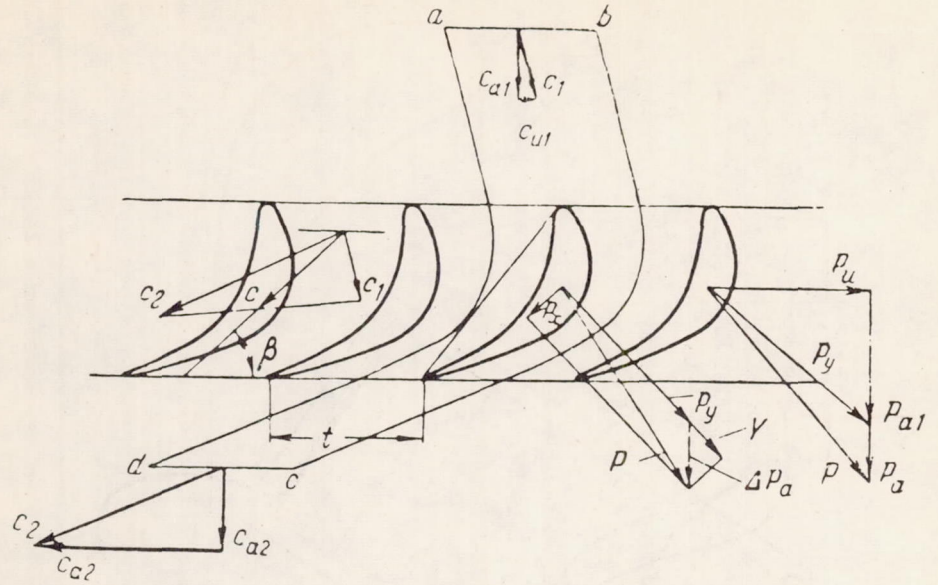


(a) Turbine (converging) lattice.

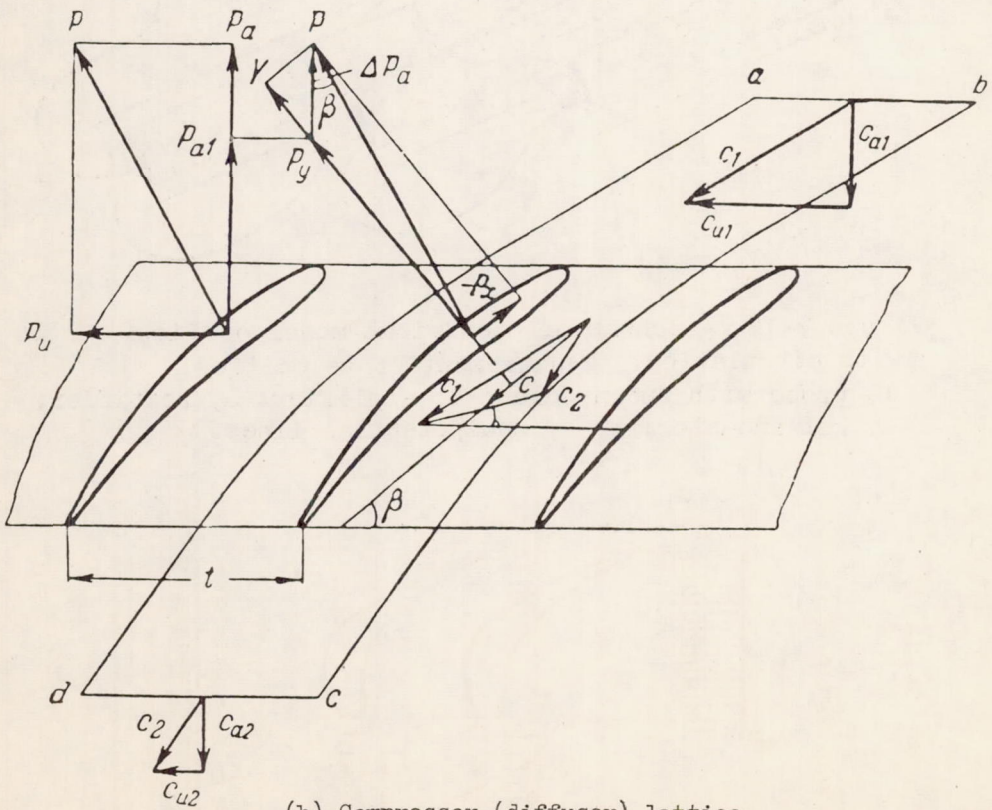


(b) Compressor (diffuser) lattice.

Figure 7-17. - Forces acting on profile in lattice.

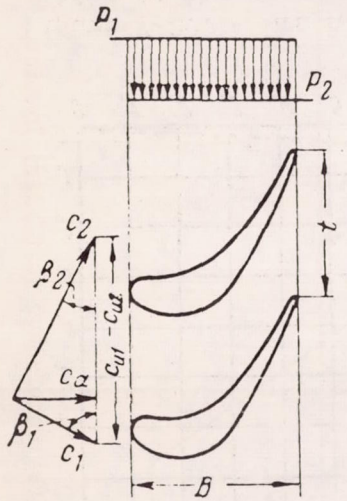


Figure 7-18. - Determination of coefficient of peripheral force.

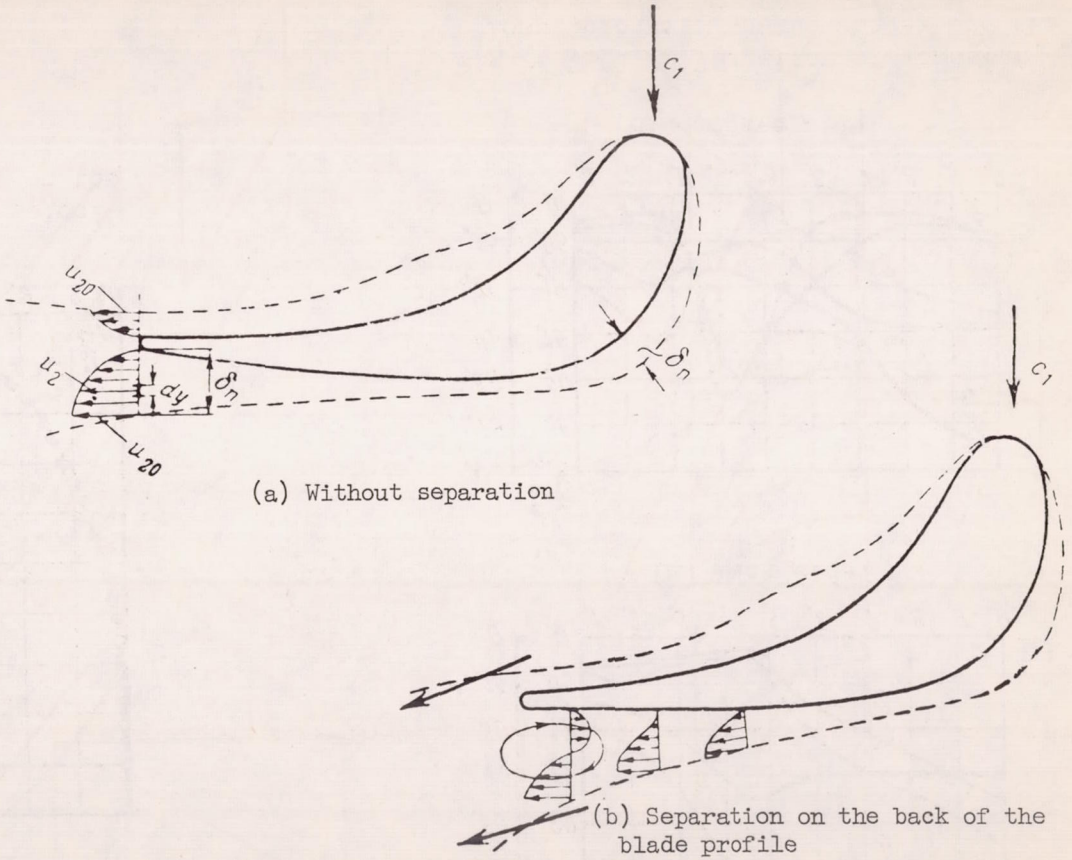


Figure 7-19. - Scheme of formation of boundary layer on a lattice profile.

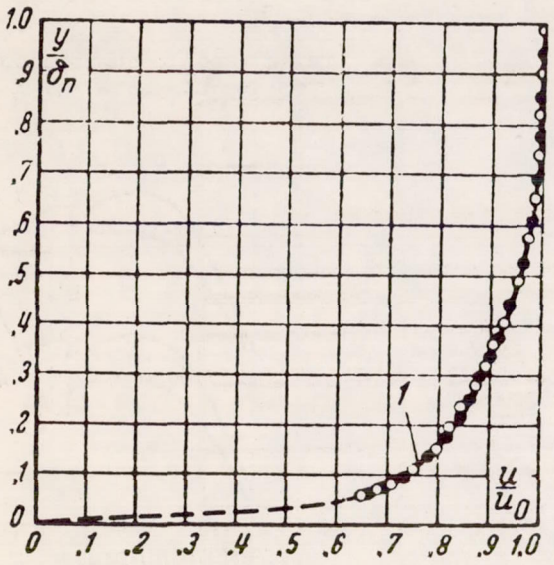


Figure 7-20. - Graph of the velocities in the boundary layer on the convex side of the blade.

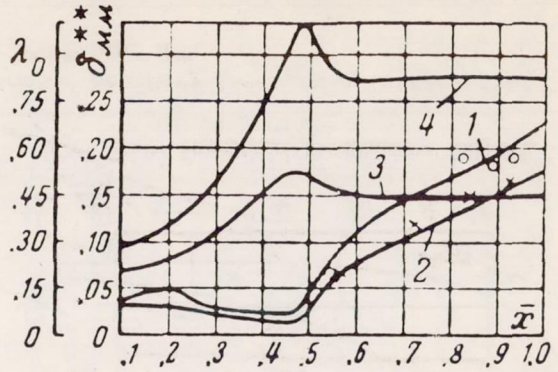


(a) Back side.

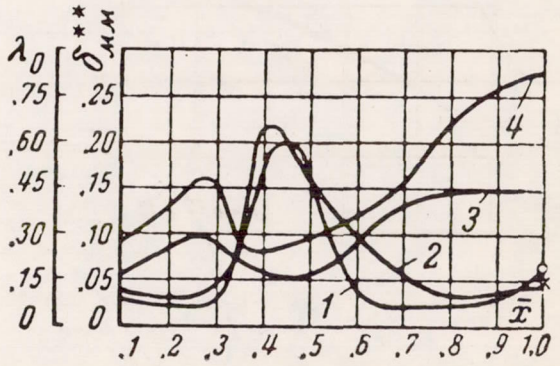


(b) Concave side.

Figure 7-21. - Variation of momentum loss thickness on the convex and the concave side of the profile of a turbine lattice.

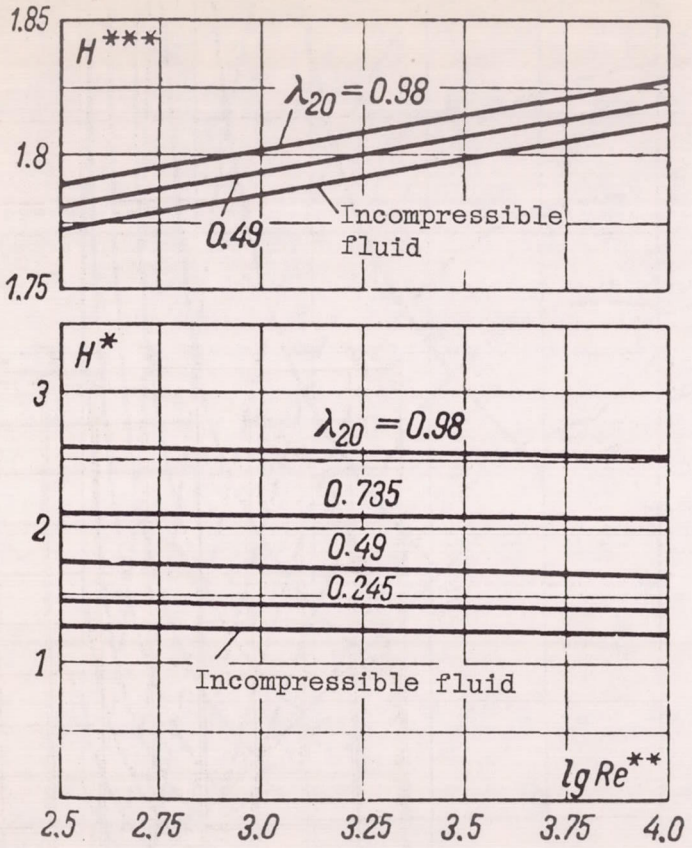


(a) For turbulent boundary layer.

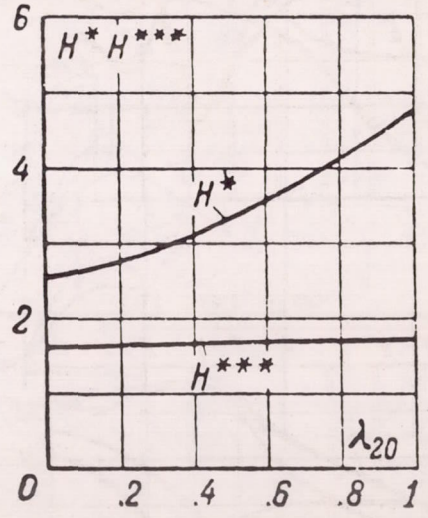


(b) For laminar boundary layer.

Figure 7-22. - Magnitudes H*** and H*.

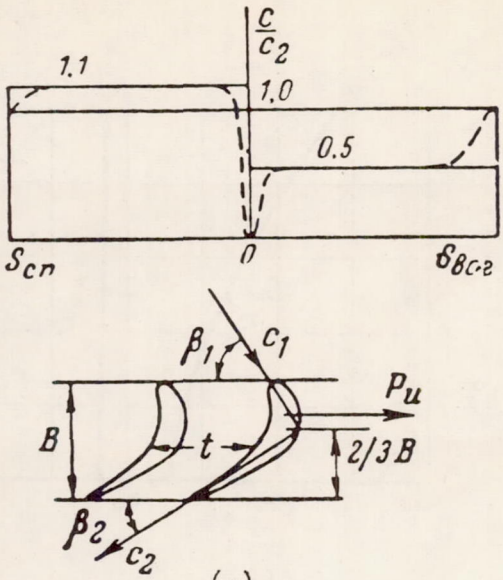


(a)

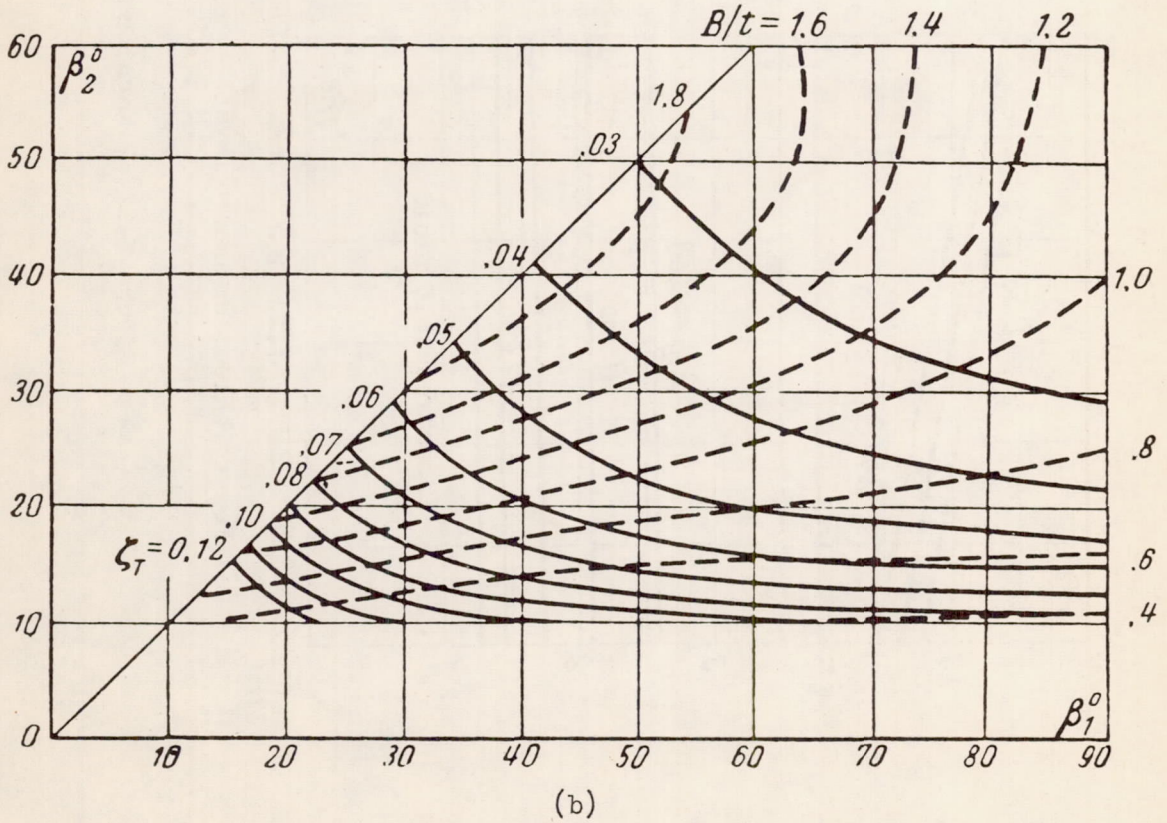


(b)

Figure 7-23. - Computed magnitudes of the friction loss coefficients in turbine lattices as a function of $\beta_1$ and $\beta_2$.

(a) $M_2 = 0.565$

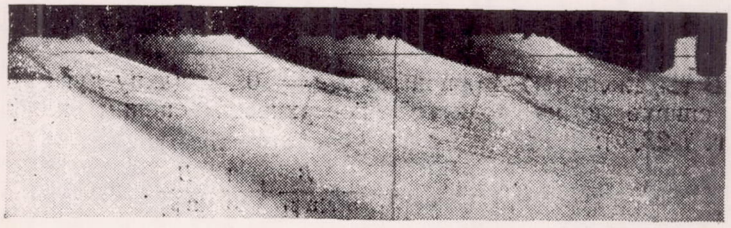

(b) $M_2 = 0.773$

(c) $M_2 = 0.940$

Figure 7-24. - Spectra of the flow of air through a reaction lattice at supersonic velocities. Relative pitch of profiles t = 0.860, inlet angle of profile $\beta_{2n} = 15^{\circ}52'$ (visualization of trailing wake).

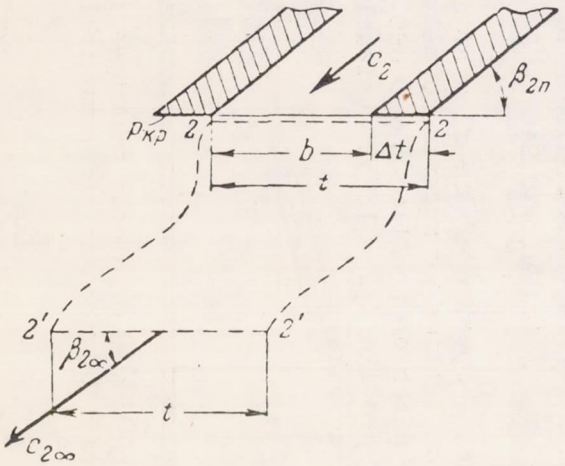


Figure 7-25. - Computation of the parameters of the equalized flow behind a lattice.

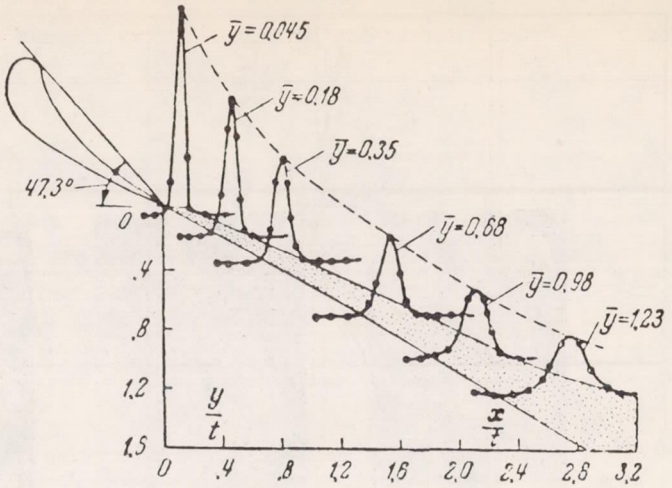


(a) Stagnation pressure.

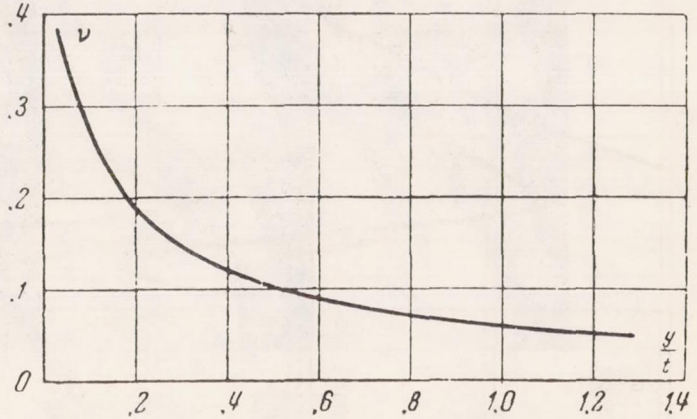


(b) Coefficient of nonuniformity.

Figure 7-26. - Variation in trailing wake characteristics of flow at small subsonic velocities as a function of the distance behind the lattice $\bar{y} = y/t$.

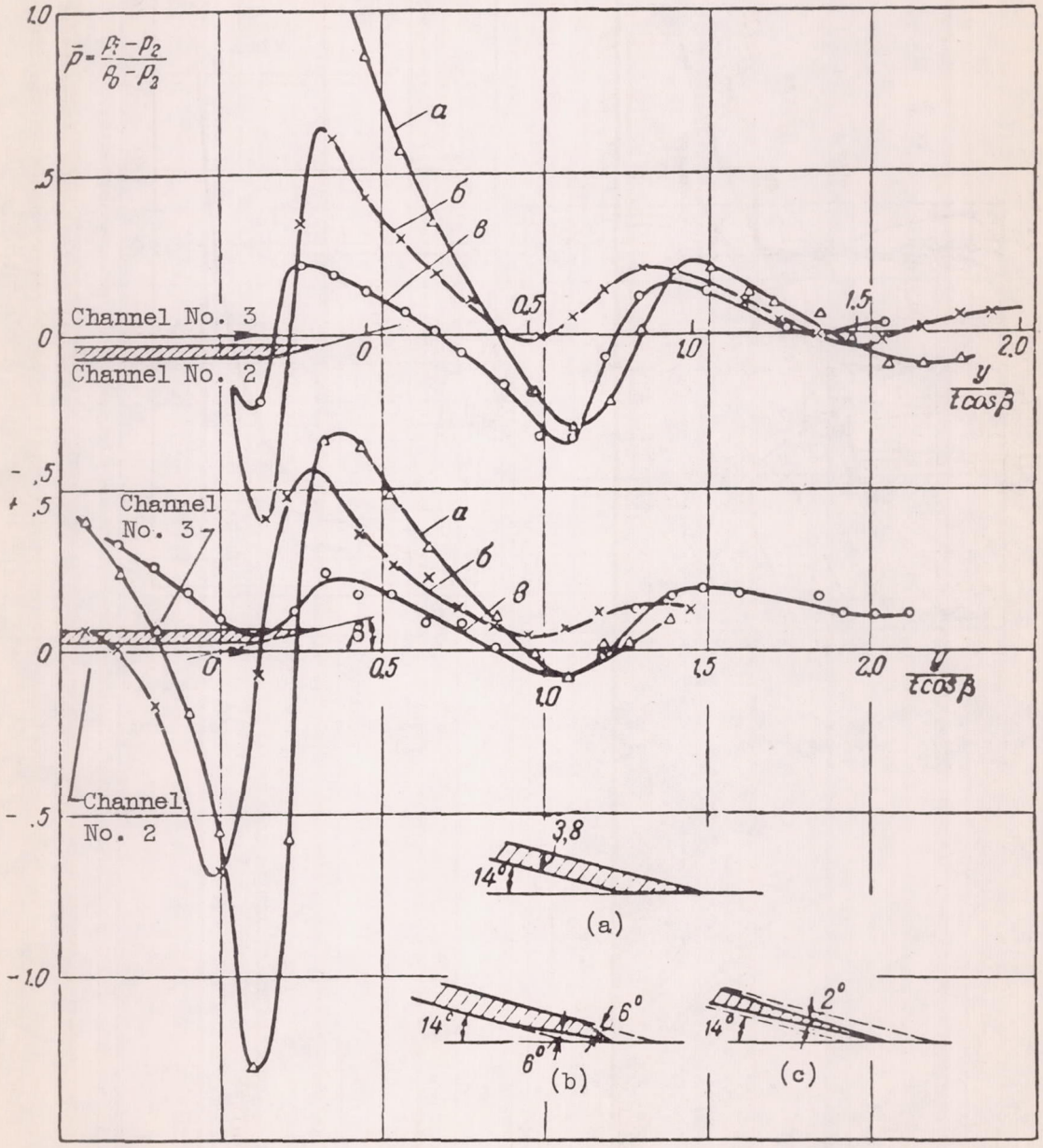


Figure 7-27. - Distribution of static pressures in the boundaries of the vortex wake behind a lattice for different trailing edges.

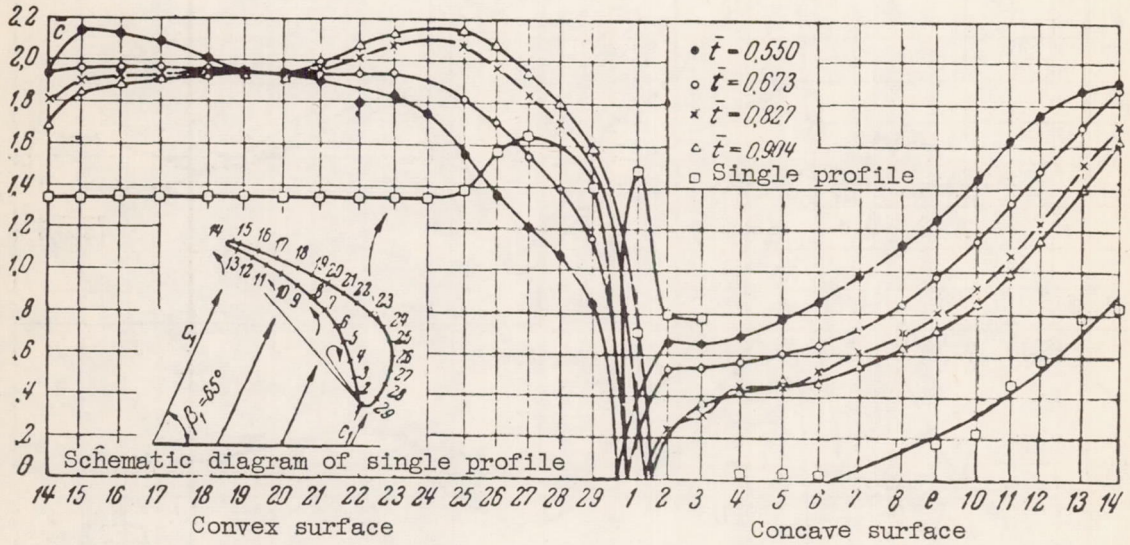


Figure 7-28. - Effect of pitch on the distribution of the velocities over a profile in a reaction lattice.

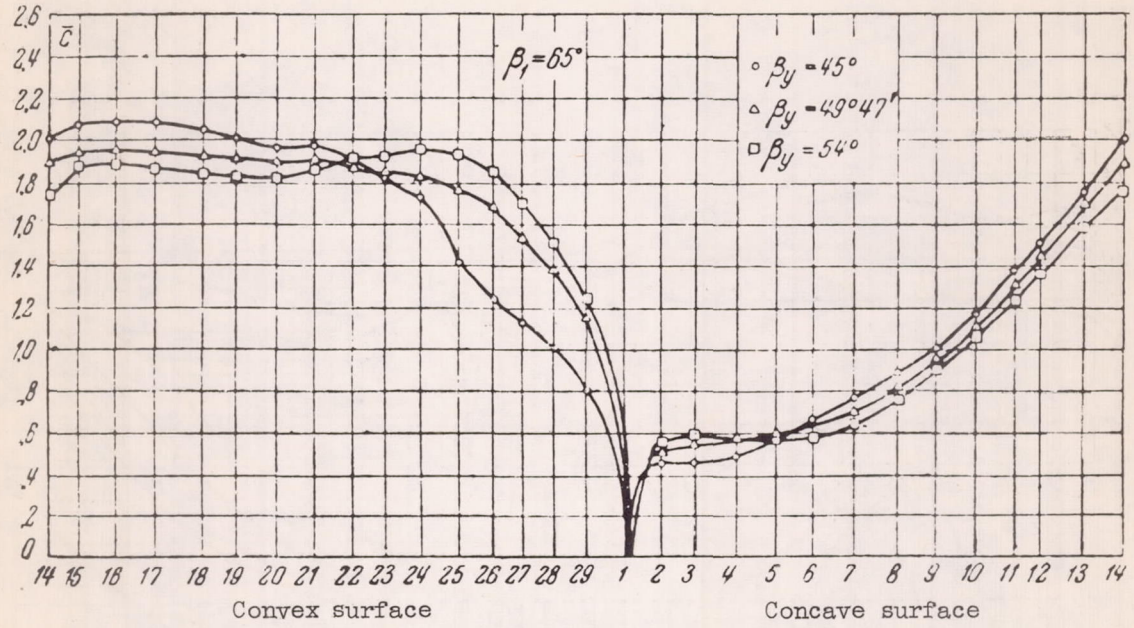


(a) Setting angle.

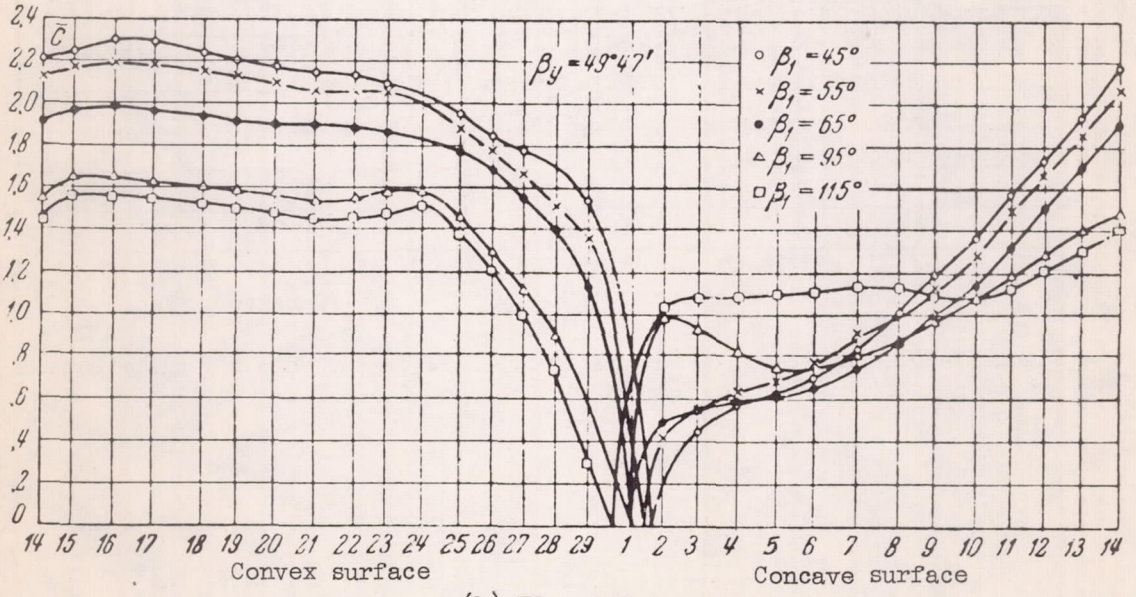


(b) Flow inlet angle.

Figure 7-29. - Effect of blade setting and flow inlet angles on the velocity distribution over a profile in a reaction lattice.

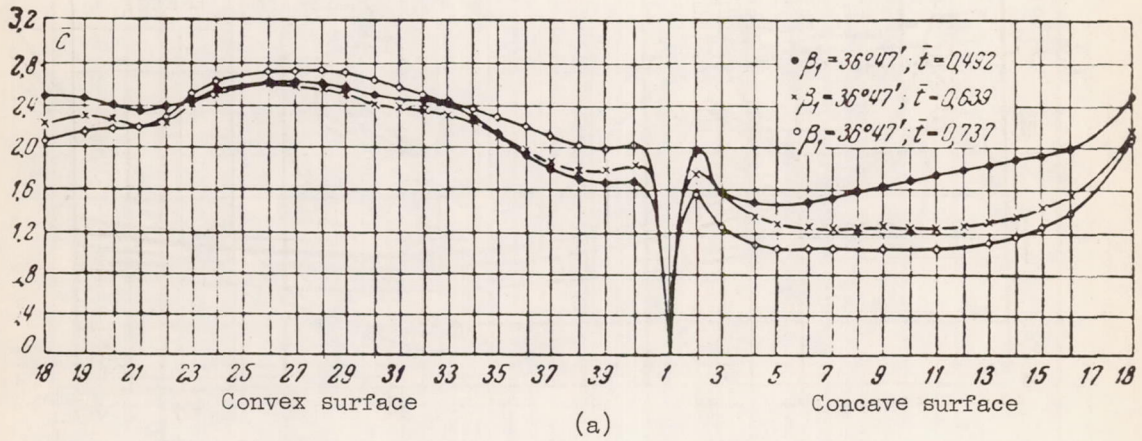


(a)

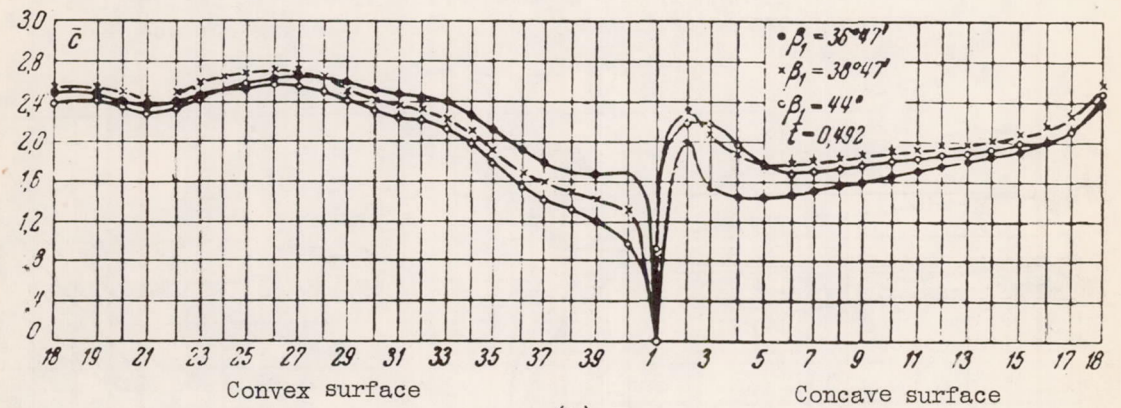


(b)

Figure 7-30. - Effect of pitch and inlet angle on the velocity distribution over a profile in an impulse lattice.

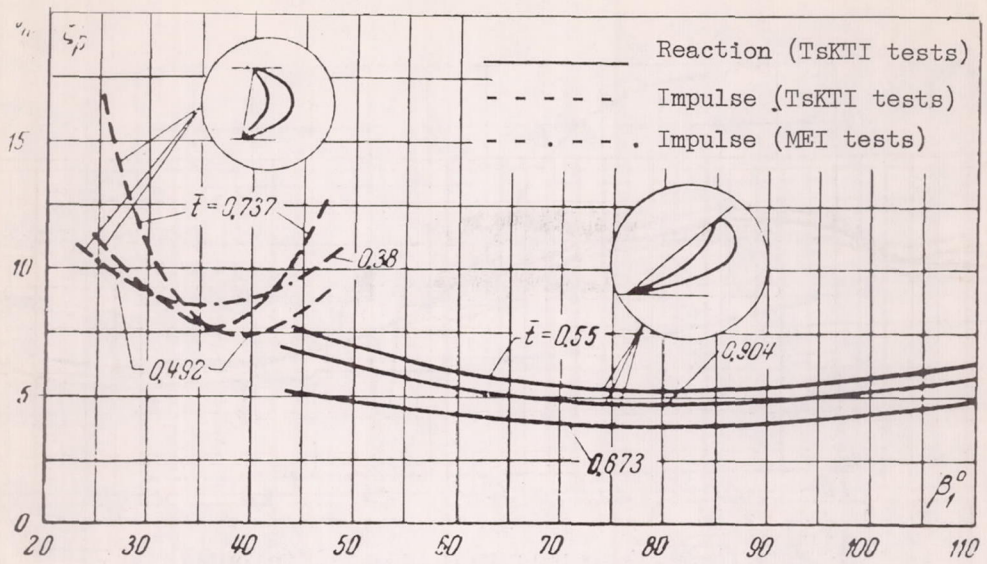


Figure 7-31. - Variation of coefficient of losses in impulse and reaction lattices as a function of the inlet angle $\beta_1$ and the pitch $\bar{t}$.

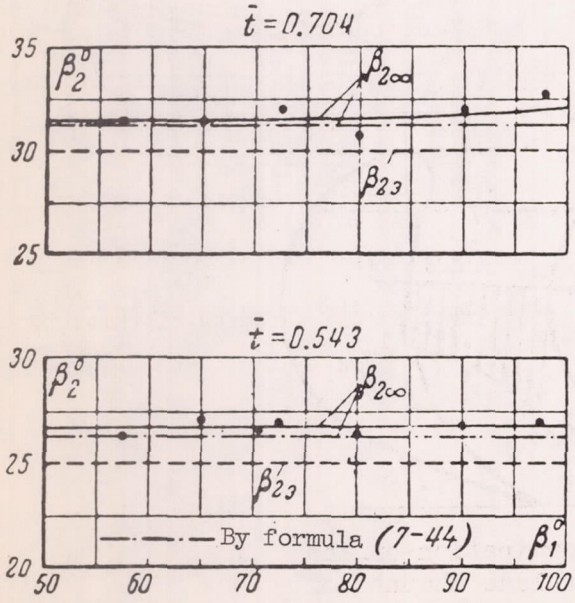


Figure 7-32. - Dependence of the mean outflow angles on the inlet angle for two values of the pitch of a reaction lattice.

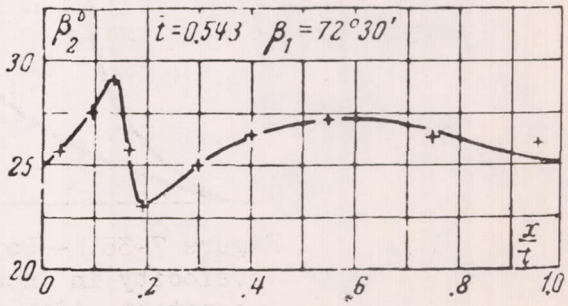


Figure 7-33. - Variation of local angles $\beta_2$ with pitch $\bar{x} = x/t$.

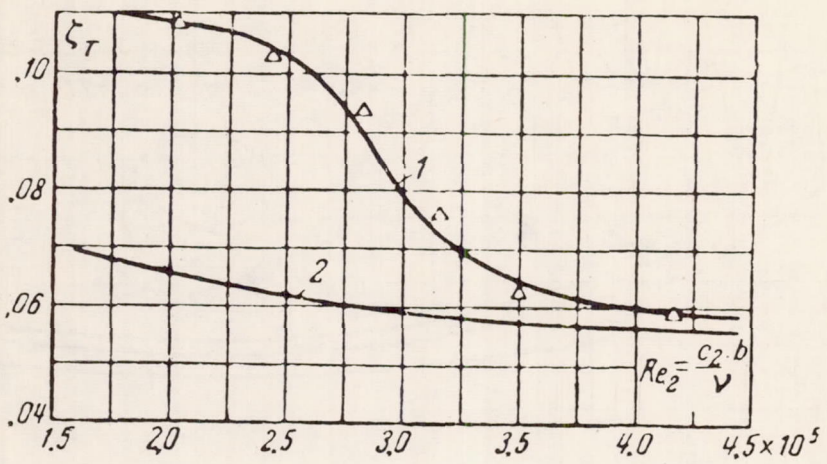


Figure 7-34. - Dependence of coefficient of friction losses in the lattice on $Re_2$.

1, with presence of flow separation; 2, with nonseparating flow (computed).

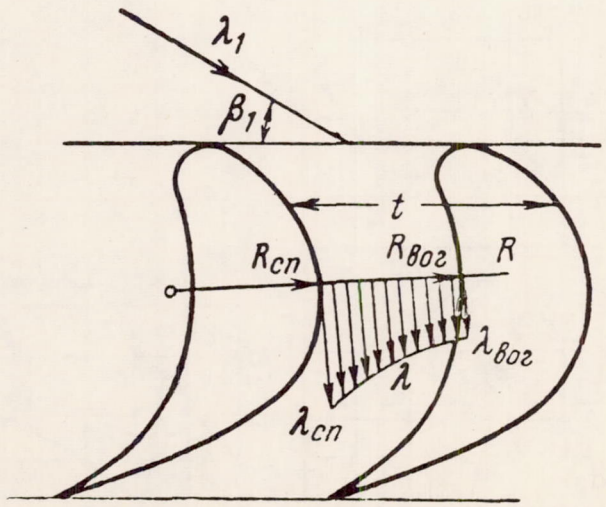


Figure 7-35. - Determination of the velocity in interblade channel of constant width and curvature.

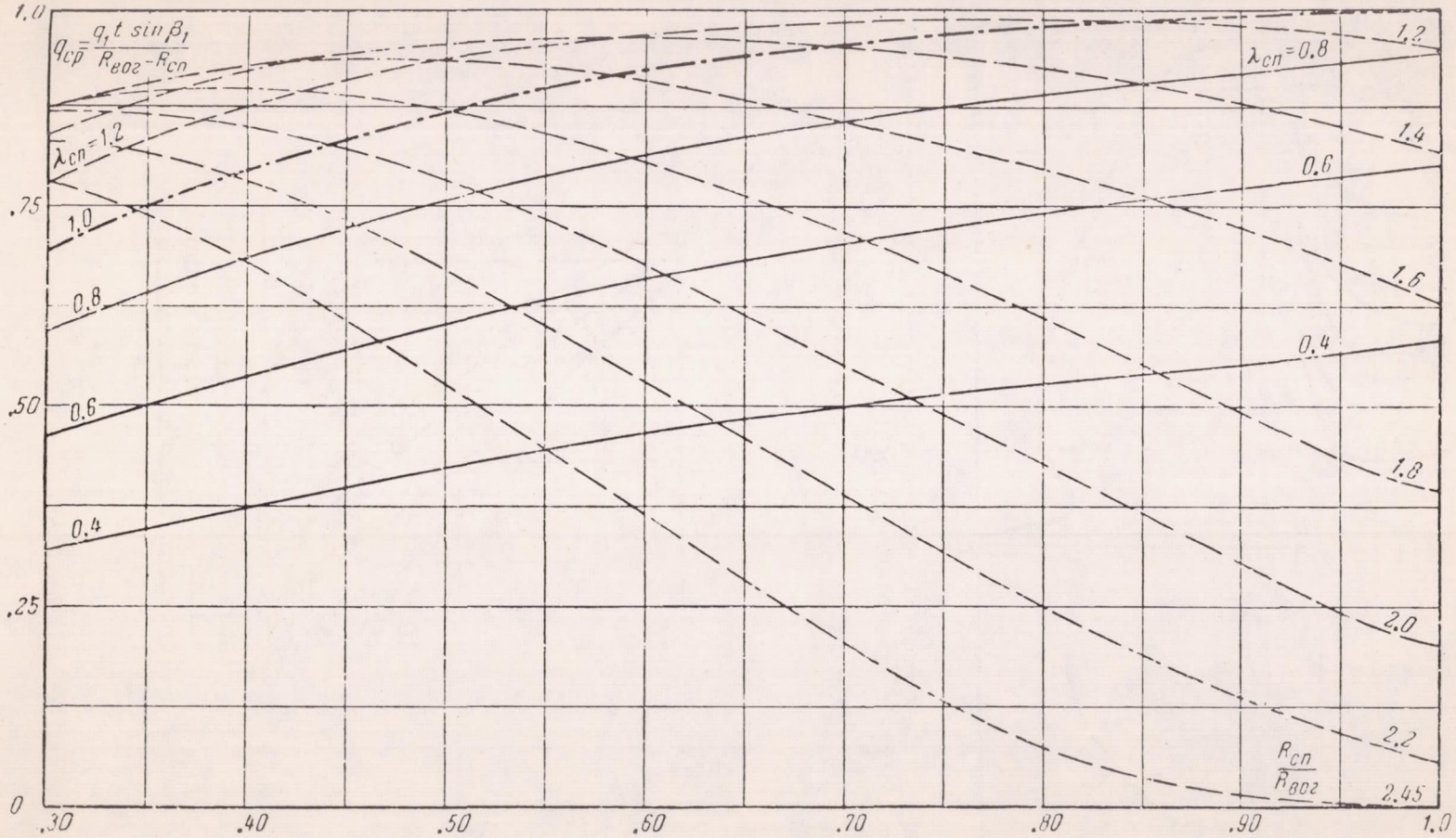


Figure 7-36. - Mean reduced flow $q_{cp}$ in curved channel (k = 1.4).

$R_{cn} = R_{convex}$
$R_{Bol} = R_{concave}$

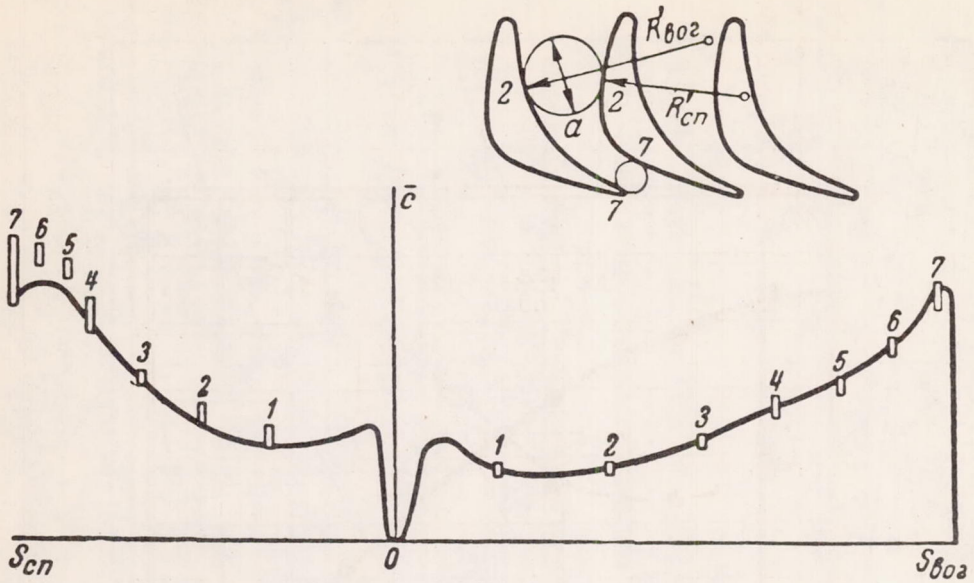


Figure 7-37. - Comparison of exact and approximate determinations of velocity in interblade channel.

_____ exact solution; □ approximate values.

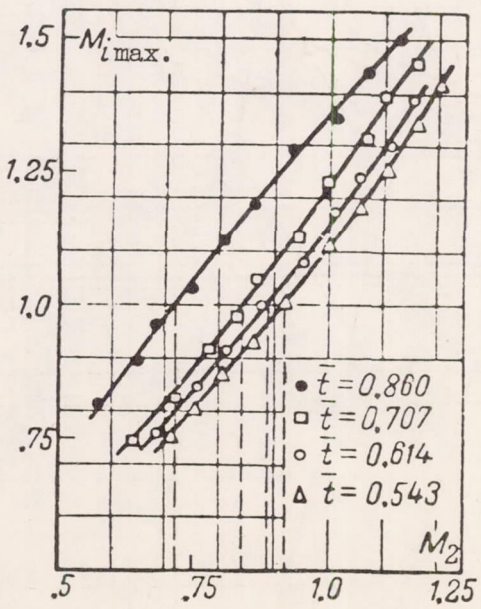


Figure 7-38. - Local maximum velocities on convex side of profile as function of $M_2$.

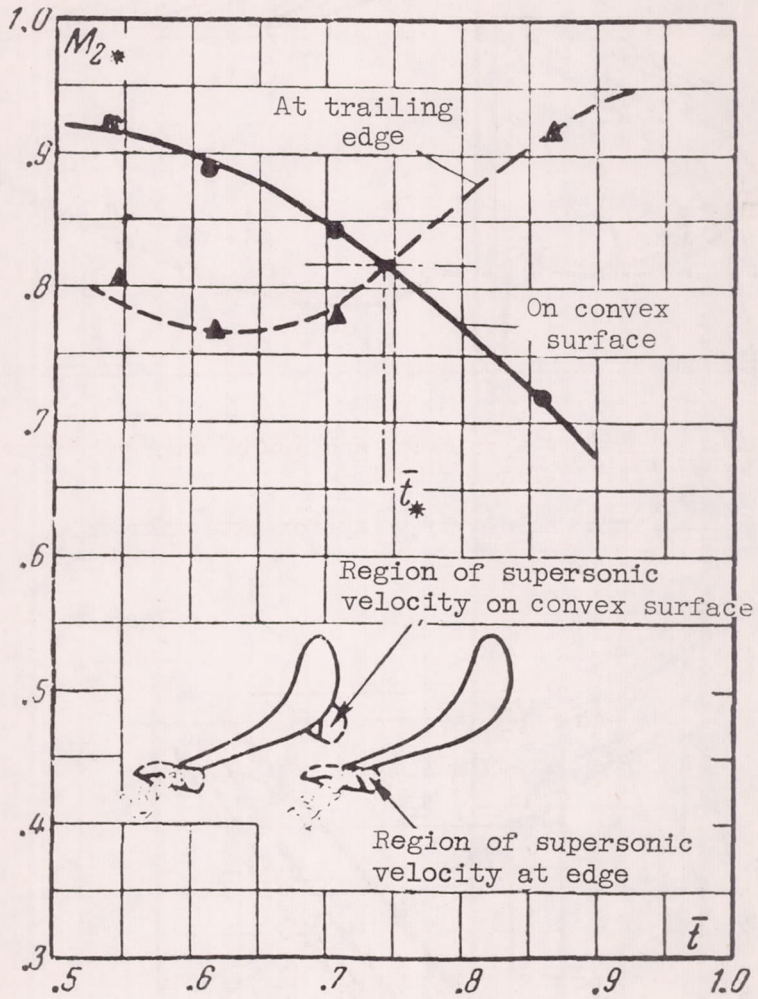


Figure 7-39. - Critical values $M_2$ as function of pitch for reaction lattice.

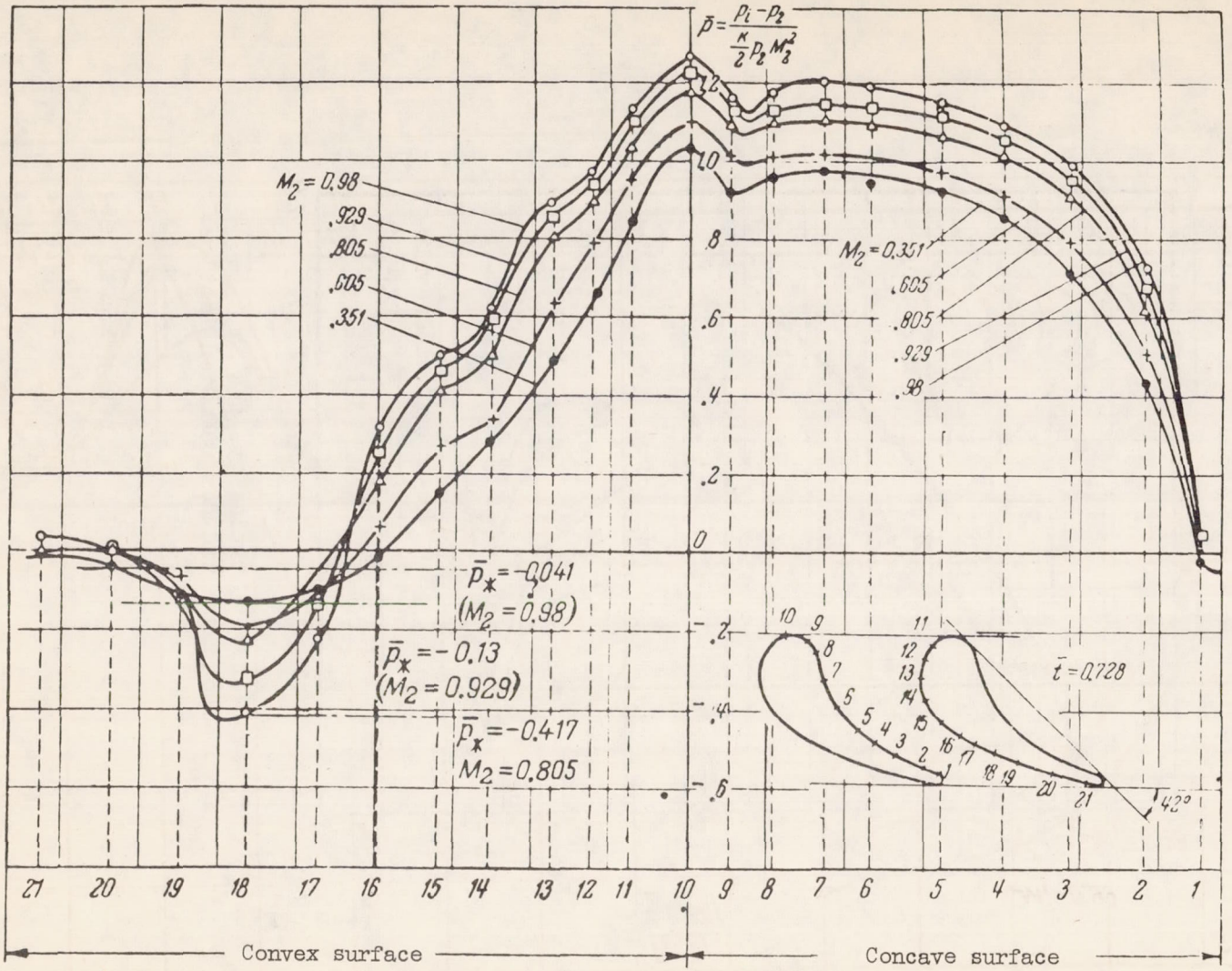


Figure 7-40. - Distribution of pressure over profile in reaction lattice for various $M_2$.

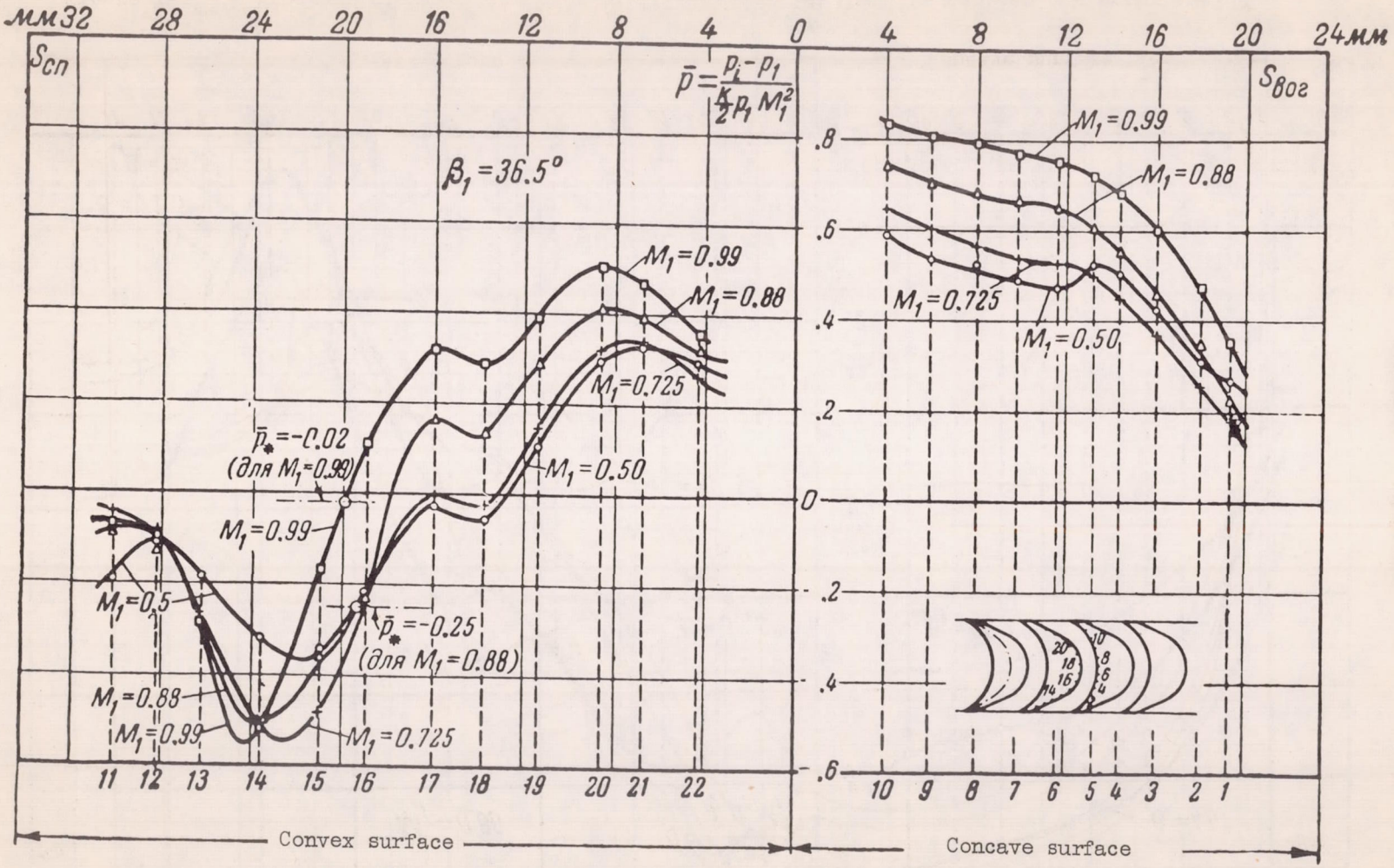


Figure 7-41. - Distribution of pressure over profile in impulse lattice for different $M_1$.

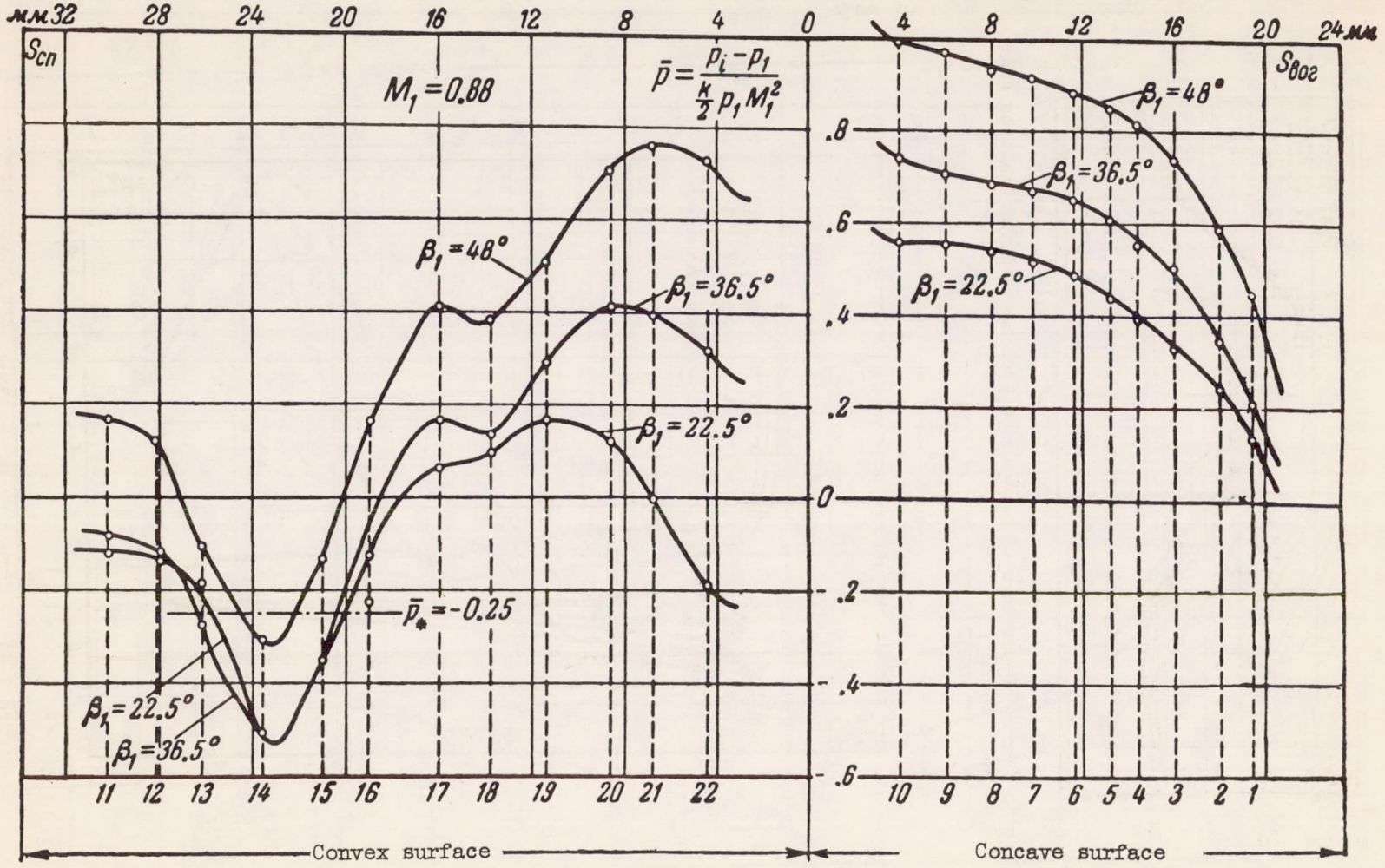


Figure 7-42. - Pressure distribution over profile in impulse lattice for various entry angles $\beta_1$.

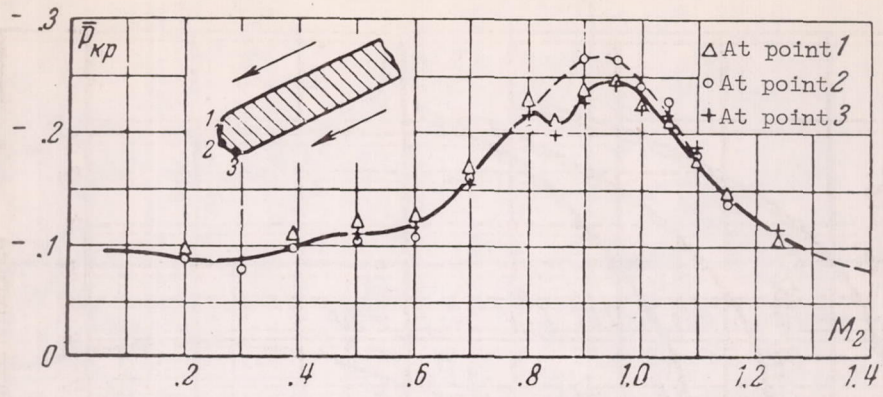


Figure 7-43. - Dependence of pressure coefficient behind trailing edge $\bar{p}_{кр}$ on $M_2$ number.

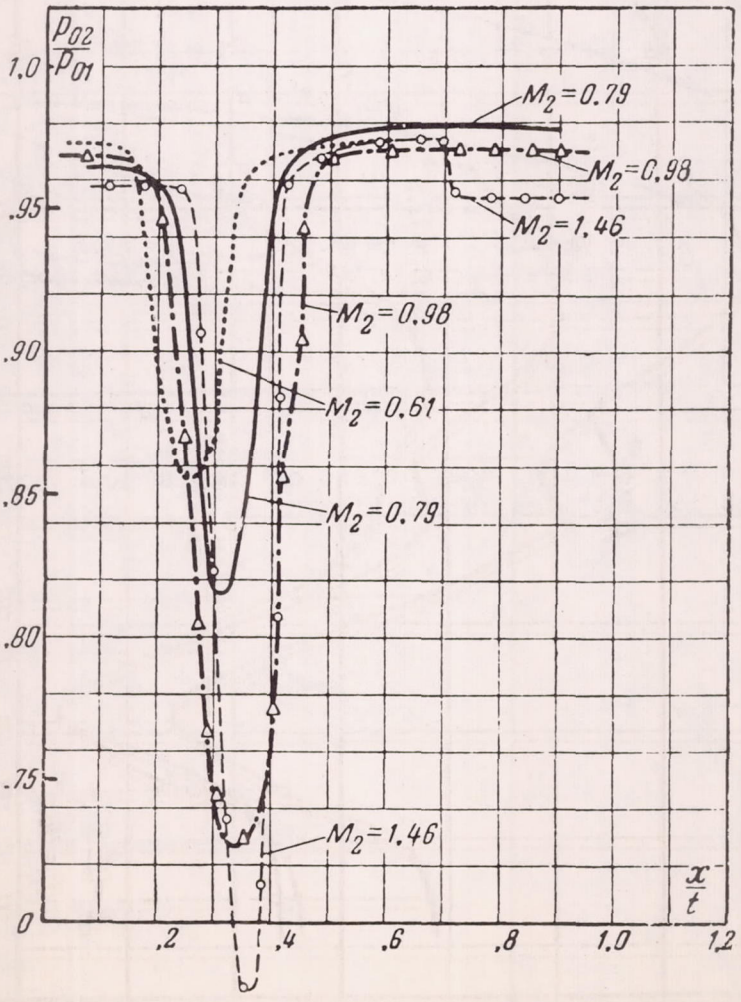


Figure 7-44. - Effect of $M_2$ on shape and dimensions of trailing vortex wake.

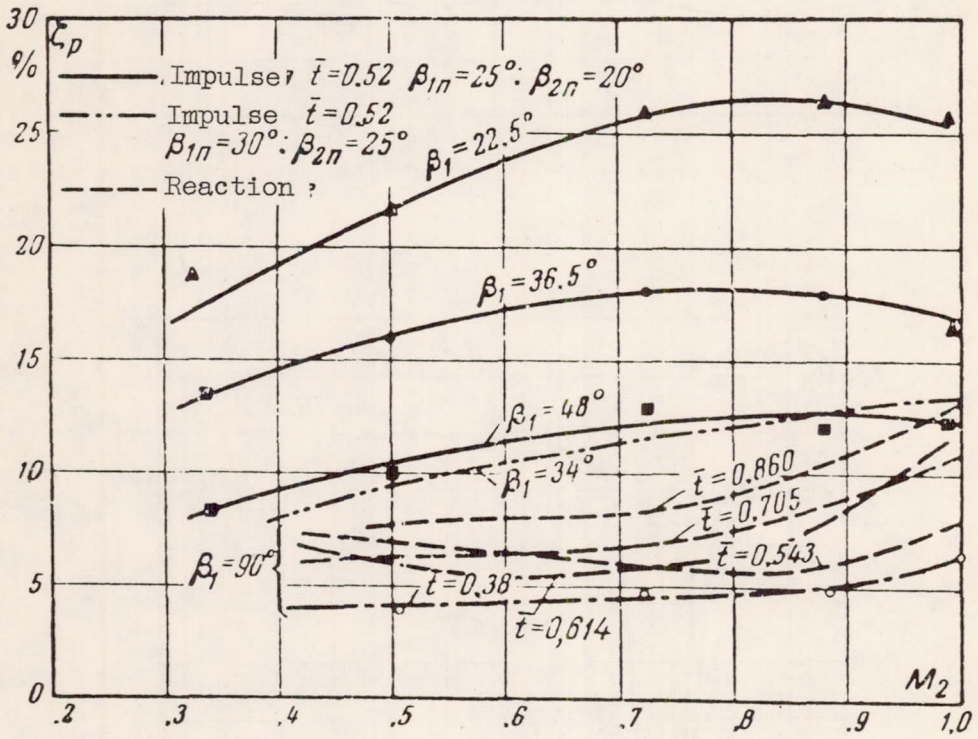


Figure 7-45. - Loss coefficient of impulse and various reaction lattices as function of $M_2$.

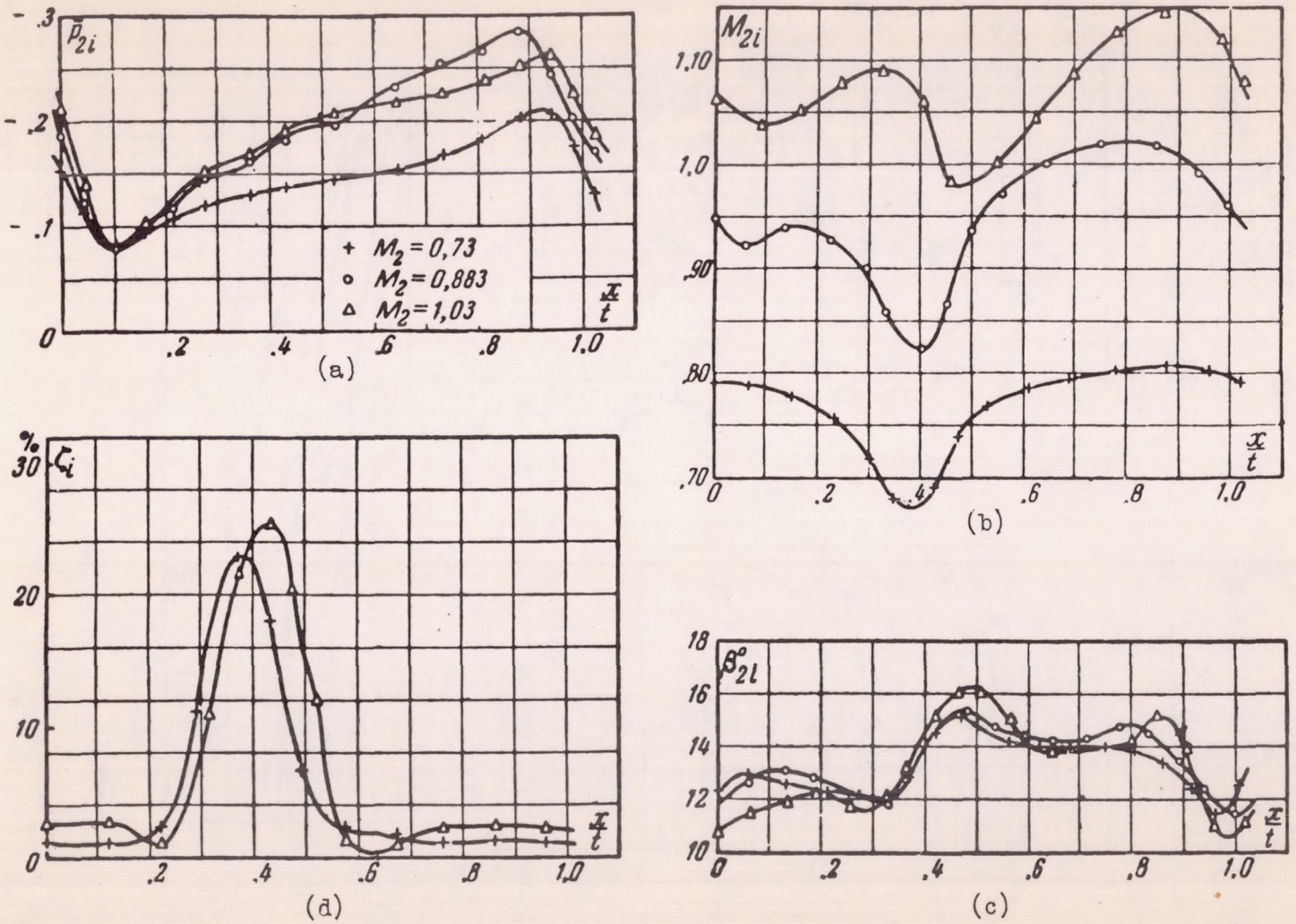


Figure 7-46. - Distribution of local pressures, velocities, angles and losses over the pitch as a function of $M_2$ at the distance $\bar{y}$ = 0.1 behind a reaction lattice.

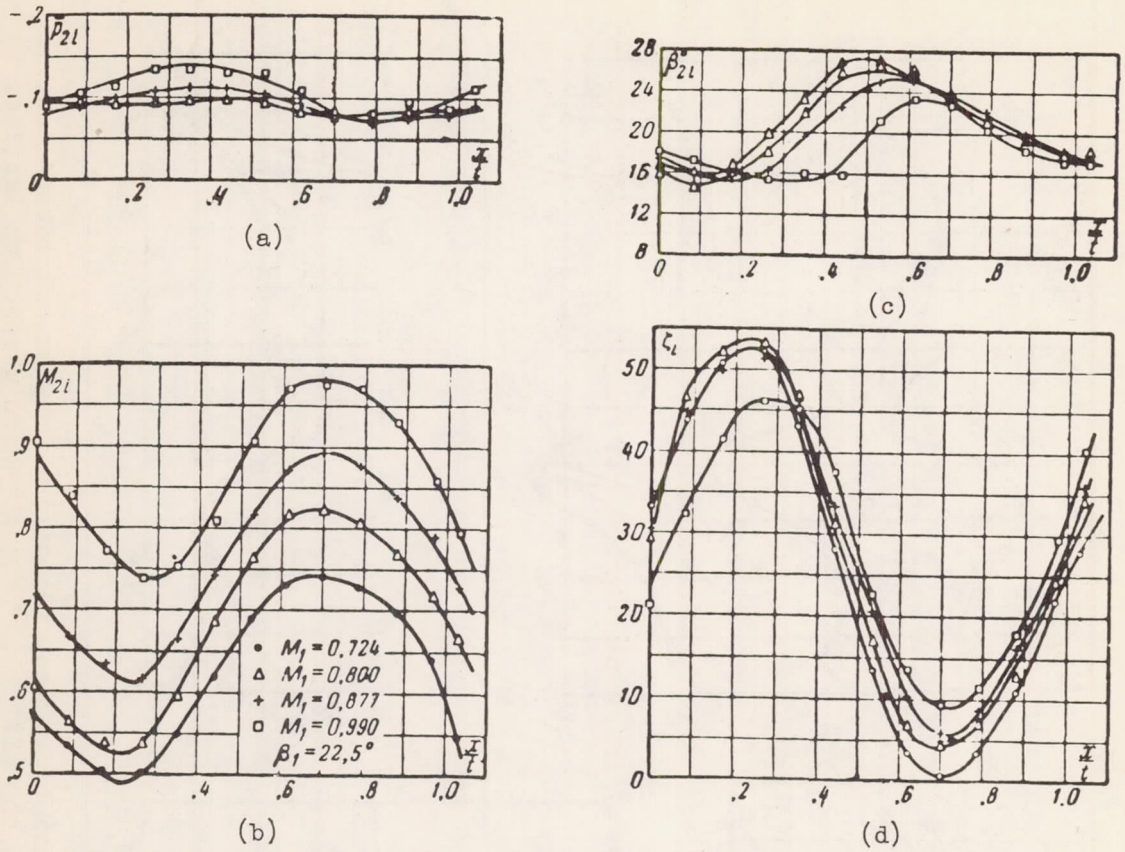


Figure 7-47. - Distribution of local pressures, velocities, angles and losses as a function of $M_2$ at the distance $\bar{y} = 0.1$ behind an impulse lattice.

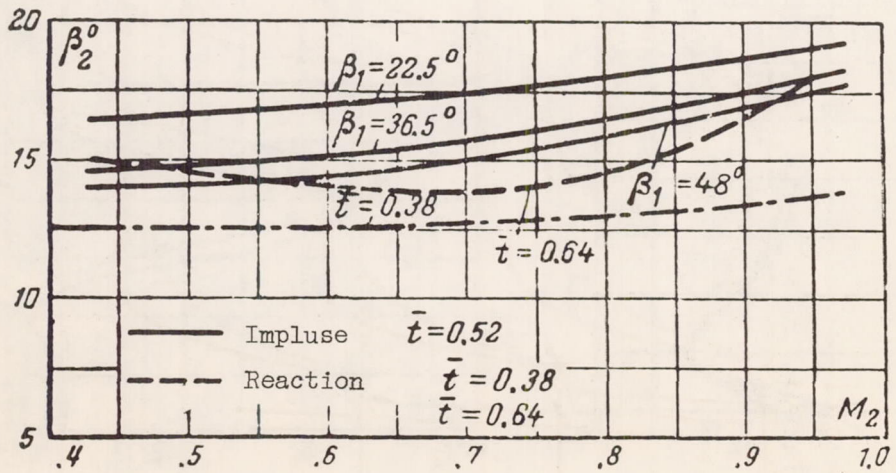


Figure 7-48. - Dependence of the mean angle of the flow behind a lattice on $M_2$.

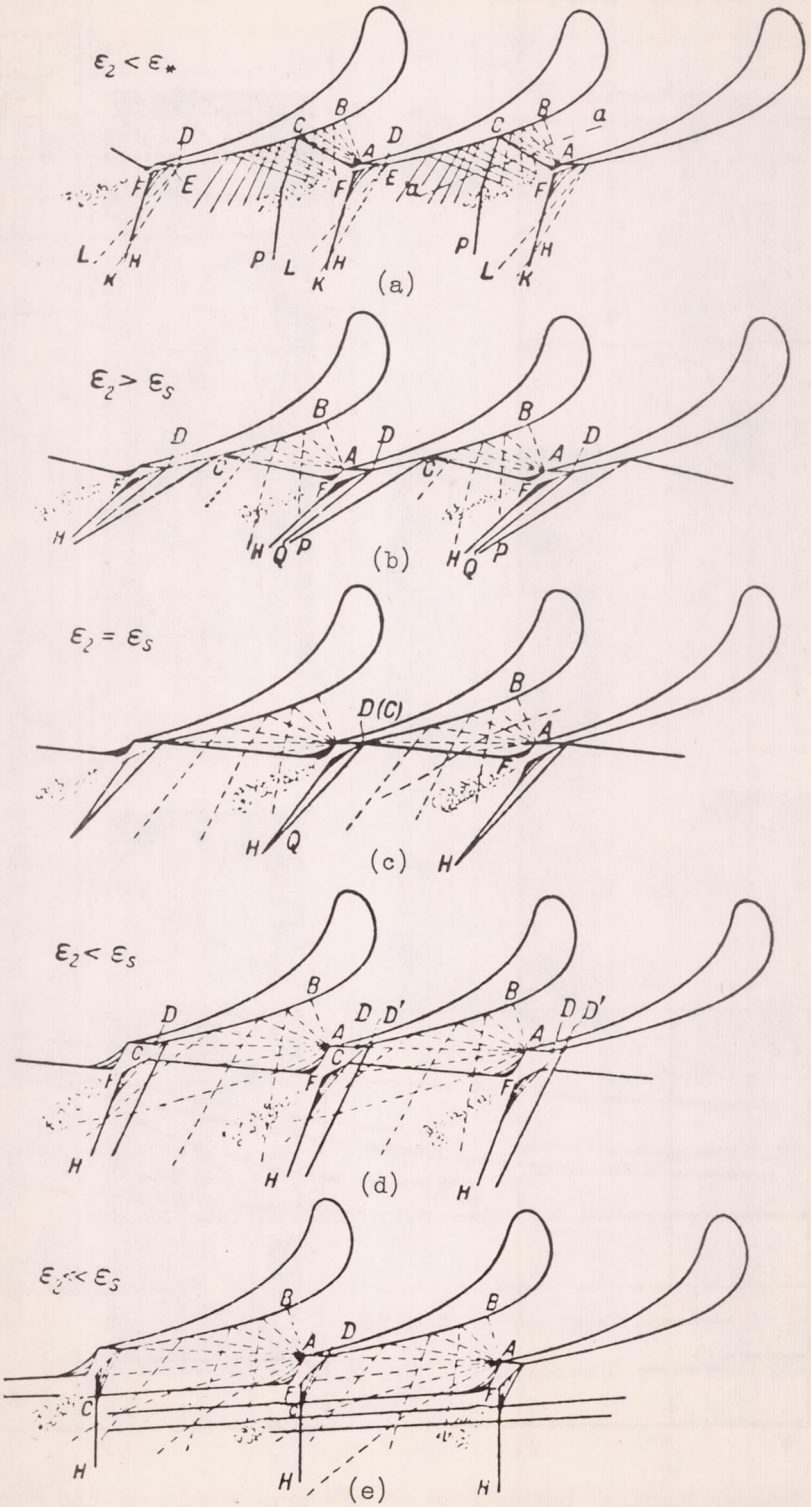


Figure 7-49. - Scheme of outflow from a reaction lattice at above-critical pressure drops.

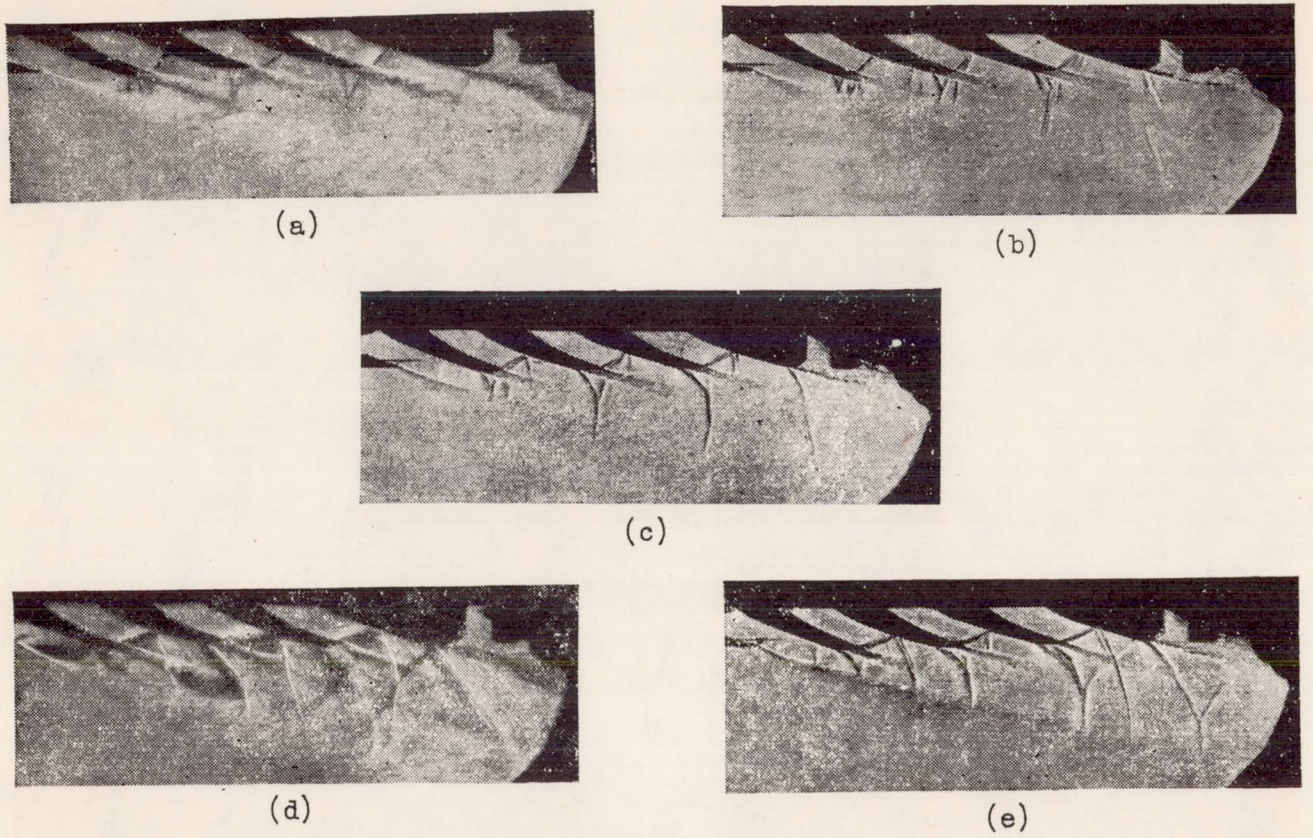


Figure 7-50. - Spectra of air flow through reaction lattice at near sonic and supersonic velocities. Relative pitch $\overline{t}$ = 0.543; exit angle of profile $\beta_{2n} = 15^{\circ}52'$.

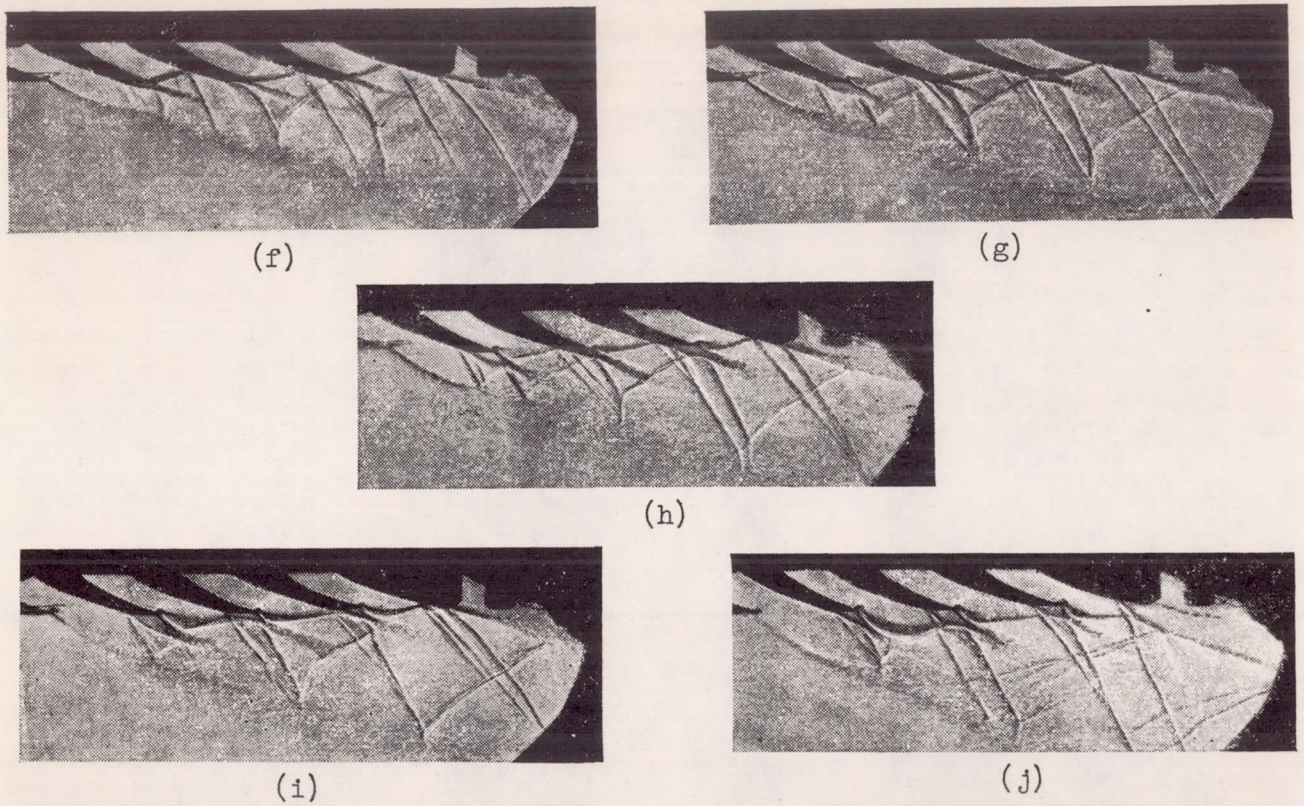


Figure 7-50. - Concluded. Spectra of air flow through reaction lattice at near sonic and supersonic velocities. Relative pitch $\overline{t}$ = 0.543; exit angle of profile $\beta_{2n} = 15^{\circ}52'$.

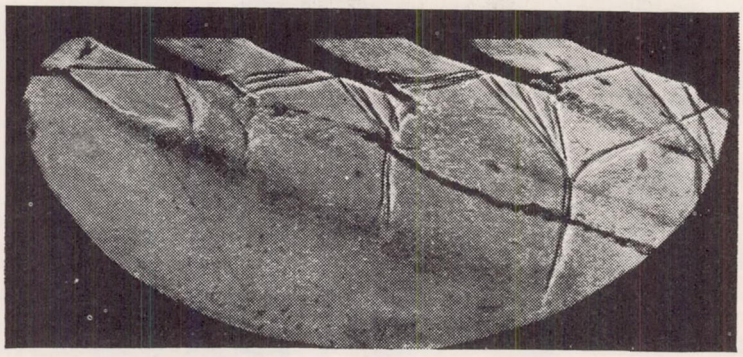

(a)

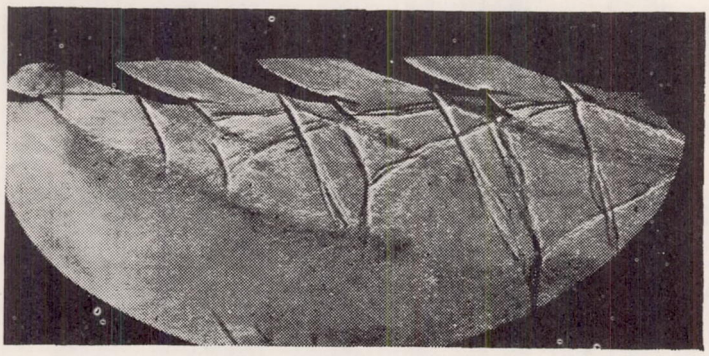

(b)

Figure 7-51. - Spectra of air flow through reaction lattice at supersonic velocities. Relative pitch of profile $\overline{t} = 0.86$; exit angle of profile $\beta_{2n} = 15^{\circ}52'$.

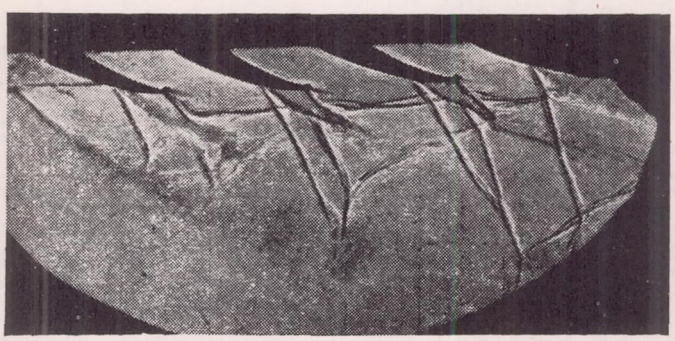

(c)

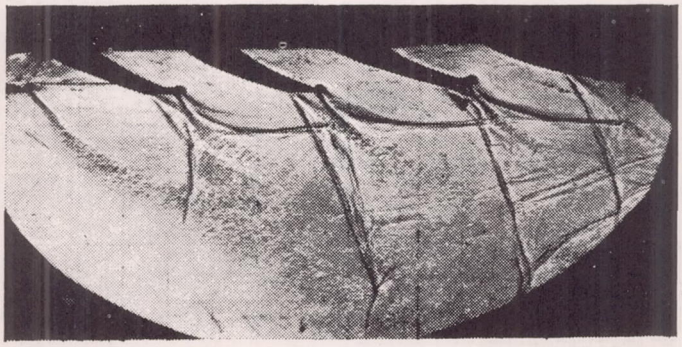

(d)

Figure 7-51. - Concluded. Spectra of air flow through reaction lattice at supersonic velocities. Relative pitch of profile $\bar{t} = 0.86$; exit angle of profile $\beta_{2n} = 15^{\circ}52'$.

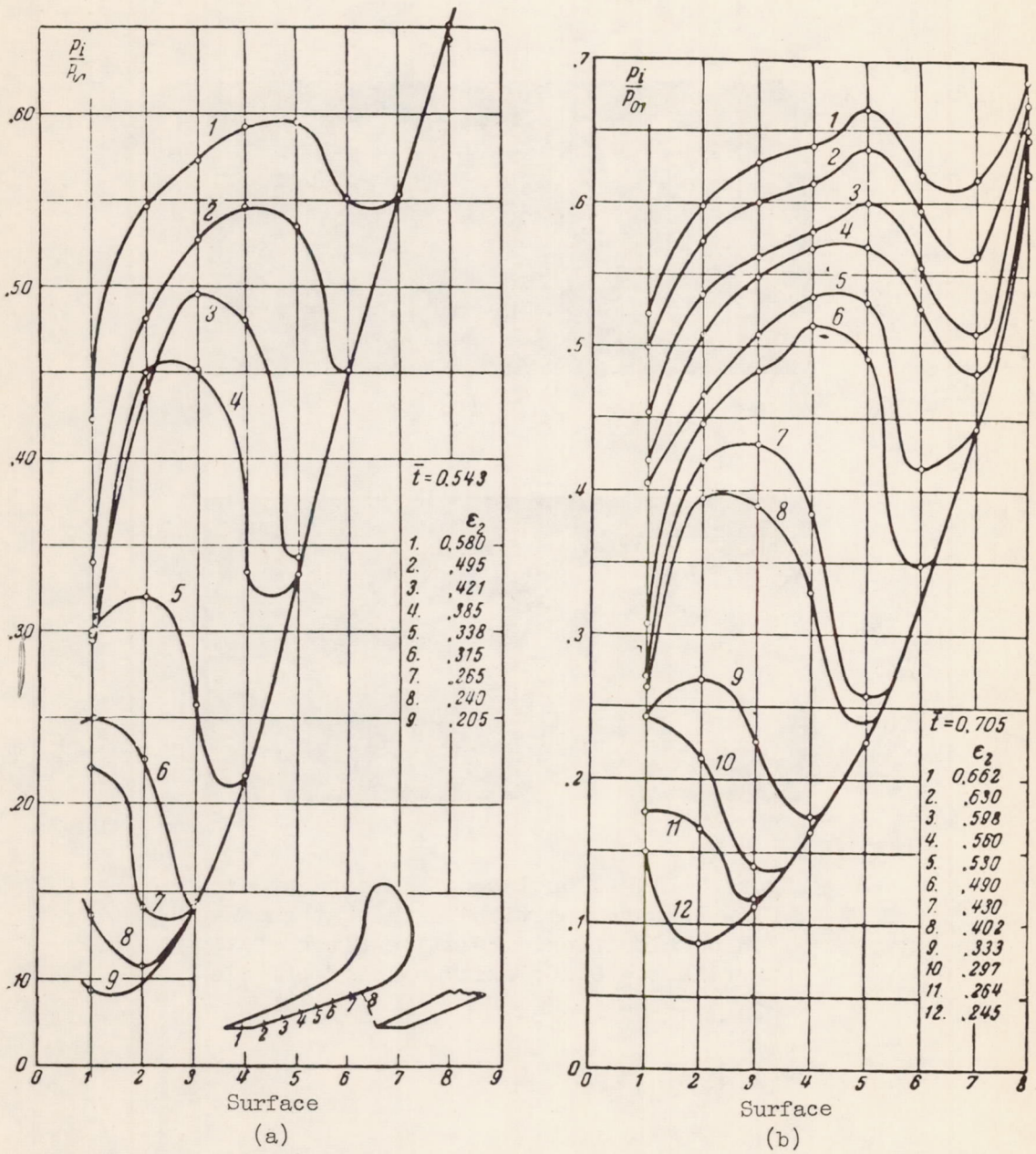


Figure 7-52. - Pressure distribution along convex surface of profile downstream of the throat at above-critical pressure drops.

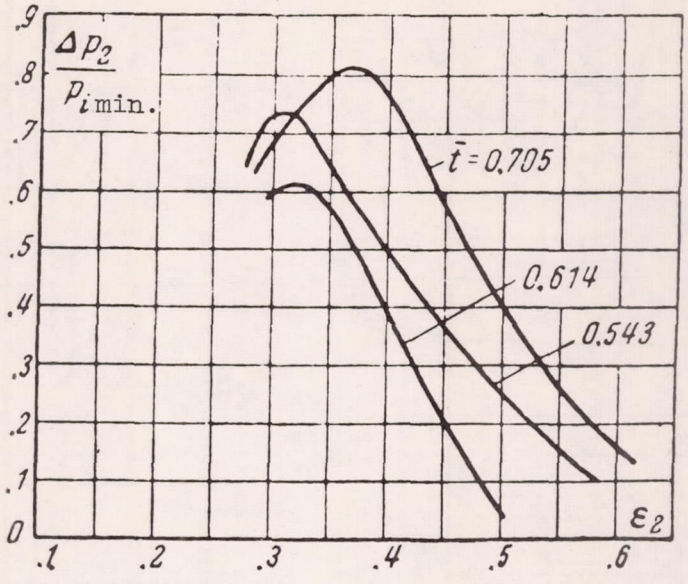


Figure 7-53. - Rise of pressure in the system of shocks on the convex surface of a blade as a function of the pressure drops in the lattice.

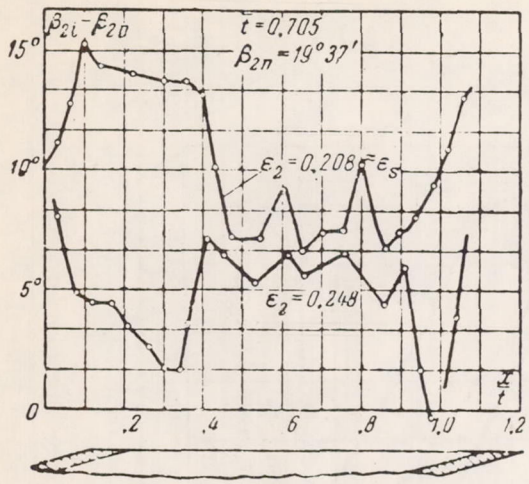


(a)

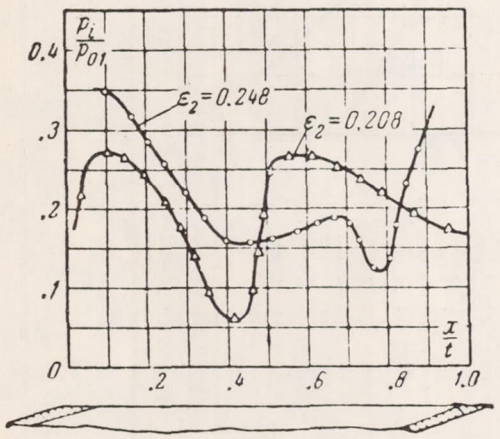


(b)

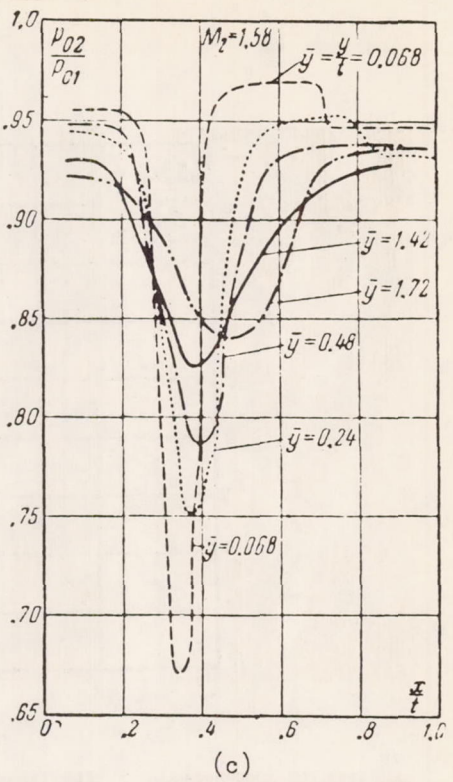


(c)

Figure 7-54. - Distribution of the flow parameters over the pitch of a reaction lattice at supersonic velocities.

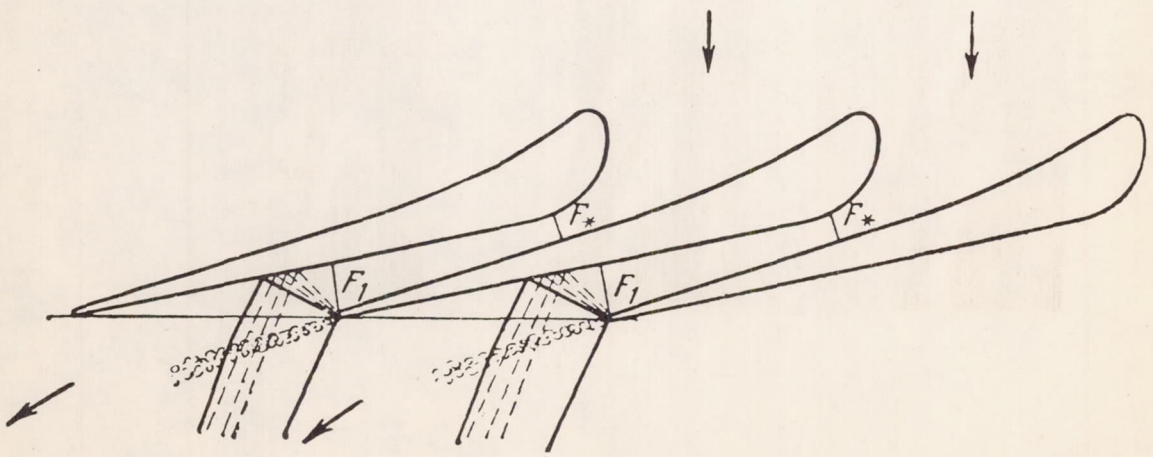


Figure 7-55. - Scheme of flow spectrum at the exit from a supersonic reaction lattice at the computed regime.

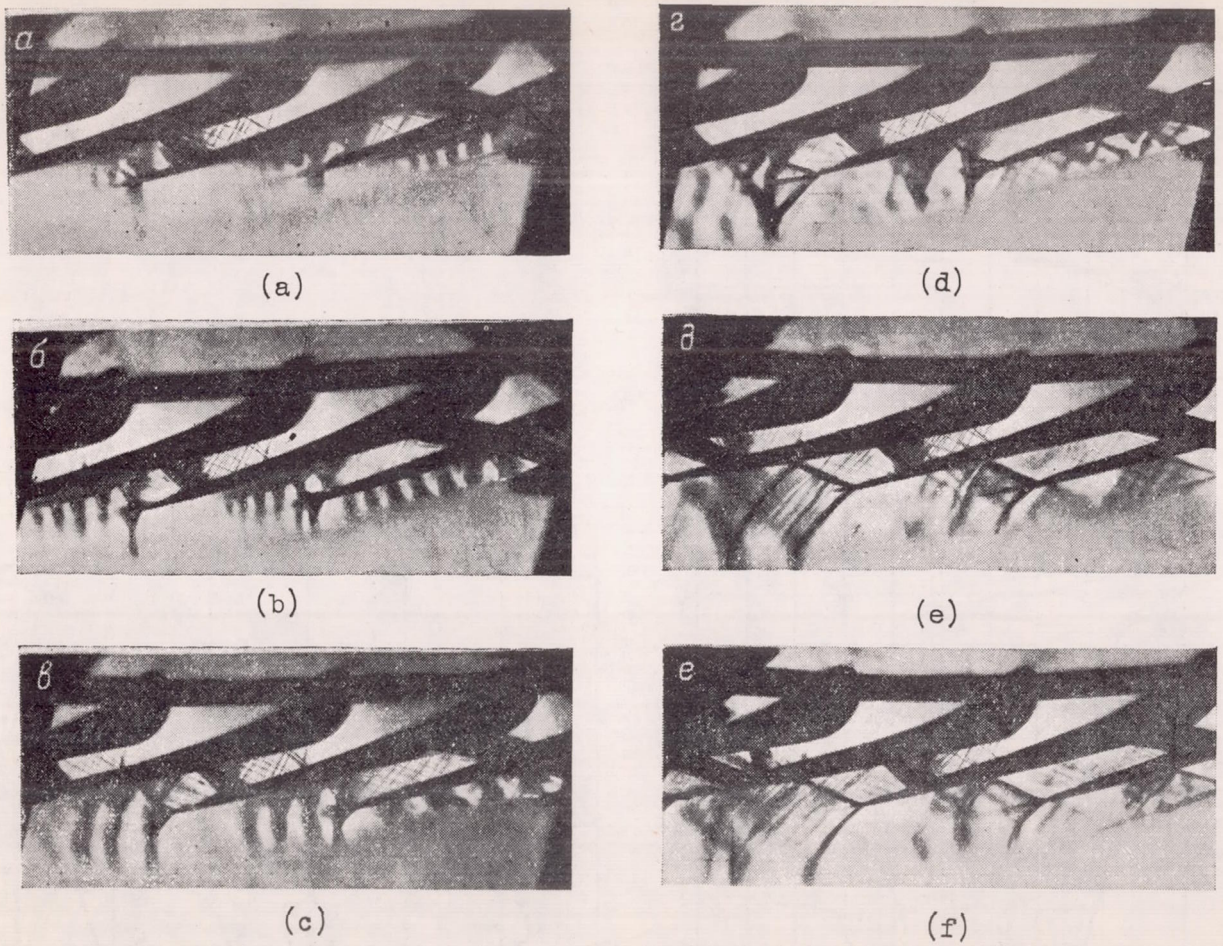


Figure 7-56. - Spectra of air flow through a reaction supersonic lattice at various regimes.

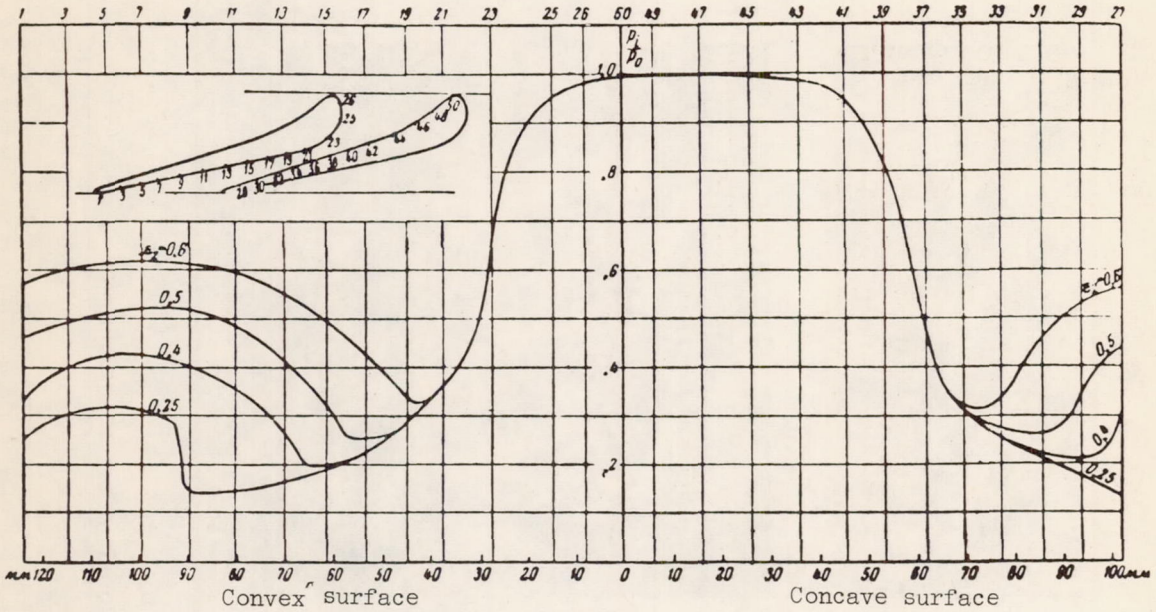


(a) Pressure distribution over profile.

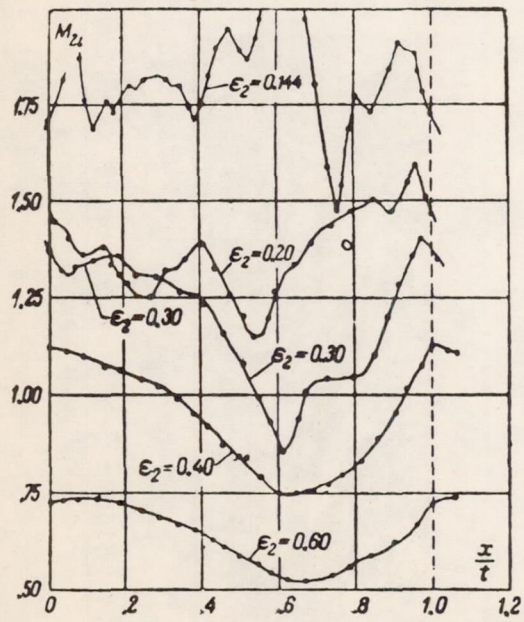


(b) Velocity distribution over pitch.

Figure 7-57. - Pressure distribution over a profile and velocity distribution over the pitch for a supersonic lattice at various regimes.

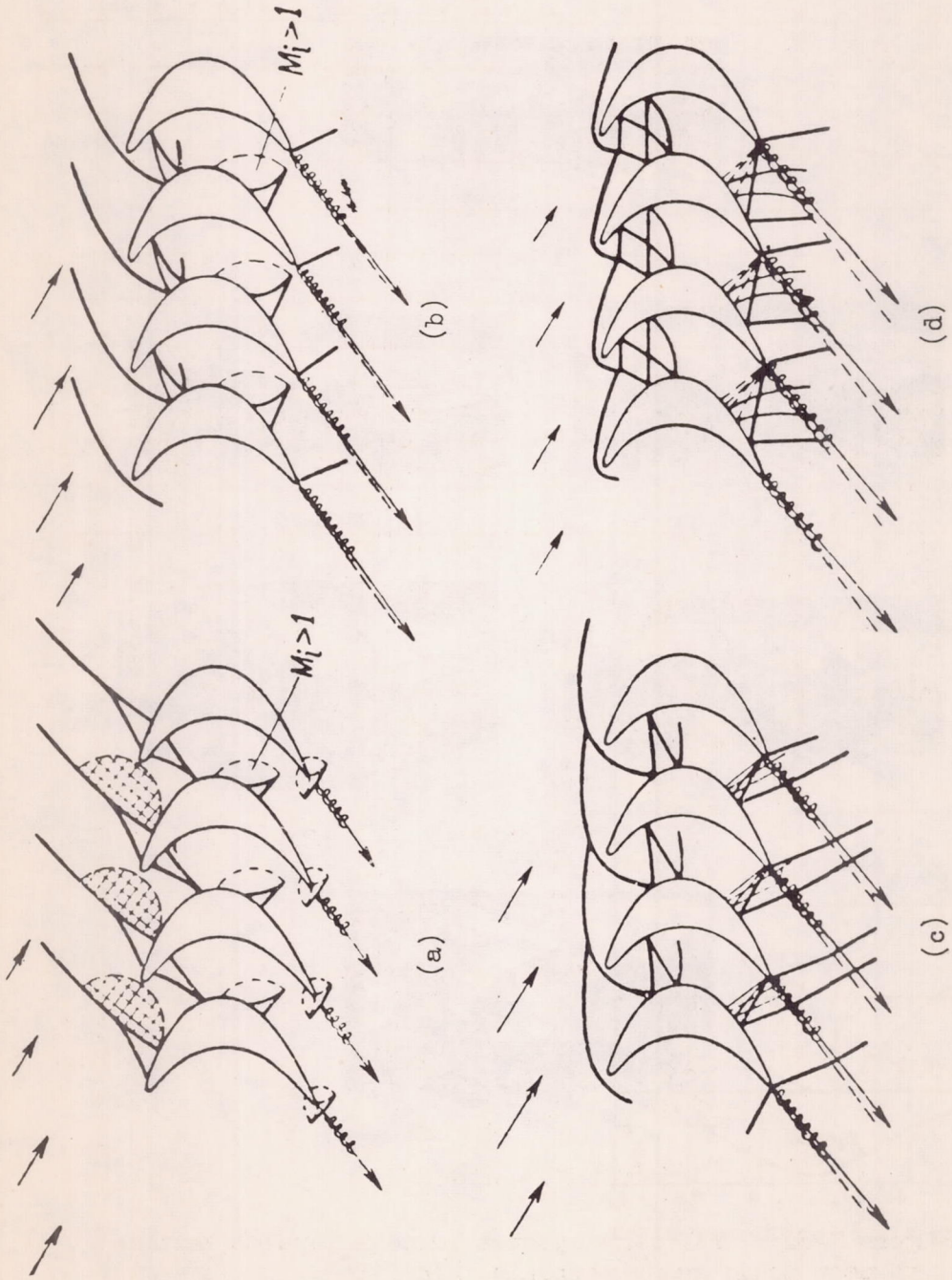


Figure 7-58. - Scheme of a supersonic flow about a lattice.

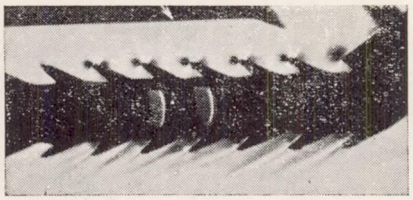

(a) $M_1 = 0.79$.

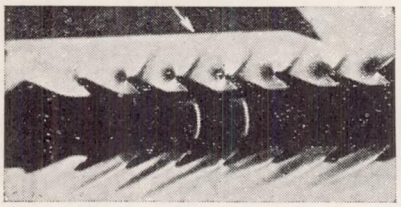

(b) $M_1 = 0.89$.

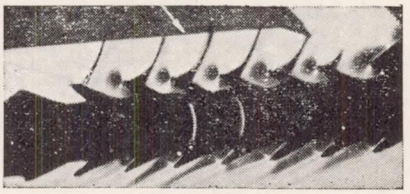

(c) $M_1 = 0.98$.

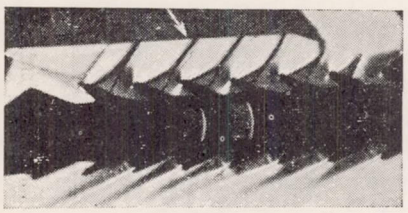

(d) $M_1 = 1.02$.

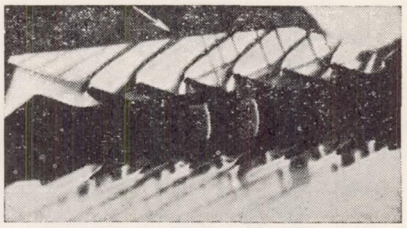

(e) $M_1 = 1.36$.

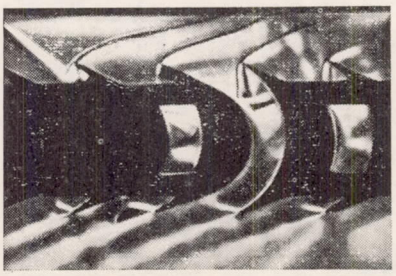

(f) $M_1 = 1.42$.

Figure 7-59. - Air flow spectra through impulse lattice at near sonic and supersonic velocities.

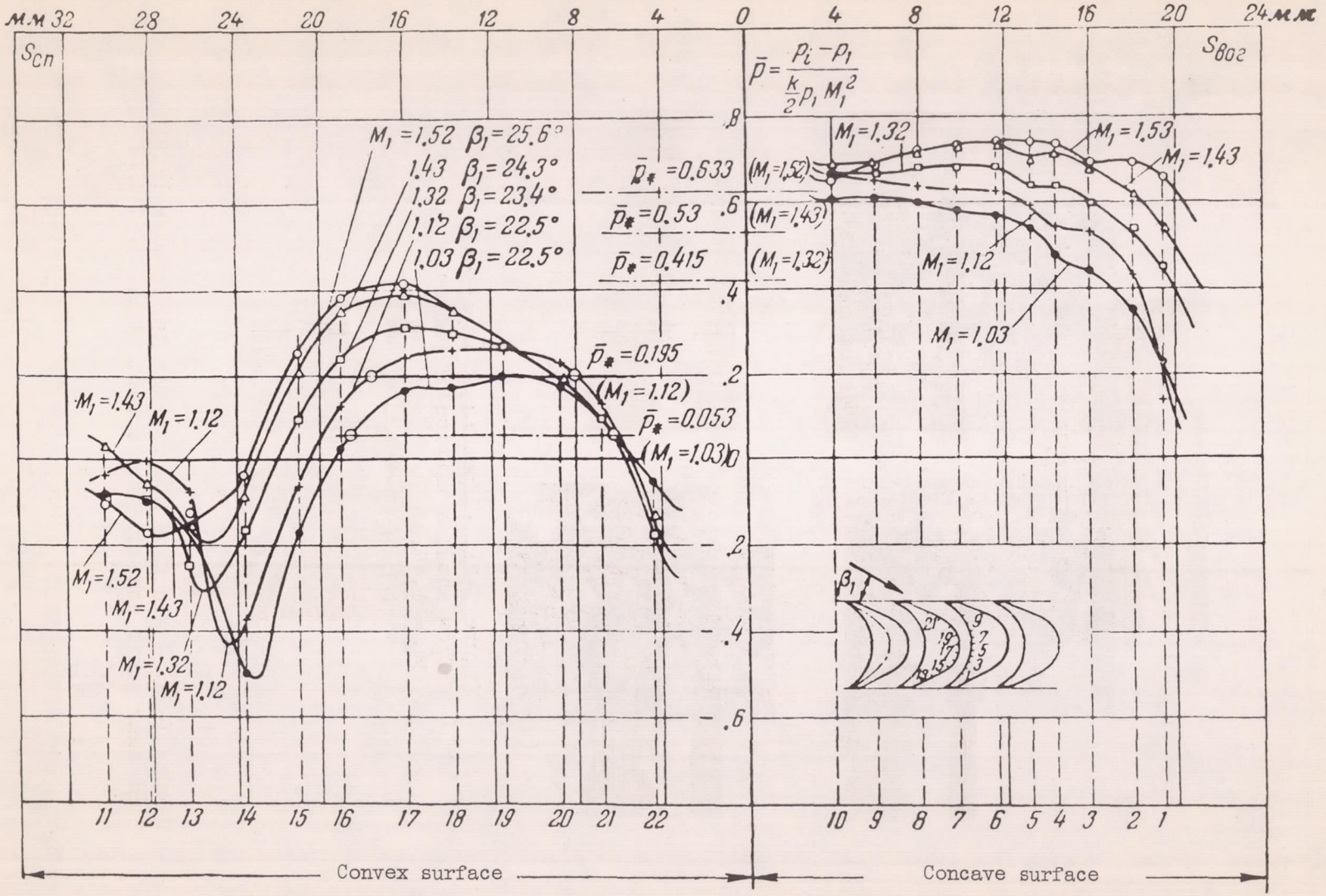


Figure 7-60. - Pressure distribution over the profile of an impulse lattice at supersonic velocities.

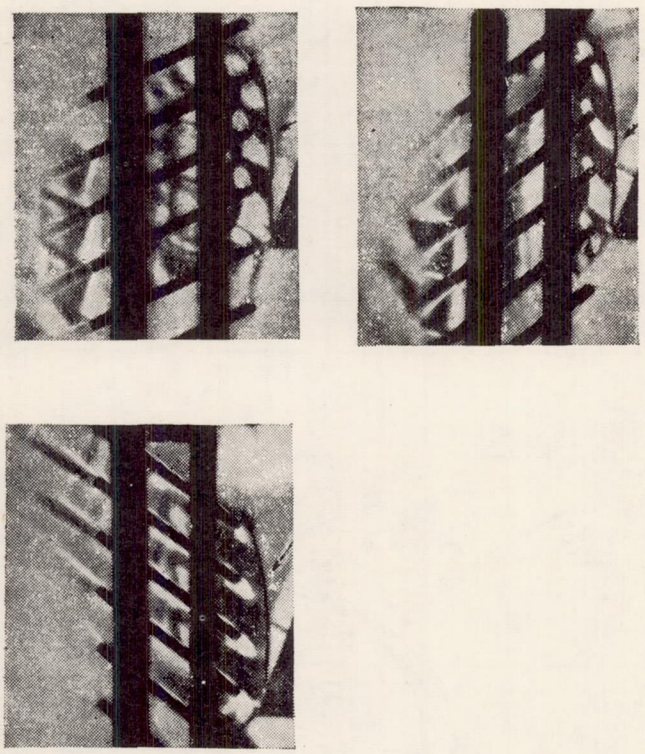

Figure 7-61. - Spectra of supersonic flow about a lattice of plates; $M_2 = 1.42$.

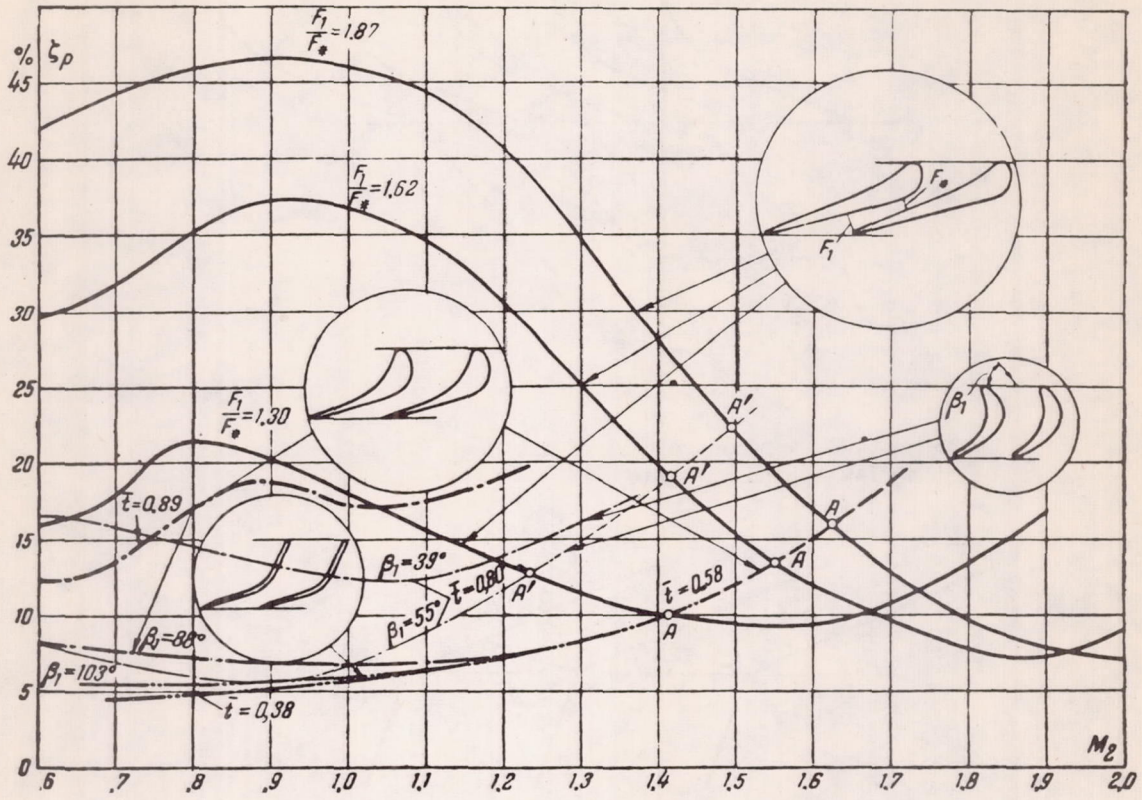


(a) Reaction lattices.

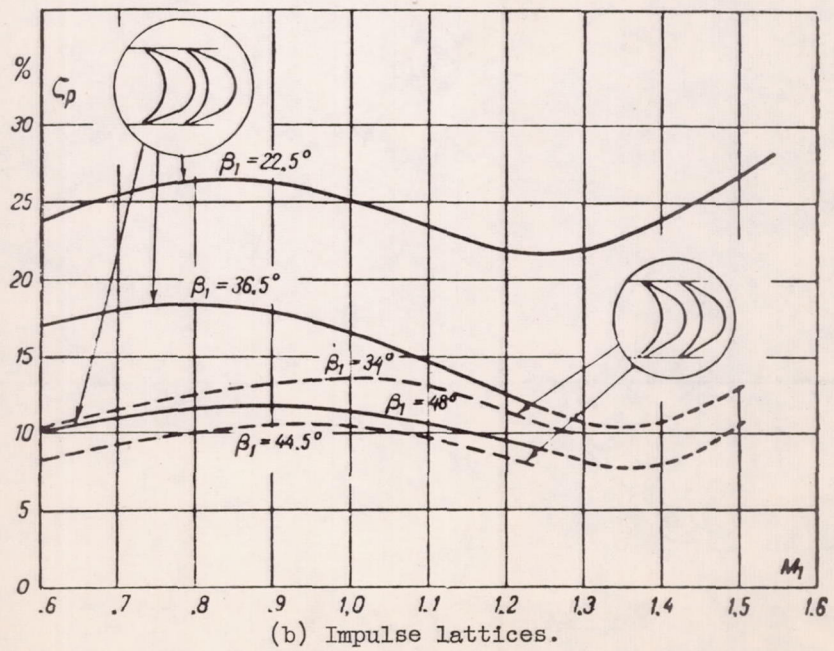


(b) Impulse lattices.

Figure 7-62. - Loss coefficient as a function of $M_2(M_1)$.

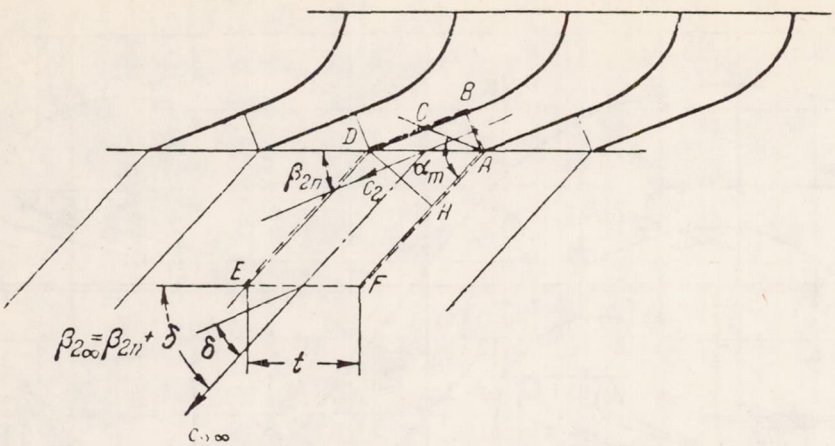


Figure 7-63. - Determination of the angle of deflection of the flow behind the throat of a lattice.

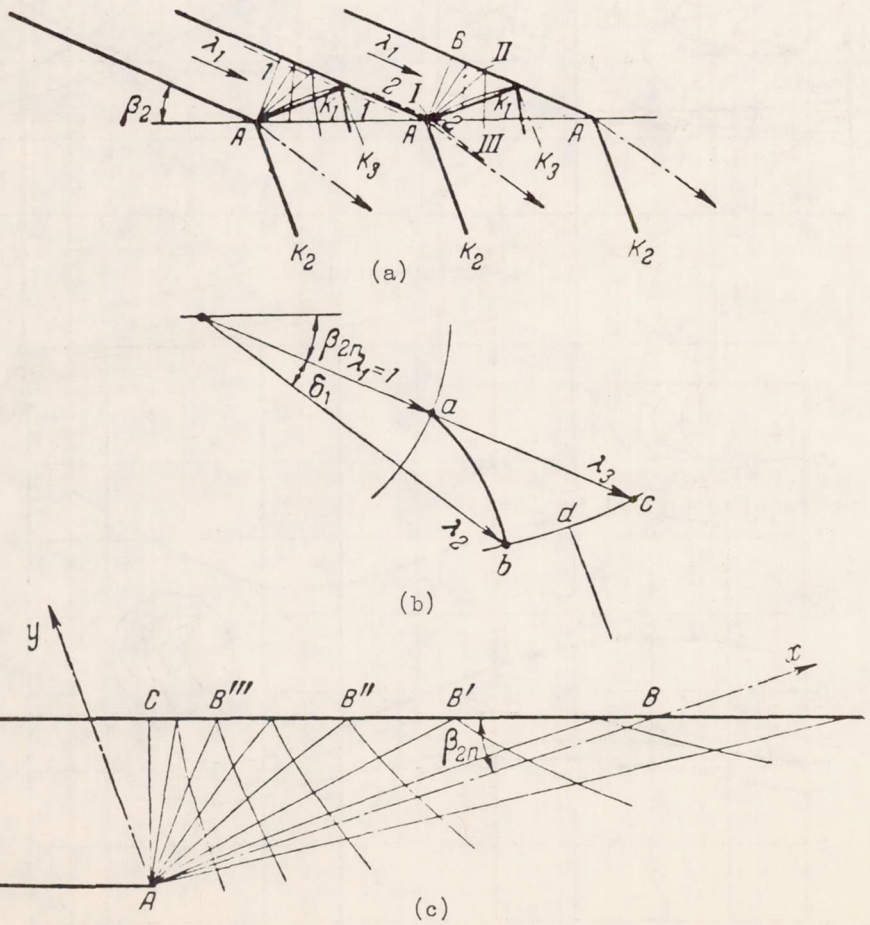


Figure 7-64. - Computation of the angle of deflection behind the throat by the method of characteristics.

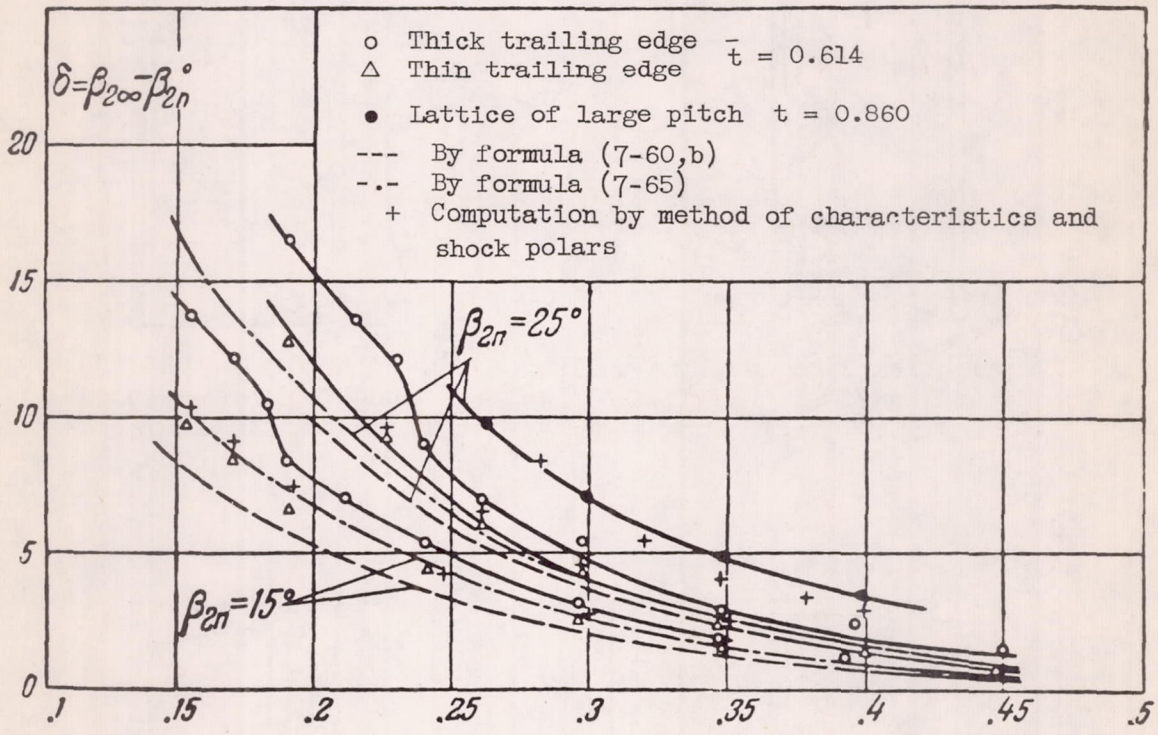


Figure 7-65. - Experimental and computed mean angle of deflection of a flow behind the throat of reaction lattices.

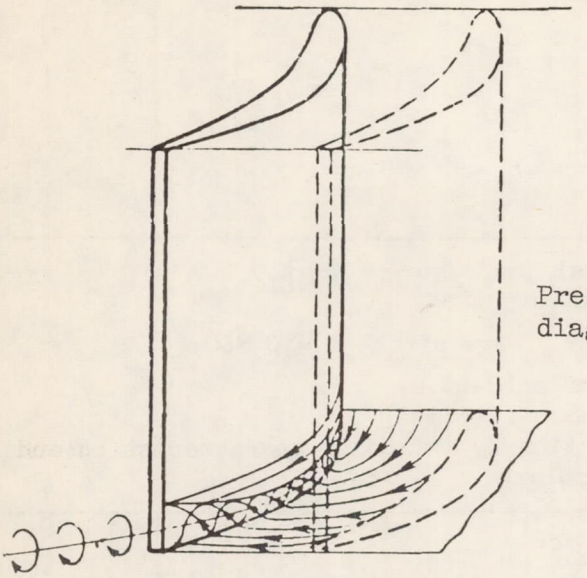

(a) Streamline on plane wall and back.

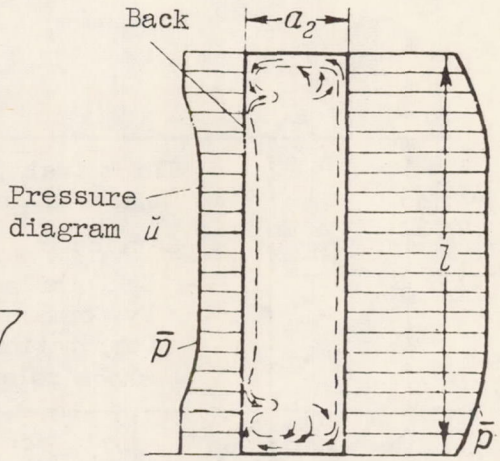


(b) Peripheral flows in boundary layer at ends of blade, thickening of layer on back of blade.

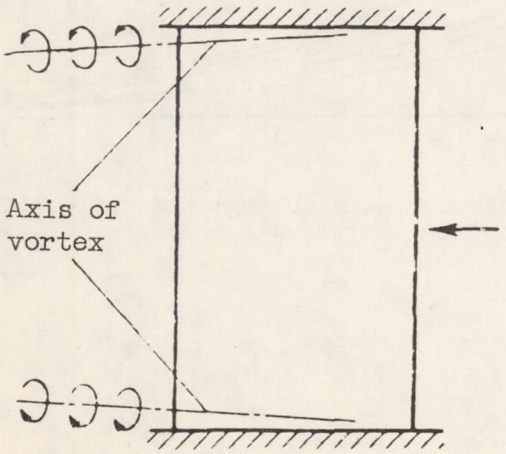


(c) Axes of vortical braids.

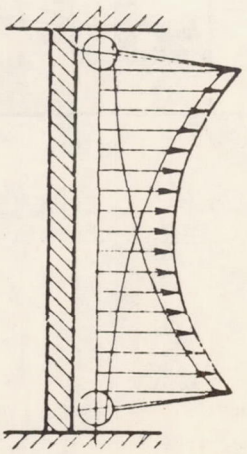

(d) Velocity field induced by vortical braids.

Figure 7-66. - Scheme of formation of secondary flows in the inter-blade channel of a lattice.

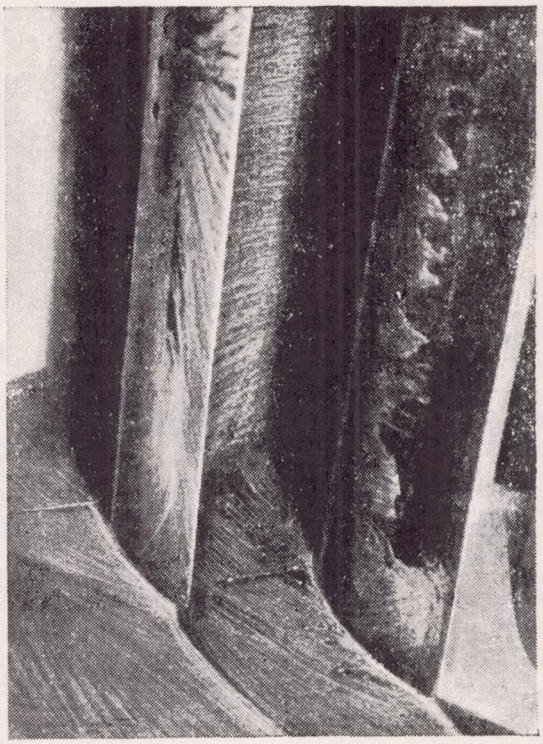

Figure 7-67. - Wakes of tip vortices in interblade channel.

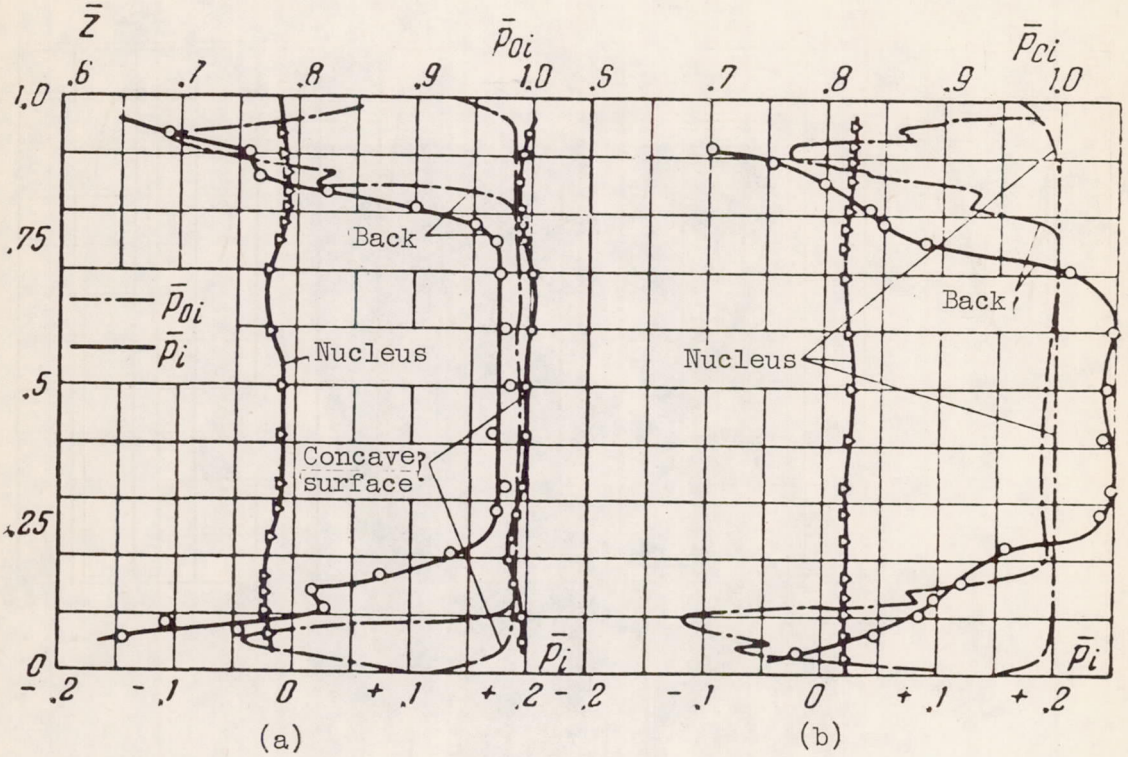


Figure 7-68. - Distribution of flow parameters over height of lattice for $M_2 = 0.78$.

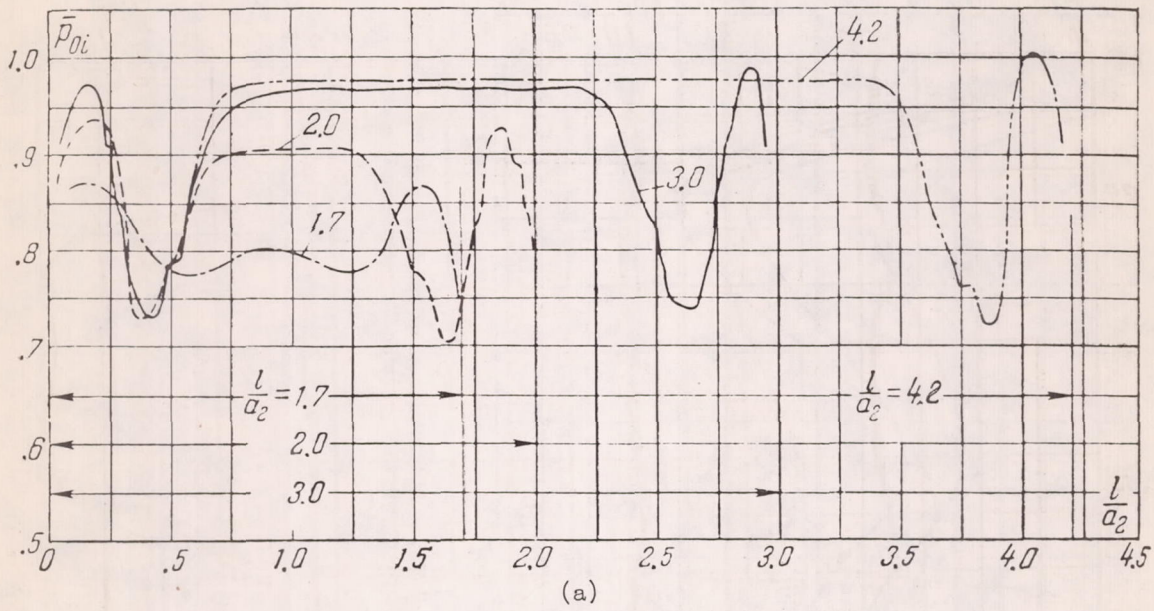


(a)

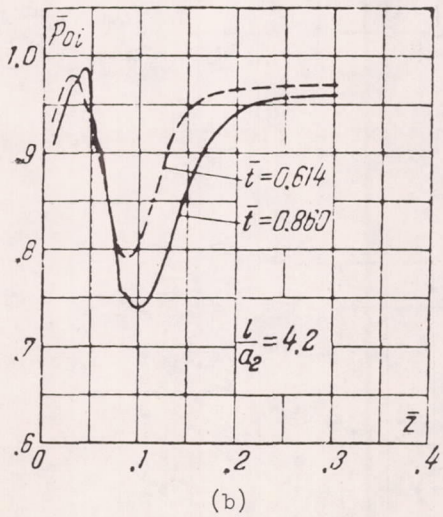


(b)

Figure 7-69. - Effect of geometric parameters of lattice on distribution of dynamic pressure over height on convex surface of blade.

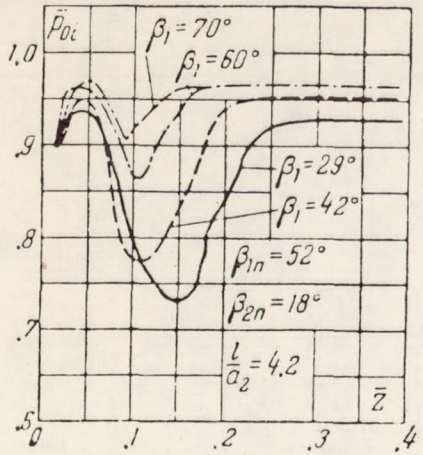


Figure 7-70. - Effect of the entry angle on the stagnation pressure distribution in the zone of vortex braids.

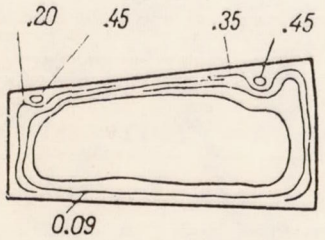


Figure 7-72. - Lines of equal coefficients of energy loss in the narrow section of a channel of a ring lattice.

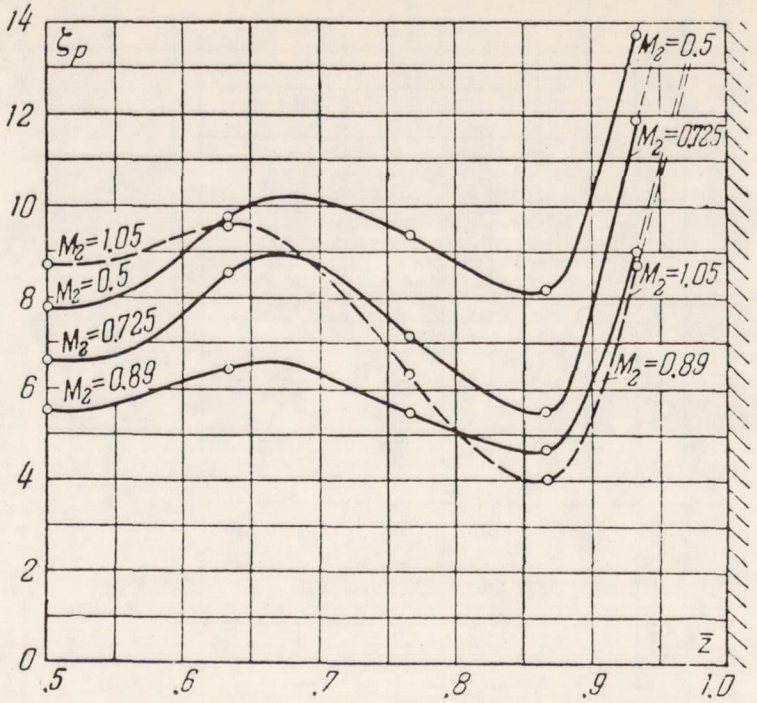


Figure 7-71. - Distribution of mean loss coefficients over height of short blade for various $M_2$ numbers.